



UNIVERSITY OF
LIVERPOOL

School of Biological Sciences

**Delivery, interaction and fate of peptide-
capped gold nanoparticles in mammalian
cells**

Thesis submitted in accordance with the requirements of the
University of Liverpool for the degree of Doctor in Philosophy

By

Umbreen Shaheen

May 2012

Dedicated to

**Mom, Dad, Sonia, Irfan, Saleha, Mobi, Bina, Ramsha, Hania, Khaleed
and Aroma**

Delivery, interaction and fate of peptide-capped gold nanoparticles in mammalian cells

Abstract

Cytosolic targeted delivery of molecular therapeutics is a crucial requirement to assess the efficacy and therapeutic potential of drugs. Recently, nanocarriers due to their easy and multidimensional use have been warmly welcomed by the scientific community, actively involved in designing delivery systems for *in vivo/in vitro* application. However, the endosomal entrapment of almost all types of nanoparticle-based delivery vehicles is a significant limitation. At present, most of the available non-viral and non-invasive delivery systems have shown modest results in addressing this problem. Gold nanoparticles are an interesting model system due to ease of functionalization, reduced toxicity and optical properties.

Here viral peptides (HA2 or/and TAT) and bacterial toxin assisted delivery strategies have been employed for cytosolic delivery of the peptide or mix monolayer of peptide and PEG-capped gold nanoparticles. HA2 functionalized gold nanoparticles were seen to interact with the endosomal membranes, but did not disperse into the cytosol. However, the presence of HA2 peptide at the surface of gold nanoparticles increased the overall cellular uptake of gold nanoparticles and this trend was found to depend upon the coverage density of HA2 peptide. Similar results were obtained for several HA2 analogues.

The pore forming bacterial toxin SLO was used to deliver the peptide and /or CCALNN-PEG-capped gold nanoparticles. Increased endocytosis of moderately PEGylated gold nanoparticles, but no cytosolic localization was observed by either gold nanoparticle imaging, *i.e.*, optical microscopy (photothermal) or electron microscopy. Surprisingly, the membrane impermeable dextran polymers of up to 150 kDa sizes were successfully delivered to the cytosol of SLO treated cells.

Finally, a pH sensitive polymer nanoparticle based delivery system (hydrogel) was employed for intracellular delivery of gold nanoparticles. The polymer particles decorated with evenly and sparsely present PEGylated CALNN-capped gold nanoparticles were localized to the cytosol, but gold nanoparticles were not able to detach from the hydrogels. The hydrogel inside the endosomal vesicles expanded in volume, but were not able to break the endosomes and release the attached gold nanoparticles.

Acknowledgments

The author is warmly grateful to Dr. Raphaël Lévy, primary supervisor not only for his all time available support and guidance for PhD but also for his very kind attitude. The author is thankful to the Higher Education Commission of Pakistan (HEC) for financial support. The research presented in this manuscript is the result of collaboration with many people from the School of Biological Sciences (University of Liverpool), Physiology Department (University of Liverpool), Chemistry Department (University of Liverpool) and also an international collaboration with Brett H Helm (Lawrence Berkeley National Laboratory, California, USA).

Ian Prior and Alison Beckett are thanked for training, guidance and allowing the use of transmission electron microscopy facility. Dave Spiller, Violaine Sée and Marco Marcello are also thanked for training and helpful guidance for fluorescence confocal microscopy. Violaine Sée is also thanked for giving initial stock of cell culture to establish our own and also for help with first optimization experiment with SLO and occasional general scientific discussions. The author is thankful to Dave Fernig as well for useful scientific and general discussions.

The author also appreciates Yann Cesbron for a 3 year long collaboration producing some crucial data together using his photothermal microscopy skills. The photothermal microscopy images presented in chapter 3 came from this collaboration. Christopher P Shaw has synthesised the nanoparticles for the group. In this manuscript, 5 nm gold nanoparticles and some of the 10 nm nanoparticles were prepared by Chris. Paul Free must be thanked for tissue culture training and for initial start up in the laboratory. Daniel Nieves and Lara Bogart should be thanked for their help with the photothermal microscopy work presented in chapter 4. The photothermal images included in chapter 4 were obtained by Dan.

The author would like to thank Thomas McDonald for his guidance while making attempts for zeta potential measurements for hydrogels.

The author is also thankful to all the people from Lab D, C and B who were great support in one way or the other. And, last but not least, the author is grateful to Irfan for his help at home while writing this manuscript and thanks to Aroma for keeping me smiling.

List of Figures

Fig. 1.1 Intracellular fate of positively charged and negatively charged SPIONs	9
Scheme 1.1 Different strategies and ligand shells for capping gold nanoparticles	13
Fig. 1.2 Different natural strategies for intracellular uptake (endocytosis)	19
Fig.1.3 A clathrin-coated vesicle	21
Fig. 1.4 Caveolae formation and endocytosis of GNPs	22
Fig. 1.5 Macropinocytosis	23
Fig. 1.6 Phagocytosis	24
Fig. 1.7 Clathrin-independent endocytosis	25
Fig. 2.1 HA2 peptide increases cellular uptake of gold nanoparticles	42
Fig. 2.2 Intracellular localization of HA2 functionalized gold nanoparticles: effect of PEG	44
Fig. 2.3 Increasing the proportion of dCCALNNHA2 in the monolayer of gold nanoparticles increases cellular uptake	45
Fig. 2.4 (PEGylated vs none PEGylated) Mixing two types of CCALNN-HA2 gold NPs to enhance cytosolic delivery of HA2 peptide	49
Fig. 2.5 Attaching HA2 <i>via</i> the C-terminus <i>versus</i> N-terminus: effect of HA2 orientation on cellular localization	51
Fig. 2.6 HA2-fused TAT peptide for intracellular delivery of FITC-TAT peptide	53
Fig. 2.7 Intracellular delivery and Quantification of CALNN-HA2/CALNN-TAT assisted delivery of gold nanoparticles	54
Fig. 2.8 Entry mechanism of TAT PEG-capped gold nanoparticles; macropinocytosis	56
Fig. 2.9 Intracellular localization of TAT PEG-capped gold nanoparticles after 2 h	57
Fig. 2.10 Intracellular localization of TAT PEG-capped gold nanoparticles after 24 h	58
Fig. 2.11 Intracellular localization of TAT PEG-capped gold nanoparticles after 48 h	59
Fig. 3.1: Permeabilization of cells with Streptolysin O	70
Fig. 3.2 SLO assisted delivery of fluorescein-conjugated dextran of increasing MW (Permeabilization confirmation).	72

Fig. 3.3 Tuning surface chemistry to control endocytotic uptake (PEG effect)	75
Fig. 3.4 Streptolysin O induced increase cellular uptake of CALNN or/and CCALNN-PEG functionalised gold nanoparticles.	77
Fig. 3.5 SLO effect: Quantification based on mean photothermal intensities for 0, 10 and 20% CCALNN-PEG conditions with/without SLO.	78
Fig. 3.6 Localization of gold nanoparticles in SLO treated HeLa cells (electron microscopy study)	80
Fig. 3.7 Localization of gold nanoparticles in +/- SLO samples (Photothermal microscopy)	81
Scheme 4.1 Functionalization of hydrogels with gold nanoparticles	90
Fig. 4.1 Gold nanoparticles distribution on hydrogel surface	93
Fig. 4.2 Entry inside the cells: via phagocytosis/direct translocation	94
Fig. 4.3 Direct translocation into the cells	96
Fig. 4.4 Low pH induced endosomal breakage by hydrogels?	99
Fig. 4.5 Increased cellular uptake of gold nanoparticles in the presence of hydrogel (Electron microscopy)	101
Fig. 4.6 Increased cellular uptake of gold nanoparticles (GNPs) due to hydrogels (photothermal microscopy)	102

List of Tables

Table 2.1 Viral peptide HA2, TAT and derivatives	41
Table 2.2 Types of HA2 gold nanoparticles with N-C or C-N orientations	50
Table 3.1 Monolayers of gold nanoparticles for PEG titration	74
Table 4.1 Experimental conditions for gold nanoparticles functionalized hydrogels	91

List of Abbreviations

CPP Cell penetrating peptide
DTT Dithiothreitol
FDA Fluorescein diacetate
TEM or EM Transmission electron microscopy
ICP-AES Inductively coupled plasma atomic emission spectroscopy
IR Infrared
LISNA Laser induced scattering around a nano-absorber
nM Nano molar
NP or NPs Nanoparticle
GNPs gold nanoparticles
PHI Photothermal heterodyne imaging
PI Propidium iodine
ROI Region of interest
SAM Self-assembled monolayer
SD Standard deviation
SE Standard error of the mean
SLO Streptolysin O
SPR Surface plasmon resonance
UV Ultraviolet
PEG Poly ethylene glycol
nm Nanometer
KDa Kilo Dalton
KV kilo volt
h hour or hours
FITC-TAT Fluorescein isothiocyanate fused-TAT
MW molecular weight

Contents

1. Introduction	1
1.2 Review of different nanomaterials	3
1.2.1 Polymeric nanoparticles.....	3
1.2.2 Liposomes	4
1.2.3 Semiconductor nanocrystals or Quantum dots	5
1.2.4 Carbon nanoparticles	7
1.2.5 Super-paramagnetic iron oxide nanoparticles (SPIONs).....	7
1.2.6 Silver nanoparticles	9
1.2.7 Gold nanoparticles	10
1.3 Ligand Shells.....	12
1.4 Techniques for the detection of gold nanoparticles.....	13
1.4.1 Transmission electron microscopy	14
1.4.2 Photothermal microscopy.....	17
1.5 Research problem: vesicular entrapment of nanoparticles	18
1.5.1 Sequestration of nanoparticles.....	18
1.5.2 Review of endocytic mechanisms	19
1.5.3 Transfection methods and their consequences.....	25
1.6 Addressing the research problem: bio-inspired strategies.....	27
1.6.1 Viral peptides in SAM of gold nanoparticles for cytosolic delivery	27
1.6.2 Toxin assisted gold nanoparticles delivery	29
1.6.3 Hydrogel.....	30
1.7 Bibliography	31
2. Intracellular delivery of gold nanoparticles using viral peptides.....	38
2.1 Viral peptides: Haemagglutinin subunit 2 (HA2)	38
2.2 Viral peptides: Trans-activator of transcription (TAT)	39
2.3 HA2 and TAT assisted gold nanoparticles delivery	40
2.4 Results.....	41
2.4.1 Nanoparticle-bound HA2 increases cellular uptake of gold nanoparticles	41
2.4.2 Effect of PEGylation on the localization of HA2- capped gold nanoparticles	43
2.4.3 Increasing percentage of HA2 in SAM increases the cellular uptake	44
2.4.4 Mixing two types of HA2 gold nanoparticles to enhance cytosolic delivery	46
2.4.5 N-C or C-N terminus orientation of HA2 peptide does not alter the cytosolic delivery of gold nanoparticles.....	50

2.4.6 FITC- TAT peptide and HA2 fused TAT peptide for cytosolic delivery	52
2.4.7 TAT and HA2 increases cellular uptake of gold nanoparticles.....	53
2.4.8 TAT-functionalized gold nanoparticles enters the cells mainly via macropinocytosis	55
2.5 Discussion.....	59
2.5.1 HA2 increases cellular uptake of gold nanoparticles	59
2.5.2 Cytosolic delivery of gold nanoparticles?	60
2.5.3 TAT: entry mechanism and cytosolic delivery	61
2.6 Conclusion and future perspective	63
2.7 Bibliography	65
3. Bacterial toxin assisted delivery of capped gold nanoparticles.....	67
3. 1 Streptolysin O: Mechanism of pore formation	67
3.2 Streptolysin O assisted intracellular delivery.....	68
3.3 Choosing the right conditions	69
3.3.1 Optimization of SLO amount.....	69
3.3.2 SLO-assisted cellular uptake of FITC-dextran (proof of principle)	71
3.4 Gold nanoparticles co-incubation with SLO.....	73
3.5 Effect of PEGylation (tailoring the nanoparticles surface properties to avoid endocytosis).....	73
3.6 Streptolysin O-assisted delivery; increased cellular uptake of gold nanoparticles	76
3.7 SLO assisted delivery of gold nanoparticles (cellular localization)	79
3.8 Discussion.....	82
3.9 Conclusion and future perspective	85
3.10 Bibliography	86
4. Intracellular delivery of gold nanoparticles using polymer nanoparticles	87
4.1 Polymer nanoparticles	87
4.2 Polymer nanoparticles for delivery of gold nanoparticles.....	90
4.3 Results.....	92
4.3.1 Effect of PEGylation and concentration of gold nanoparticles on the interaction with hydrogel	92
4.3.2 Interaction of hydrogels with the cell membrane	93
4.3.3 Cytosolic localization of hydrogels: direct translocation through cell membrane	94
4.3.4 Did endosomal breakage help cytosolic delivery of gold nanoparticles?.....	97
4.3.5 Increased cellular uptake of gold nanoparticles	100
4.4 Discussion.....	103
4.5 Conclusion and future perspective	107

4.6 Bibliography	108
Conclusion.....	109
Materials and methods.....	112
1 Materials	112
2 Methods.....	113
2.1 Peptide stock solutions	113
2.2 Gold nanoparticle synthesis.....	113
2.3 Formation of peptide self-assembled monolayers for gold nanoparticles (general procedure)	114
2.4 Formation of peptide self-assembled monolayers containing 5% CALNN-TAT 95% PEG- ligands	114
2.5 Nanoparticles purification procedure.....	115
2.6 Nanoparticles purification procedure for 5% CALNN-TAT 95% PEG-containing gold nanoparticles	116
2.7 Streptolysin O (SLO) preparation	116
2.8 Optimization of the optimum Streptolysin O amount.....	116
2.9 Formation of nanoparticles-decorated hydrogels	118
2.10 Cell culture and nanoparticle incubation (general procedure).....	118
2.11 Cells treatment with gold nanoparticles (with/without SLO).....	119
2.12 Cells treated with fluorescent isothiocyanate-dextran (FITC-dextran)	120
2.13 Cell proliferation assay: Thiazolyl blue tetrazolium bromide (MTT assay)	120
2.14 Transmission electron microscopy	120
2.15 TEM image analysis for gold content.....	121
2.16 Gold nanoparticles sizing by TEM	121
2.17 Confocal microscopy	122
2.18 Photothermal microscopy.....	122
2.19 Bibliography	125
Appendix.....	126

CHAPTER 1

1. Introduction

In this PhD thesis, different strategies have been evaluated for the cellular internalization of peptide and polyethylene glycol (PEG) capped gold nanoparticles. As nanoparticles and their intracellular delivery is the main theme of this manuscript, a general overview of bionanotechnology is given below, and, in particular, the different nanoparticles used for biological applications that require intracellular delivery are presented.

The term nano derives from the Greek word "dwarf". Nanotechnology involves studying, applying and designing materials in the nanometre to micrometre size range.¹ Nanobiotechnology or bionanotechnology refers to the use and design of nanomaterials for biological applications or the use of biological systems to produce or modify nanomaterials. In Klostranec and Chan's words "the marriage of nanomaterials with biology have produced a new generation of technologies having great impact on biological and biomedical research".²

This field is highly interdisciplinary and due to its multifaceted impact on science, the publications in all types of journals, *i.e.*, biology, physics, chemistry, materials science *etc.* are exploding.^{1, 3} The expansion of nanotechnology can be illustrated by estimating the production of nanoparticles, which is predicted to increase by 25 times from 2,300 tons in 2006-2007 to 58,000 tons in 2020.⁴ In this context, improving our understanding of the interaction of nanoparticles with cells is particularly important.

With the advent of molecular biology that describes cellular events at the molecular level, nanobiotechnologies could contribute to solving the challenges of imaging and sensing at the nanoscale. Nanomaterials have similar dimensions as complex organic biomolecules such as DNA and proteins. They have much larger surface to volume ratio than the respective bulk materials. Gold as a bulk has a distinct golden colour, while gold nanoparticle suspensions have different colours, which vary from black to cherry red colour, depending on their sizes. The quantum related magnetic and electrical properties, size related optical properties and ability to carry different compounds, *e.g.*, drugs, molecular probes and proteins, make them suitable for biological applications.

Diverse kinds and shapes of nanomaterials have been synthesized so far. The shapes include nanorods, nanosheets, nanowires, nanotubes, carbon nanotubes, liposomes, micelles, etc. The materials include organic (e.g., fullerenes, polymers, lipids, surfactants), inorganic (e.g., gold, silver, iron oxide, cadmium selenide) as well as combinations of the two into core-shell materials. In biology, these nanomaterials are being used as diagnostic and therapeutic tools, detectors, spectroscopic markers, trackers, transfection vectors and for drug delivery.^{5,6}

Silver nanoparticles are increasingly being utilized as antimicrobial agents in cosmetics, air fresheners, medicine and in cleaning products like washing powders.⁷ Biodegradable polymer nanoparticles and liposomes are considered as safe non-viral delivery vehicles for drugs and genes.⁸⁻¹⁰ Super-paramagnetic iron oxide nanoparticles (SPIONs) have been in routine use as contrasting agent for magnetic resonance imaging (MRI).¹¹ Carbon nanotubes and nanoparticles have been used for strengthened tissue scaffolds, drug carriers, diagnostic devices and fluorescent-contrast agents.¹²

Gold nanoparticles are considered efficient probes for medical and biological diagnostics and applications. They owe this status because of their easy synthesis, chemical stability, high biocompatibility, limited cytotoxicity, distinct optical properties and their high affinity for sulphur compounds, which facilitates functionalization.¹³⁻¹⁵ Apart from direct use of gold nanoparticles as delivery and imaging agents, biological probes, therapeutic remedy and transfection vectors, gold is also used as a coating on other types of nanomaterials to enhance their working efficiency.^{16 11}

Quantum dots (Qdots) are fluorescent nanoparticles with dimensions in the range of 2-10 nm. The conventional technique for live cell imaging is fluorescence confocal microscopy. Qdots smoothly fit in with this imaging technique, due to their fluorescent properties and their long term and intense fluorescence emission compared to organic dyes. Apart from bioimaging and detection, Qdots are also being utilized for delivery purpose by adding biofunctional ligands on their surface.¹⁷

Each of these nanomaterials has their own advantages and limitations, which will be discussed below. The emphasis is particularly on the cellular interaction and intracellular fate of nano materials.

1.2 Review of different nanomaterials

1.2.1 Polymeric nanoparticles

Polymeric nanoparticles are based either on synthetic biodegradable polymers, *e.g.*, poly lactic acid (PLA), polyesters, poly(cyano)acrylates, polyethylenimine or natural polymers, like albumin, gelatin, chitosan, dextrane, alginates, starch and hyaluronic acid. Polymeric nano or micro materials are suitable for cellular drug delivery due to a wide range of polymeric materials to choose from according to need and also due to the ease of production, ease of surface modification, versatility in synthetic chemistry, encapsulation efficiency of the payload, polymer degradation and feasibility of scale-up.^{18, 19} General biological application of polymeric nanoparticles is drug or gene delivery. A proposed mechanism for cargo release from polymer nanocarrier is through biodegradation of the polymer carrier once it has reached the target site. To increase the circulation time and to reduce cytotoxicity, PEGylation of polymeric particles is recommended.⁸ It was noticed that the molecular weight of the polymeric particles plays a role in defining most of the biological properties and responses, not only at cellular level, but also at the whole body level.²⁰

Won *et al.* have reviewed the nano-carriers for organelle targeted RNA/DNA intracellular delivery. Particularly the reducible polymers and peptides, cationic polymers and peptides and nuclear localized signal peptides complexes with polymer and DNA/ RNA (NLS-polymer-DNA complex) have been discussed. Reducible polymers contain internal disulfide bonds, which exhibit high stability in extracellular environments, but rapidly reduce inside the cells thus, releasing the entrapped cargo. The results have been discussed in terms of gene silencing or gene expression, *i.e.*, end effect of the particle delivery, but this review did not discuss how the cargo was able to reach the target organelle or cytoplasm. Instead it was concluded that there are very few studies, which give the full scenario of the fate of nano carriers once inside the cells.²¹ In another review the potential of naturally occurring polymers with stimuli- responsive properties was discussed in terms of gene delivery. The natural polymers are generally biocompatible and stimuli- responsive properties were incorporated into the system either using pH, temperature or redox responsive element. Still few studies were reported with successful efficient endosomal release of the cargo using these polymers.²² Efficiency of targeted delivery and localization inside the cells is still an active area of research with a range of outcomes depending on the conditions in each

study. In our work, we have used cationic core-shell polymer colloids (a gift from Brett A. Helms, Lawrence Berkeley National Laboratory California) for gold nanoparticles delivery. These polymer particles or hydrogels of 200-160 nm size are pH sensitive and should break lysosomal vesicles at low pH. Bayles *et al.* have done localization studies for Qdots functionalized with these polymer particles using confocal fluorescence microscopy and concluded that they were able to break out of endosomes, delivering the Qdots to cytosol.²³ Our results will be presented and discussed in chapter 4.

1.2.2 Liposomes

Liposomes are vesicles formed by one or several phospholipid bilayers surrounding an aqueous core. Liposomes were designed to deliver drugs, enzymes, genes and therapeutic peptides to various biological targets. Lipids can degrade easily in a biological environment, thus, the cargo, which needs to be delivered safely to the target, is separated from the nanocarrier readily. The presence of hydrophobic and hydrophilic domains allows the flexibility of loading a wide range of therapeutic agents. Generally, hydrophilic biomolecules are encapsulated within the central aqueous core, whereas hydrophobic biomolecules are incorporated into the lipid membrane.^{24, 25} Stealth liposomes, which have been developed by incorporating PEG-coated lipids in the formulation, exhibit extended blood circulation time *In vivo* compared to conventional liposomes, containing only natural phospholipids.²⁶ pH sensitive liposomes have also been developed for drug delivery, but there are few reports about their therapeutic potential.^{27, 28}

A nice review by Johnston *et al.* on the challenges faced by colloidal delivery systems summarizes the 'nano-carriers' interaction *in vivo* and *in vitro*. There is no simple rule describing cellular interaction with nano carriers. Cellular interaction of nanoparticles is highly dependent on the cell type, nature of the surface ligands, size of the particles and overall charge.²⁹ To illustrate how subtle changes in nanoparticle composition can affect the final outcome, we consider below a recent example of peptide-decorated liposomes. Liposomes having a high density of positively charged octarginine peptide (R8) or the octlysine peptide (L8) on their surface, showed macropinosytic mediated cellular uptake by NIH 3T3 cells. The macropinosome is considered as an inherently leaky vesicle and in most cells its acidification occurs even before fusion with the lysosomes.^{30, 31} The intracellular fate of the liposomes functionalised with L8 showed vesicular localization and exhibited very low

transfection efficiency when delivering siRNA. In contrast, R8 liposomes have shown escape from the early endosomal compartment and showed significantly higher transfection efficiency.³² This study suggests that the intracellular fate and consequently the transfection efficiency are dependent upon the surface chemistry of the nano carrier and on the way the cargo enters the cells. This same idea was strengthened by another comparative study, which estimated transfection efficiency by high density R8 coated liposomes and by less densely R8 coated liposomes. The former showed three fold higher transfection efficiency than the later. It was found that R8-rich liposomes entered via macropinocytosis and were, therefore, able to escape the early endosomes, while liposomes with lower R8 surface coverage entered the cells via clathrin-mediated endocytosis and were subjected to degradation due to lysosomal entrapment.³³ These observations are of particular interest in the context of our work, as we noticed trends of preference in cellular uptake mechanism with TAT and PEG-capped gold nanoparticles, which will be discussed in chapter 3.

In spite of some successful attempts mentioned above, evading the cellular or whole body defence mechanisms remains a major challenge.²⁹ The other barrier for liposomal-assisted cargo delivery is the targeted release of contents, while maintaining stability during transportation. The drug or cargo is often released before reaching the target due to instability and leakage of liposomes.²⁵ Furthermore following inefficient release from liposomes, most of the cargos can be trapped inside lysosomal vesicles and degraded thus, never reaching their targets in the cytosol or in the nucleus.^{9 3}

1.2.3 Semiconductor nanocrystals or Quantum dots

Quantum dots (Qdots) are fluorescent nano-materials having size-dependent optical properties. These nanocrystals are either composed of different elements, *e.g.*, CdSe, CdTe, CdS, ZnSe, InP, InAs or consist of core/shell systems such as CdSe/ZnS and CdSe/ZnSe.

Qdots are available commercially in 5 or 6 different colours: the emission wavelength of a Qdot can be continuously tuned by changing the particle size. A single light source can be used for simultaneous excitation of all different-sized Qdots thus, enabling multiplex fluorescence imaging.³⁴

Qdots emit photons by exciting electrons in response to optical or electrical stimuli. The amount of energy required to induce the electrons to become excited, is dependent upon the

band gap energy. This band gap energy in turn is related to the Qdot's size, shape, and composition. This dependence is due to the quantum confinement effect and will only occur when the size of the nanostructure is on the order of a few nanometres (< 20 nm).²

In biology, Qdots are attractive because of their similar quantum yields and much reduced photobleaching rates compared to traditional organic fluorophores.³⁵ Michalet *et al.* reviewed the use of Qdots for labelling whole cell using microinjection, electroporation or by phagocytosis. Detection and tracking of microorganisms using Qdots is also reported, *e.g.*, detection of gram- positive bacteria and tracking of *Dictyostelium discoideum* at single cell level. *In vivo* long term imaging of live animal using Qdots was found brighter and stable compared with organic dyes.³⁶

Cytotoxicity due to the release of Cd²⁺ or Se²⁻ ion due to improper coating, interference with cellular processes, irregular blinking, variability in surface chemistry preventing effective biofunctionalization, physical damage during transfection procedure, vesicular sequestration after cellular internalization and nonspecific binding were identified as potential risks and limitations for biological and biomedical applications of Qdots.^{17, 36, 37}

Nirmal *et al.*, explain blinking in the following way:

"Surface defects in the crystal structure act as temporary "traps" for the electron or hole, preventing their radiative recombination. The alternation of trapping and untrapping events results in intermittent fluorescence (blinking)".^{36, 38}

Like other nanomaterials, endocytosis, and the possible degradation in endocytic compartments, hampers the potential usage of Qdots inside living cells. Unfortunately, there is no systematic critical review available, which scrutinizes and compares the small number of studies reporting departure from the generally observed scenario of endosomal trapping. The reviews of this field tend to mention the same few studies, which have shown cytosolic or nuclear localization of either CPP-coated Qdots or NLS and PEG functionalized Qdots via microinjection and electroporation.^{17, 36, 39, 40}

Shao *et al.* have reviewed the biomedical applications of Qdots including, *in vitro* and *in vivo* delivery, labelling, sensing, photodynamic therapy and imaging. Qdot based delivery systems for *in vitro* applications result mainly in vesicular localization unless some active delivery methods are employed such as electroporation or microinjection. Electroporation

of Qdots was found to be toxic to cells and microinjection was regarded as expensive, low through put, time consuming and required relative specification of working conditions.⁴⁰

1.2.4 Carbon nanoparticles

There are different kinds of carbon nanomaterials like C60, single walled nanotubes (SWCNTs) and multi-walled nanotubes (MWCNTs).⁴¹ The SWCNTs is composed of carbon atoms, arranged in benzene rings forming graphene sheets, rolled up in cylinder shape. The MWCNTs are formed by several concentric layers of rolled graphite. The SWCNTs can be very long and very thin (a few nm).¹² Their light weight, high tensile strength, thermal/chemical stability and conductivity have led to biological applications such as tissue scaffolds, diagnostic or biosensing devices, fluorescent-contrast agents and drug carriers.¹²

Shvedova *et al.* have presented a review of medical applications and pulmonary toxicity of SWCNT. The review also covers other aspects such as, synthesis, industrial significance of nanomaterials along with *in vitro* / *in vivo* uptake and toxicity of CNTs. It was concluded that SWCNTs with some biological moiety adsorbed on their surface, are readily engulfed by different types of cells (human, mouse and rat lung cells) compare to poor or no cellular uptake shown by unmodified SWCNTs.⁴² In another study the cellular localization of 6-aminohexanoic acid-derivatized single-wall carbon nanotube (AHA-SWNTs), with overall negative surface charge, was found vesicular. These AHA-SWNTs showed a dose-dependent cytotoxicity in human epidermal keratinocytes (HEKs).⁴³

The cytotoxicity measurement assays based on dyes (like MTT) are questioned due to the recently discovered optical interference and physical interaction of CNTs with the dyes. It was also generalized that purified CNTs (with less iron contamination) were less toxic than unpurified. Still the *in vitro* / *in vivo* toxicity of SWCNTs and MWCNTs is a reasonably established fact, which needs consideration for any biological application of CNTs.⁴²

1.2.5 Super-paramagnetic iron oxide nanoparticles (SPIONs)

SPIONs are superparamagnetic nanoparticles composed of a core (~ 5-20 nm diameter) of Fe₃O₄ or YFe₂O₃ coated with any organic or inorganic molecules, usually polymers, for preventing their oxidation and aggregation. Superparamagnetism arises due a quantum size effect. The bulkmaterial's ferromagnetic properties change to paramagnetism, as the size approaches the nanometre scale. The magnetic properties, therefore, highly depend upon

particles size: for high magnetic susceptibility, the recommended diameter is in the range of 6 to 15 nm.⁴⁴ Suitable coating for preventing oxidation, maintaining consistent magnetic properties, small size and ease of biofunctionalization for targeted delivery are the basic requirements for designing a SPIONs system for biological application.

SPIONs are utilized *in vivo* as contrasting agents for magnetic resonance imaging (MRI) and for localized hyperthermia treatment of cancerous cells or tissues. For MRI, these magnetic nanoparticles are directed to an organ, tissue and tumour. For hyperthermia, the SPIONs are heated in alternating magnetic fields. Other biological applications include protein purification, cell separation, immunoassay and drug delivery.¹¹

Regarding cellular delivery, high transfection efficiency was obtained with magnetic nanoparticles bound antisense oligodesoxynucleotides (ODN) through magneto-transfection procedure. In this approach, the magnetic particle bound cargo was delivered under magnetic field guidance. It was shown that 84% human umbilical vein endothelial cells were transfected within 15 minutes, while nuclear localization of the SPIONs was observed within 2 h. whereas, the same level of transfection efficiency was observed with conventional transfection method, which required a longer exposure time of 24 h and that long exposure time caused cytotoxicity.⁴⁵

In another study, the localization of uncoated SPIONs and PEG-coated SPIONs was found to be vesicular, while lactoferrin or ceruloplasmin functionalized SPIONs were shown to remain attached to the surface of the plasma membrane. It was concluded that the cellular delivery and localization of biofunctionalized SPIONs was strongly dependent on the type of functional ligands present on the SPION surface.⁴⁶ The intracellular fate of positively charged and negatively charged SPIONs has been compared by Mahmoudi *et al.* They conclude that positively charged SPIONs were able to reach the nucleus and mitochondria, while negatively charged SPIONs got attached to the outer membrane of the HeLa cells. However, the provided evidence (TEM images reproduced in figure 1.1, B & D) does not support the claims, as no nuclear or mitochondrial localization can be seen; instead, the localization appears to be endosomal and lysosomal.⁴⁷ Overall, the intracellular localization scenario for SPIONs is similar to the other nanomaterials discussed in this chapter.

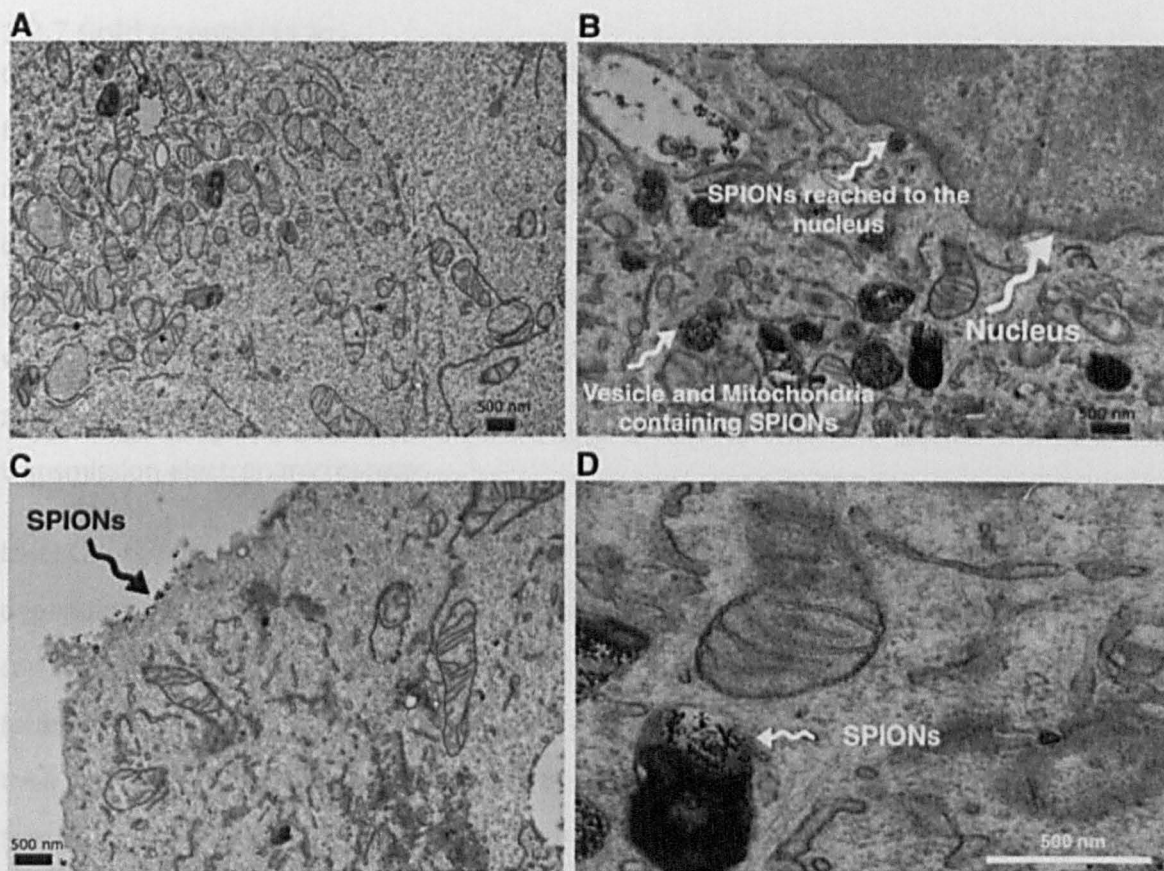


Fig 1.1 Intracellular fate of positively charged and negatively charged SPIONs.

TEM images of HeLa cells; (A) control (B, D) positively charged SPIONs, (C) negatively charged SPIONs. The figure was adapted with permission and the arrow signs and inset picture annotations are adapted as such from the original figure (Mahmoudi, Sant *et al.* 2011).

1.2.6 Silver nanoparticles

Silver nanoparticles, like gold nanoparticles show distinct size- and shape-dependent optical properties. They can be synthesized using sodium borohydride or citrate reduction methods.⁴⁸ Sharma *et al.* have reviewed different synthesis methods and antimicrobial properties of silver nanoparticles. Although the exact mechanism causing antimicrobial activity is still not understood, silver nanoparticle coatings have been in use on various textiles and on certain medical implants.^{7, 49}

To the best of our knowledge, there is no study, which has used silver nanoparticles for delivery purposes. Indeed, they should not be a material of 'choice' for cellular delivery due to their toxicity, characterized by inducing apoptosis in different mammalian cell lines.^{50, 51} Lee *et al.* have observed the concentration dependent cytotoxicity trend of silver nanoparticles along with nanoparticles of aluminium and of cadmium. Silver nanoparticles were found to be more toxic than the other nanoparticles in this particular study.⁵¹

1.2.7 Gold nanoparticles

Gold nanoparticles are popular nanomaterials due to the ease of synthesis and functionalization.⁵² Biomolecules can easily be attached to the surface of gold nanoparticles using thiol, phosphine or amine bioconjugation strategies.⁵³⁻⁵⁵ Molecular self-assembly of biomolecules on the nanomaterials is a common approach to introduce required functionality to the surface of the nanomaterials.^{56, 57} Gold nanoparticles are compatible with many imaging and detection techniques like, photothermal microscopy, absorption spectroscopy, fluorescence spectroscopy, Raman spectroscopy, electrochemistry, and transmission electron microscopy.

Like Qdots, the gold nanoparticles exhibit different colours in the visible spectrum depending upon their size. Contrarily to Qdots, the particles are not fluorescent, but they can be detected optically thanks to their strong scattering (dark field) or absorbance (photothermal) cross-sections. The size- and shape-dependent optical properties are due to their surface plasmon resonance (SPR). The surface plasmon resonance can be defined as the collective oscillation of conduction-band electrons stimulated by an electromagnetic field (incident light).

The electric field of an incoming light wave induces an oscillation and consequently polarization of the electrons with respect to the much heavier ionic core of a spherical nanoparticle. A net charge difference is only felt at the nanoparticle surface. This creates a dipolar oscillation of all the electrons with the same phase. When the frequency of the electromagnetic field becomes resonant with the coherent electron motion, a strong absorption in the spectrum is seen, which constitutes the origin of the observed colour.

The frequency and width of the surface plasmon absorption band depend on the size and shape of the metal nanoparticle, as well as on the dielectric constant of the metal itself and of the medium surrounding it. As the shape or size of the nanoparticle changes or the surface geometry changes, it causes a shift in the electric field density on the surface. This causes a change in the oscillation frequency of the electrons, generating different cross-sections for the optical properties including absorption and scattering. This is why the optical properties of gold nanoparticles depend upon their shape and size.

Gold nanorods are advantageous for deep tissue imaging because of their two plasmonic emissions in the visible and in infra-red spectroscopic regions.⁵⁸ Gold nanorods were found non-toxic, but the detergents, *e.g.*, cetyltrimethylammonium bromide (CTAB) involved in the synthesis of the gold nanorods are the main cause of potential toxic effects as they remain present in the surrounding medium of gold nanorods. The CTAB-associated toxicity was reduced by PEG coating of gold nanorods and by removal of excess of CTAB in surrounding medium.⁵⁹ However, detergents such as CTAB are important for the synthesis of nanorods rather than spheroids. Thus, it is difficult to replace the detergent except after synthesis in a ligand exchange reaction.

Gold nanoparticles are biocompatible and exhibit no cytotoxicity compared to Qdots, silver nanoparticles and SPIONs. In few studies, the cytotoxicity of gold nanoparticles was found associated with the ligands coating present on their surface and the overall charge.⁶⁰⁻⁶² The use of gold conjugates as labels for electron microscopy is well established over several decades.⁶³ Gold nanoparticles can quench the fluorescence of a fluorescent dye molecules present in close vicinity.⁶⁴ This property, along with size-dependent optical properties, has been utilized for delivery and diagnostics of nucleic acid.^{65, 66} Pissuwan *et al.* have reviewed the use of gold nanoparticles for cellular delivery of pharmaceutical products ranging from antibodies, vaccines, antibiotics, oligonucleotides, peptides and cancer drugs. The controlled release of drugs conjugated with gold nanoparticles, in the presence of an external (light) or internal stimuli (pH) constitute innovative applications of gold nanoparticles.⁶⁷ Seferos *et al.* have found that the DNA conjugated gold nanoparticles (DNA-AuNP) showed more stability toward enzymatic degradation compared to molecular DNA under conditions where the concentrations of electrolytes affect enzymatic activity. It was concluded that the local sodium ion (Na^+) concentration is the factor that causes enhancement in DNA stability.⁶⁸

An amphipathic proline-rich peptide sweet arrow peptide (SAP) was conjugated with gold nanoparticles via cysteine for intracellular delivery. All the techniques applied to see the intracellular localization of CPP conjugated gold nanoparticles showed endosomal uptake.⁶⁹ No cellular uptake of uncapped citrate stabilized gold nanoparticles was documented, which is rather surprising, since such nanoparticles would be expected to bind biomolecules (via thiol and amines) in the cell culture medium and on the cell surface. This would be expected

to result in cellular uptake. Indeed, a previous study demonstrated the cellular uptake of uncapped citrate stabilized gold nanoparticles.⁷⁰

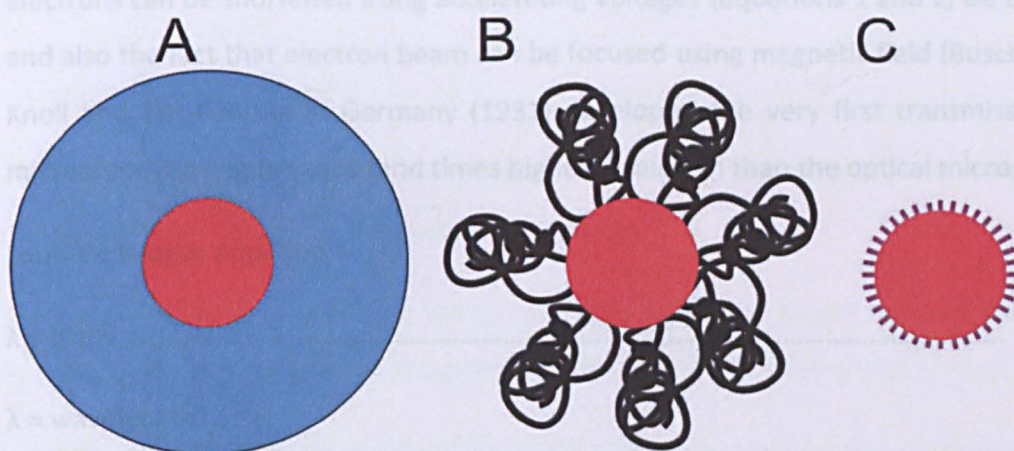
Apart from a few individual studies, which showed some extent of cytosolic or nuclear targeting,^{71, 72} vesicular entrapment and the subsequent enzymatic degradation of gold nanoparticles conjugated biomolecules is recognized as the common barrier for reaching the cellular machinery, by a wide science community.^{3, 66, 67, 73, 74}

1.3 Ligand Shells

Ligand shells are charged or uncharged molecules or ions present on nanoparticles surfaces. The function of these ligand shells is to provide necessary colloidal stability to gold nanoparticles to prevent their fusion and aggregation.⁷⁵ For citrate stabilized gold nanoparticles, the citrate itself acts as a stabilizing shell, but the stabilizing capacity of citrate is limited; it is insufficient in solutions containing electrolytes and/or biological molecules. Moreover, citrate doesn't provide the gold core with any functionality necessary for biological application, e.g., targeting and delivery. So, hundreds of successful attempts have been done so far to replace the weakly bound citrate ligand shell with suitable biofunctional ligand shells, e.g., peptides, polymers, oligonucleotides and proteins using a ligand exchange reaction. The success of ligand shell exchange reaction owes a lot to the affinity of thiols for gold. Thus, ligands with one or more thiols can effectively anchor onto the gold and replace the citrate. The desirable properties for ligand shells that will enable nanoparticles to operate in a biological environment are water solubility, high affinity for gold, a small size and an ability to form a compact monolayer. In addition, it is desirable that the ligand shell has controlled or low non-specific interactions, a high stability *in vitro*/ *in vivo* and some sort of active functionality. The issue of non specific binding as a parameter of stability of nanoparticles has recently been highlighted in a review on ligand shells for quantum dots.⁷⁶ The encapsulation strategy and the core of polymers impart a substantial increase in nanoparticle hydrodynamic diameter, thus they do not meet the above criteria. In contrast, self assembly of shell of small ligands result only a small increase in nanoparticle size.

In a recent review, Thanh *et al.* have listed different types of ligand shells used for capping gold nanoparticles. Among these, EG terminated alkane thiols (commonly termed thiolated-

PEG, though they typically have 2-6 EG units and so are EG oligomers) has been identified as good ligands, which fulfils all the basic properties listed above for a good ligand shell, however, they are not so versatile. Thiolated-PEG and peptidols have been demonstrated to impart the highest stability and the most comprehensive opportunities for functionalization.^{77, 78} Interestingly, peptides with terminal EG units are not the best ligands, thus various mix monolayers of thiolated-PEG and any other suitable targeting bio-ligand are often used for capping gold nanoparticle.⁷⁸



Scheme 1.1 Different strategies and ligand shells for capping gold nanoparticles. A) Encapsulation of gold nanoparticle in silica shell B) polymer-capped gold nanoparticle C) small ligand self-assembled monolayer-capped gold nanoparticle.

Most of the Ligand shells can be lost easily in physiological environment, e.g., in cellular matrix around the cells or inside the cells, either due to ligand shell exchange reaction or due to proteolysis. Chemical modification of ligand shell, either due to ligand exchange reaction or due to proteolysis, leads to a loss of integrity and result in a different material from that introduced into the biological system, which is likely to have new and unpredictable properties and functionality.

1.4 Techniques for the detection of gold nanoparticles

There are several techniques available to detect gold nanoparticles. These techniques include dark-field light-scattering imaging, surface enhanced Raman spectroscopy (SERS), photothermal imaging and electron microscopy. We have used photothermal microscopy

and electron microscopy for imaging and detection of gold nanoparticles. These two techniques are described in more detail below.

1.4.1 Transmission electron microscopy

Transmission electron microscopy (TEM or EM) is a transmission based technique, which allows the imaging of thin pieces of metals, cells and tissues at high resolution. In 1930, after reaching the theoretical limits of the resolution (at that time) for optical imaging, there was a need for an elaborated imaging technique in order to observe the more fine details of physical structures. With the development of understanding that the wavelength of electrons can be shortened using accelerating voltages (equations 1 and 2, De Broglie 1924) and also the fact that electron beam can be focused using magnetic field (Busch 1926), Max Knoll and Ernst Ruska in Germany (1931) developed the very first transmission electron microscope, having ten thousand times higher resolution than the optical microscope.

Louis De Broglie equation

$$\lambda = h/mv \dots \dots \dots \text{equation 1}$$

λ = wavelength

h = Planck's constant

m = mass of the electron

v = velocity of the electron

As mv depends on the accelerating voltage \sqrt{V}

$$\lambda = \sqrt{1.5/V} \text{ nm} \dots \dots \dots \text{equation 2}$$

1.4.1.1 Resolution

The maximum theoretical resolving power of a microscope is about half the wavelength of the illuminating light. What we can see with a light microscope is limited by the wavelength of light (ranges between 400-700 nm for visible light). So the best resolution, which can be achieved with the light microscope is $\geq 0.2 \mu\text{m}$. The transmission electron microscope (TEM) operates on the same basic principles as the light microscope, but uses electrons instead of light. Their much lower wavelength (ranges between 0.006-0.0039 nm at 120 kV) makes it possible theoretically to get a resolution a hundred thousand times (0.002 nm) better than

with a light microscope. This high resolution, however, is not possible to achieve due to practical constraints, which include, difficulty to align parts of the machine perfectly, instability in high voltage and lens circuit, lens aberrations, image artefacts and diffraction effects.

The relationship of different optical variables, which affects the theoretical resolving power of the microscope, is defined by following equation:

$$r = 0.61\lambda/n \sin \alpha \dots\dots\dots \text{equation 3}$$

Where

r = resolution of microscope

λ = wavelength of illumination (electrons at 200 kV have the $\lambda \sim 0.0025$ nm). Wavelength is inversely proportional to the velocity of electrons.

α = aperture angle of the lens, which refers to half angle of the illumination a lens can accept. A lens with wide α will accept more information from the object viewed.

n = refractive index, which is a measure of the optical density of medium (refractive index of vacuum ~ 1)

To get the widest possible acceptance angle, the lens focal length must be as short as possible. Generally, by decreasing the focal length, the magnification is increased and *vice versa*. Unlike the glass lenses of an optical microscope, it is possible to change the focal length of an electromagnetic lens by changing the amount of DC current running through the coil of wire and also by changing the accelerating voltage. This allows focusing the image and changing the magnification at the same time.

The dependence and relation of the focal length of the electromagnetic lens on voltage and current is defined by follows equation

$$f = K (V/I^2) \dots\dots\dots \text{equation 4}$$

Where

f = focal length of the lens

K = constant

V = voltage

I = current

The description given in this section (section 1.4.1) about transmission electron microscopy is adapted and modified from books by Weakley, B.S. and Agar, A. W. *et al.*^{79, 80}

1.4.1.2 Working principle

A light source, at the top of the microscope emits the electrons. This light source is usually a filament made up of lanthanum hexaboride (LaB_6) or tungsten (W). The emitted electrons from the filament, travel through vacuum in the column of the microscope and are directed toward the sample under high accelerating voltage (100-120 kV). These electrons are focused into a thin beam by electromagnetic lenses. The highly focused and monochromatic electron beam, then passes through a thin sample (<100 nm). Depending on the density of the sample, some of the electrons are scattered and disappear from the beam. At the bottom of the microscope the unscattered or transmitted electrons hit a fluorescent screen, which gives rise to a "shadow image" of the sample with its different parts displayed in varied contrast according to their density. The image can be studied directly by the operator and also can be captured by a camera (adapted and elaborated from link-www.nobelprize.org/educational/physics/microscopes/tem/index.html).

There are three different types of motions of electrons in TEM, which affect the image quality. These are unscattered or transmitted electrons, elastically scattered electrons and inelastically scattered electrons. The unscattered or transmitted electrons pass through the specimen straight forward without interacting with the specimen. The transmission of unscattered electrons, through the specimen, is inversely proportional to the specimen thickness. Thick areas will appear dark due to fewer transmitted electrons and thinner areas will appear lighter due to more transmitted electrons through. The elastically scattered electrons result from interaction with the atoms of the specimen in elastic fashion (no loss of energy) and they transmit through the remaining portions of the specimen. The inelastically scattered electrons (losing energy) transmit through the rest of the specimen. The quality or contrast of an image depends on the illumination conditions and the selection of transmitted electrons, *e.g.*, unscattered, elastically scattered or highly scattered.⁸¹

1.4.1.3 Significance

In spite of the difficult and time-consuming specimen processing for TEM imaging, there is no other technique, which can replace the electron microscopy because according to Eskelinen *et al.* "It is still indispensable and needed to directly look at the details of ultra small structures and also act as an ultimate source of information for confirming and verifying results obtained by other methods".⁸² In this PhD, it has been an important tool for imaging gold nanoparticles inside cells. The two limitations of this technique are 1) only a small number of cells can be studied and 2) live cell imaging is not possible. The cells need to be fixed and processed by dehydration, stained with heavy metals for contrast and embedded in plastic, so that they can be cut into thin sections for imaging.

1.4.2 Photothermal microscopy

Unlike TEM, photothermal microscopy can operate on live cells, as it is non-disruptive. Photothermal microscopy allows the imaging of various nano-objects based on their absorption cross-section. It can detect gold nanoparticles of a few nanometres. The absorption cross-section of nanoparticles varies with the diameter of the absorbing nano-object in a slower manner than the scattering cross-section (as d^3 instead of d^6) and, therefore, absorption-based microscopy becomes more sensitive than dark field for small nanoparticles. For gold nanoparticles excited with a wavelength of 523 nm in water, the absorption is thus, typically dominating over the scattering for diameters below 40 nm.⁸³⁻⁸⁵

The instrument used in this PhD is described in details in the thesis of Yann Cesbron, a member of the group who has set-up this microscope in Liverpool.⁸⁶ Briefly, a green laser (523 nm) is used to warm up any nanoparticle, which is present in the focal beam, and a red laser (633 nm) allows detection of the change of temperature. More precisely, the green laser is modulated in time, *i.e.*, turned on/off, at a frequency of ~500 000 times per second. If a nanoparticle is present in this modulated green laser beam, there will be a pattern of change of temperature and, therefore, of refractive index. The red laser detects this change of refractive index. A lock-in detection is used to extract the signal at the modulation frequency. A piezoelectric device is used for scanning. The signal is then sent to a computer to build the image.

1.5 Research problem: vesicular entrapment of nanoparticles

1.5.1 Sequestration of nanoparticles

Among the biological applications of nanomaterials, targeted cellular delivery of drugs and other therapeutic agents, *e.g.*, antisense oligonucleotides, is getting more and more attention from the medical and biosciences community. After realizing the potential applications of nanotechnology in general pharmaceuticals and in cancer research, the investment has increased in this field. Scientists are looking forward for a new generation of nanomedicine and nanodevices, which will somehow improve or replace conventional treatments. Some nanomedicines and nanodevices are already approved by health authorities, in different parts of the world, as treatment and drug delivery.⁸⁷ Still there are issues related to the efficiency of these nanovectors for targeted release of the cargo, once entered into the biological system. Among these issues, one is endocytic uptake of nanomaterials. This is a major limitation for applications of nanomaterials in drug delivery, as well as for intracellular biomolecular imaging and sensing.

Following the first contact of a delivery vector/foreign material with the cells, one of the main cell mechanisms, which come into action, is endocytosis. Endocytosis is the natural cellular uptake mechanism for many materials from endogenous molecules, *e.g.*, receptor ligands to pathogens (bacteria, viruses) to water and nutrients. After the material has been taken up by endosomes, it progresses in the endocytic pathway to another type of intracellular vesicles called the lysosome where enzyme-mediated degradation occurs. The degraded or processed material is either used by the cell as substrates for cellular biosynthesis or exocytosed, *i.e.*, recycled out of the cell. Nanovectors carrying therapeutic contents meet the same fate of vesicular entrapment, which leads to degradation due to the enzymes present in lysosomes thus, making the delivery process ineffective. Different types of nanoparticles discussed in section 1.2 of this chapter showed little or no cytosolic delivery, because of the endosomal entrapment. This observation is valid for gold nanoparticles as well.^{71, 74, 88} The scenario for cellular localization of gold nanoparticles conjugated or carried by additional carriers, is not different either. For example Chithrani *et al.* found that although liposomes increased the gold nanoparticles (1.4 nm) delivery into cancer cells by 1,000-fold, the localization of particles was vesicular.⁸⁹

So it is clear that endosomal entrapment of nanocarriers regardless of their size, shape or composition, is a major research problem, which should be addressed in order to utilize the full potential of nanoparticles assisted delivery systems.

Below a brief introduction to the different endocytic cellular uptake mechanisms, is given. As a general observation based on this research work and the literature, we note that nanoparticles utilize almost all types of endocytic uptake mechanisms. The preference for one or other type of mechanism generally depends upon the size, charge and surface chemistry of nanoparticles.

1.5.2 Review of endocytic mechanisms

The types of endocytosis (Fig. 1.2) are categorized according to the particular molecular mechanisms involved; they are differentially triggered by the particular properties of foreign materials, the cell type and physiological conditions. During the course of this work, we have observed particular endocytic mechanisms involved in the uptake of different types of nanoparticles and nanoparticle assemblies. In this section, the mechanisms for phagocytosis, clathrin-mediated endocytosis, caveolae-mediated endocytosis, clathrin- or caveolae-independent endocytosis and macropinocytosis, are briefly described and illustrated with exemplary electron microscopy pictures from the literature or our own investigations.

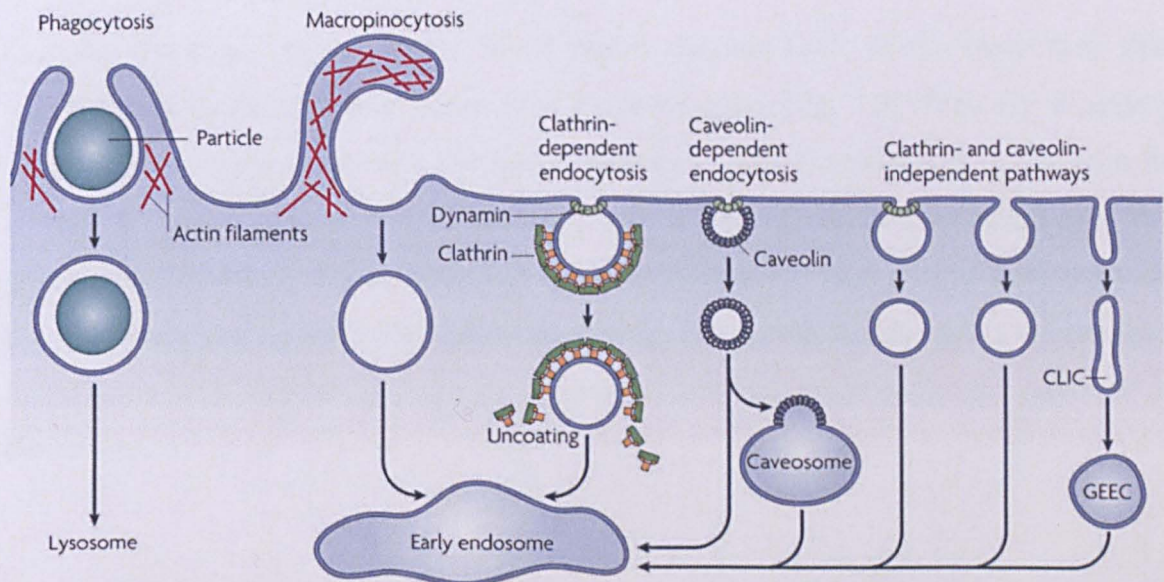


Fig. 1.2 Different natural strategies for intracellular uptake (endocytosis)
Figure adapted with permission from Mayor *et al.*⁹⁰

1.5.2.1 Clathrin-mediated endocytosis

Clathrin-mediated endocytosis is a type of receptors-mediated endocytosis (RME). The receptor-bound ligands enter the cell by the formation of clathrin-coated vesicles (CCVs). The functional unit of CCVs is a triskelion and the functional unit of the triskelion is a protein called clathrin. The triskelions self-assemble into cages called clathrin-coated vesicles, in the presence of dynamin, which helps the vesicle to pinch off from the coated pit.

After the binding of a ligand to plasma membrane receptors, a signal is transduced through the membrane, leading to membrane coating, and formation of a membrane invagination. The receptor, its ligand, and anything in close proximity, are then internalised in clathrin-coated vesicles (Fig. 1.2). Once internalised, the clathrin-coated vesicle uncoats, a prerequisite for the vesicle to fuse with other membranes, and individual vesicles fuse to form the early endosome. Since the receptor is internalized with the ligand, the system is saturable and uptake will decline until receptors are recycled to the surface. We observed many clathrin-coated vesicles (example in figure 1.3), which often did not contain any nanoparticles.

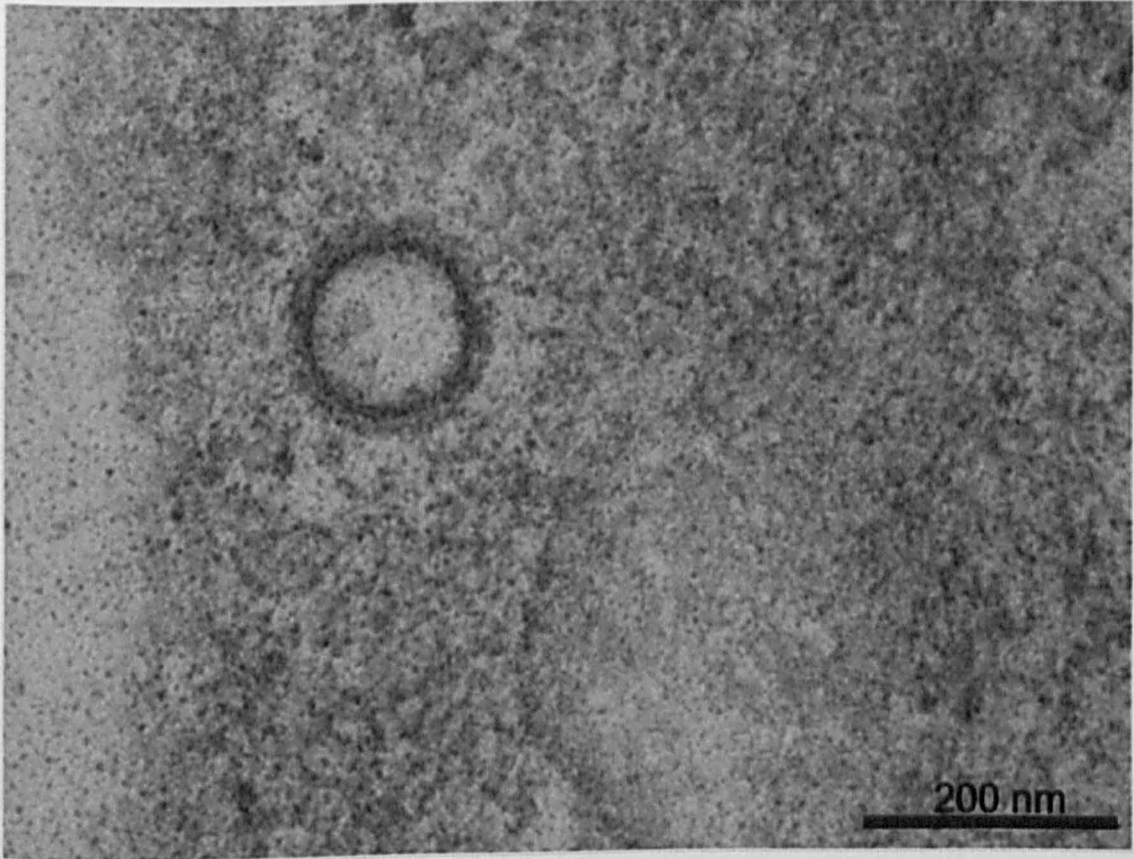


Fig.1.3 A clathrin-coated vesicle

HeLa cells are fixed after 6 h incubation with CALNN-capped gold nanoparticles (no gold nanoparticle visible in this image)

1.5.2.2 Lipid raft/ caveolae mediated endocytosis

Caveolae are small (approximately 50–60 nm in diameter) pits in the membrane that resemble the shape of a cave hence their name caveolae (Fig. 1.4). They are especially abundant in smooth muscle cells, fibroblasts, adipocytes, and endothelial cells. They consist of the cholesterol-binding protein caveolin, with a bilayer enriched in cholesterol and glycolipids. Dynamin protein is required for pinching off these flask shaped caveolae from the cell membrane for further endocytic trafficking. The protein family cavin1-4 have been found complexed together with caveolin and affect the size, morphology and curvature of the structures.⁹¹

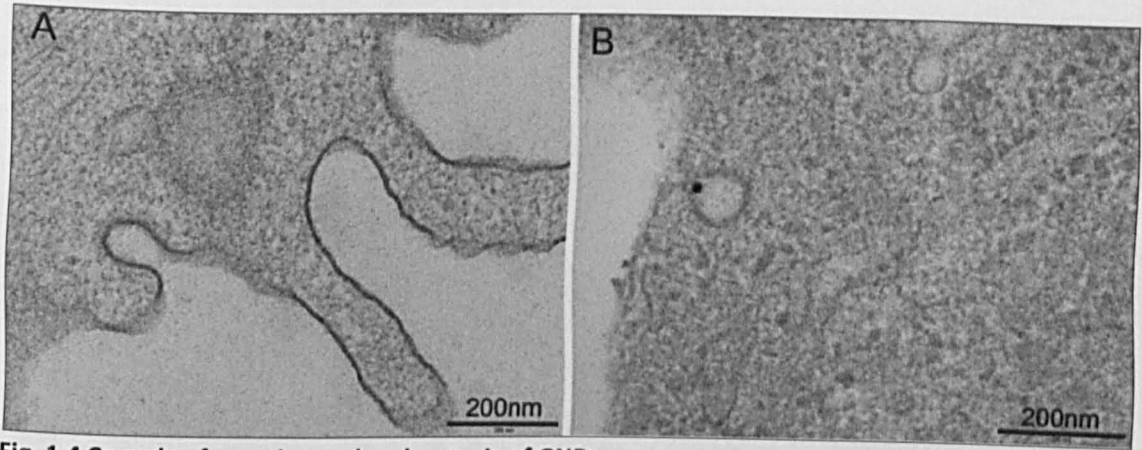


Fig. 1.4 Caveolae formation and endocytosis of GNPs

A) Caveolae formation, B) Cellular uptake of oligonucleotide functionalized gold nanoparticles 10 nm by HeLa cells.

1.5.2.3 Macropinocytosis

Macropinocytosis occurs from highly ruffled regions of the plasma membrane. The rims of membrane folds to form a pocket (Fig. 1.5, D) by fusing back with the cellular membrane, which then pinches off into the cell to form a large vacuole or vesicle (0.5-5 μm in diameter) filled with large volume of extracellular fluid and molecules within it. The filling of the vesicle occurs in a non-specific manner. The vesicle then travels into the cytosol and fuses with other vesicles such as endosomes and lysosomes. There is evidence of actin filaments involvement in macropinosome formation.⁹²

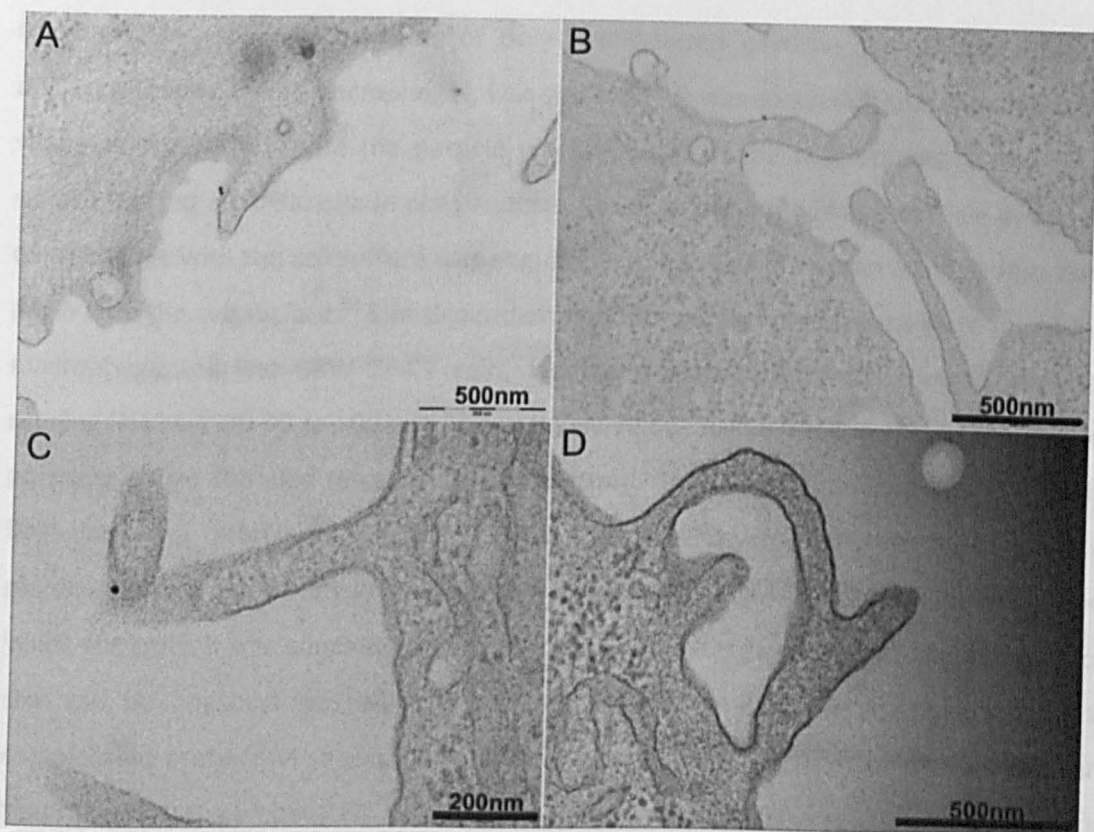


Fig. 1.5 Macropinocytosis

A, B) 5% CALNN-TAT and 95% (both mole/mole) PEG functionalized gold nanoparticles (14 nm) on the surface of HeLa cells after 10 minutes incubation.

1.5.2.4 Phagocytosis

Phagocytosis is regarded as a special type of endocytosis occurring in mammalian cells especially in macrophages, neutrophils and also in some non-professional phagocytes like epithelial and endothelial cells, but at a comparatively lower rate.⁹³ It is the process by which cells bind and internalize particle of around 100 nm- 0.5 μm diameter (Fig. 1.6). In some studies the proposed size range of particle is around 0.75 μm in diameter.⁹² These could be dust particles, cell debris, micro-organisms and even apoptotic cells. Phagocytosis is considered as a defence line against microorganisms.⁹² Uptake is triggered by binding of opsonised particles (opsonization is the adsorption of proteins like immunoglobulins, fibronectin and laminin on the particle) to cell surface receptors capable of transducing a phagocytic stimulus to the cytoplasm. This stimulus results in the polymerization and rearrangement of actin at the site of particle attachment and subsequent pseudopod extension that engulfs the bound particle into a phagosome. Under most circumstances, phagosomes rapidly fuse with endosomes and/or lysosomes exposing their contents to

hydrolytic enzymes. Phagocytosis of polystyrene-based particles (1- 10 μm) of twenty different shapes, by rat macrophages, was studied.⁹⁴ It was concluded that the local particle shape at the point where the particle was attached to the macrophage at the time of uptake, played a crucial role in phagocytosis. For example a rod shape particle at forty five degree angle with the cell surface was engulfed in much less time than a rod at zero degree angle with the cell surface.⁹⁴ Size-dependent endocytic entry mechanisms were found in the macrophage cell line RAW 264.7 cells, incubated with carboxylated polystyrene beads ranging in size from 30 to 500 nm. The particles below 30 nm were in the cytosol, while all particles above this size range were endocytosed. These particles were found to induce DNA-damaging effects.⁹⁵ Hillaireau *et al.* have reviewed the effect of size and physicochemical properties of polymer nanoparticles and liposomes on entry mechanisms inside the cells. It was concluded that particles of diameter from 200 nm to several micron size can be phagocytosed, due to the large surface area presented for opsonin and complement proteins in serum, necessary for phagocytosis. Particles below this size range have presented complicated picture for preferences of different types of endocytic mechanisms depending on the cell type.¹⁸

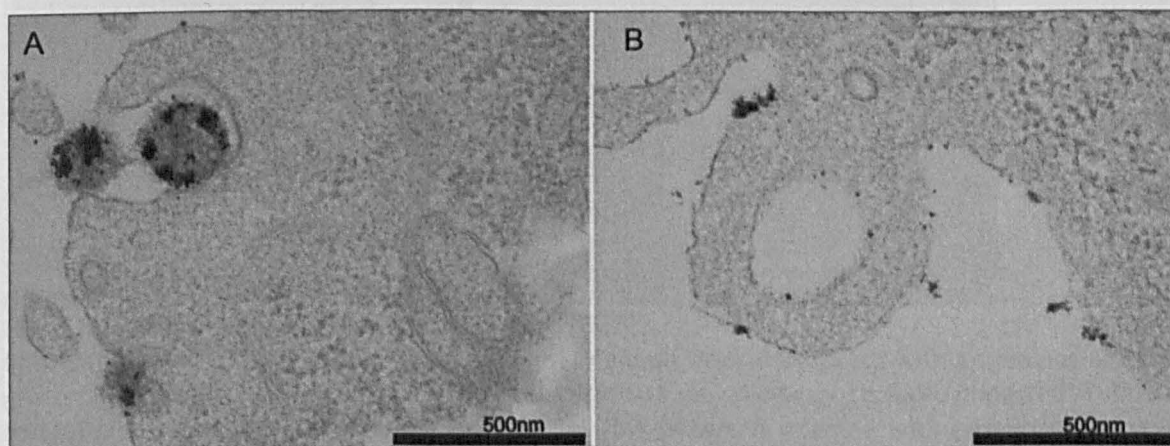


Fig. 1.6 Phagocytosis

A) Phagocytosis of CALNN- capped gold nanoparticles functionalized hydrogels by HeLa cells, B) cup shaped phagosome.

1.5.2.5 Clathrin-independent endocytosis (CLIC/GEEC)

Clathrin-independent endocytic pathways are actually cluster of many different pathways includes, the CLIC/GEEC endocytic pathways, ARF6-dependent endocytosis, flotillin-dependent endocytosis, caveolin1-mediated endocytosis, macropinocytosis and phagocytosis. Some of them have been discussed separately in this chapter. Here CLIC/GEEC

endocytic pathway will be discussed briefly. The cell surface gives rise invaginations with different types of morphologies unlike caveolae or clathrin-coated vesicles. These structures are known as clathrin independent carrier (CLICs) and GPI-AP-enriched early endosomal compartments (GEEC) (GPI-AP stands for glycosylphosphatidylinositol-anchored proteins).^{90, 91} It was found that GRAF1 protein is necessary for CLICs mediated uptake. GRAF1 sculpts the endocytic membranes into 40 nm diameter tubules and vesicles (Fig.1.7). The basic structure of GRAF protein and the mechanism of GRAF-dependent tubular uptake has been discussed in detail by Lundmark *et al.*⁹¹ We did not observe or identify such tubules for any type of the nanoparticles, in the present research.

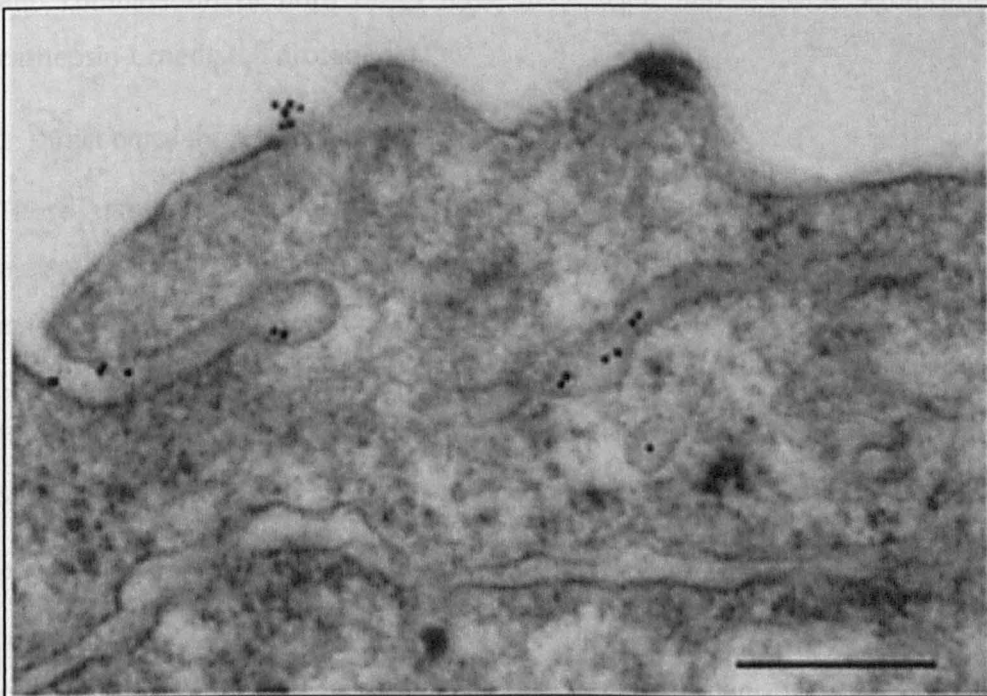


Fig. 1.7) Clathrin-independent endocytosis (CLIC/GEEC)

Chinese hamster ovary cells incubated with gold nanoparticles conjugated with antibodies against green fluorescent protein (GFP). The TEM picture is showing surface-connected tubular invaginations with the gold nanoparticles inside. This picture is adapted with permission from a study by Sabharanjak *et al.*⁹⁶

1.5.3 Transfection methods and their consequences

Generally, intracellular delivery methods can be classified into three categories based on the mechanisms of entry adopted to promote entry inside the cells.

1: Methods based on endosomal breakage

To break the endosome after internalization of the cargo, the approaches either rely on external stimulation, *e.g.*, laser excitation, chemical treatment or, on the natural changes in

the environment during endocytosis such as the pH drop inside the endosomes, for example, pH sensitive liposomes, pH sensitive viral peptides, cationic polymers, fucose and chloroquine, which can cause breakage of the endosomes at low pH due to a proton sponge effect or direct interaction with endosomal membrane.^{3, 23, 97, 98} I have tested the approach of chloroquine-mediated endosomal breakage, in the context of a work on the proteolytic degradation of peptide-capped gold nanoparticles upon cell entry. This particular study identified the cathepsin-L enzyme (an endosomal proteolytic enzyme) responsible for cleaving the peptide capping of endosomally localized gold nanoparticles. As an attempt to prevent intra-endosomal proteolysis, chloroquine, Z-FF-fmk (irreversible cathepsin inhibitor) and combination of both drugs have been used and showed significant reduction of cathepsin-L mediated proteolysis.⁷⁴

2: Direct entry through cell membrane

These methods include toxin assisted delivery and cell penetrating peptide (CPP) assisted delivery. Different naturally occurring CPPs have been identified, which help the cargo to enter the cells either by direct penetration or simply by increasing endocytosis. Direct penetration of CPPs loaded cargo is still a matter of controversy (see Chapter 2 also), however, the increased endocytosis of nucleic acids complexes with CPPs has been shown.^{99, 100}

Pore forming bacterial or plant toxins have been found to show either direct entry of cargo into the cytosol through toxin-induced pores in fixed or alive cells or increase the endocytic uptake of cargos as a consequence of repair mechanisms cells use to reseal their membrane.¹⁰¹⁻¹⁰⁵

3: Physical manipulation of cell membrane using artificial stimulation, to deliver the molecules of interest.

They include microinjection, sonoporation and electroporation/microporation. Microinjection is time consuming, less effective in terms of productivity and demands specialist skills, while with electroporation/microporation, there is always a need for optimization of the electroporation conditions according to the given cell line, cargo type, and time for electroporation for least cytotoxicity.⁴⁰ The critical use of microinjection and sonoporation for cellular delivery of nanoparticles has been reviewed by Lévy *et al.* and a

detailed summary of studies where these techniques have been used for delivering nanoparticles is published by Chou *et al.*^{3, 106} The combined conclusion out of these two reviews, about potential and limitation of these delivery techniques, was not much different from the description given here.

1.6 Addressing the research problem: bio-inspired strategies

As discussed in the previous sections, the vesicular sequestration of nanomaterials is a key issue hampering their development as delivery vectors and imaging agents. While a number of approaches summarized above (section 1.4.3) have been tested, their effectiveness for cytosolic delivery of nanomaterials is still too low for many envisioned applications.

In this work, we used peptide-capped or peptide/PEG-capped gold nanoparticles as model materials to understand the cellular interaction and intracellular fate, with a focus on their targeted cytosolic delivery. We evaluated four approaches belonging to the three main delivery categories. The first approach is inspired from the method used by some bacteria to enter mammalian cells. The second and third approaches are based on viral peptides, which the viruses use either to directly penetrate the cell (TAT) or to escape the endosomal compartment (HA2). The fourth approach builds on protocols developed for DNA transfection with pH sensitive polymers.

In the last part of this introduction, these various cytosolic delivery methods are briefly described.

1.6.1 Viral peptides in SAM of gold nanoparticles for cytosolic delivery

The following two viral peptides have been used in the ligand shells of gold nanoparticles and the intracellular localization of nanoparticles has been investigated by combining photothermal, confocal and electron microscopy study.

1. Haemagglutinin subunit HA2 (HA2) derived from influenza virus
2. Trans-activating transcriptional activator (TAT) derived from HIV-virus.

1.6.1.1 HA2 peptide for endosomal destabilization

Influenza type A viruses have evolved the technique of destabilizing endosomal membrane at low pH to gain access to the cytoplasm of host cell using HA2 peptide, which is present on their surface.¹⁰⁷

Haemagglutinin HA2 is a well-characterised, highly conserved 20-23 residue containing peptide derived from a viral protein, haemagglutinin complex glycoprotein HAO.^{108,109}

On entering the cell by endocytosis, the low pH in the endosome triggers conformational changes,¹¹⁰ causing the fusogenic HA2 peptide to get inserted into the unit membrane of the endosome. This results in the destabilization of the membrane, which in turn causes the release of endosomal contents into the cytoplasm. In the literature, there are not as many research studies of the application of HA2 peptide for cytosolic delivery^{72, 111} as available about HA2 structure, its interactions with membranes and conformational changes at low pH.^{110,112}

Synthetic wild type HA2 peptide having 23 amino acid (GLFGAIAGFIENGWEGMIDGWYG) or 20 amino acid (GLFGAIAGFIENGWEGMIDG)¹¹³ and its analogues, have been used *in vitro* to see the fusion activity successfully.¹¹⁴ HA2 peptide has also been used for cytosolic delivery of protein.¹¹¹ We used different types of HA2 peptides along with CALNN peptide and PEG for coating gold nanoparticles and did TEM and photothermal imaging based investigations for finding out their intracellular localization. The detailed discussion about the potential of HA2-functionalized gold nanoparticles for cytosolic delivery is presented in chapter 2.

1.6.1.2 Cell penetrating peptides: trans-activating transcriptional activator (TAT)

CPPs are natural or synthetic analogue peptides, which facilitate or simply increase the cellular uptake of different molecular cargos, *e.g.*, nucleic acids, plasmids and proteins. CPPs alone or in combination of nuclear localized signal peptides (NLS) and PEG, have been used in several research attempts in order to get cytosolic delivery of cargos. TAT peptide is derived from human immunodeficiency virus (HIV-1) and was the first type of CPP discovered in 1988. TAT peptide derived from a 86-101 residue containing protein also called TAT enhances the transcriptional efficiency of HIV-virus. TAT protein released out of infected cells can also act as killing toxin for surrounding healthy cell by inducing apoptosis. Berry *et al.* have claimed the nuclear localization of 5 nm sized gold nanoparticles functionalized with TAT and PEG, however, the claim was supported by quite unclear and confusing TEM images. It was also concluded that 15 nm sized gold nanoparticles functionalized with same SAM were not able to enter the nucleus due to nuclear pore size restriction.¹¹⁵ While in another study 20 nm sized gold nanoparticles functionalized with bovine serum albumin (BSA) linked peptides (4 different nuclear localized signal (NLS)

peptides), were claimed to enter the nucleus. The imaging technique used was video-enhanced colour differential interference contrast microscopy. Interestingly some images of the cells, which have been shown nuclear localization of the gold nanoparticles appeared to be dying cells.⁶¹

Using the FITC-TAT fused HA2 peptide, Wadia *et al.* have showed the increased expression of green fluorescent protein (EGFP).⁷² Kumar *et al.* have showed targeted cytosolic localization of 20 nm gold nanoparticles With TAT fused HA2 peptide containing gold nanoparticles, which were also functionalized with actin antibodies and PEG.³⁷ Sugita *et al.* have used the TAT-fused HA2 peptide for cytosolic delivery of FITC-TAT conjugated with shepherdin, an anti cancer drug. It was showed that killing activity of the cancer drug was increased, which according to the author was due to the cytosolic localization of FITC-TAT conjugated shepherdin in the presence of TAT-fused HA2. All these studies proposed the role of TAT-fused HA2 peptide, for enhancing the cytosolic delivery of biomolecules of interest. These studies are discussed critically in chapter 2.

The mode of entrance of CPPs inside the cells by direct translocation through the plasma membrane is a controversial research debate.^{116, 117} However, most studies (including our results) showed macropinocytosis as the main entry mechanism utilized by CPP.^{39, 72}

Krpetic *et al.* have reported that TAT and PEG capped gold nanoparticles leaked out of the vesicles and were then again trapped by the vesicles. However, the mechanism responsible for such behaviour was not defined.⁷¹ We have tried to probe the results described by Krpetic *et al.* and Sugita *et al.*¹¹⁸ and found some interesting results, which will be discussed in chapter 2.

1.6.2 Toxin assisted gold nanoparticles delivery

Streptolysin O (SLO) is a bacterial toxin, which is secreted by bacteria to form pores in the host cell membrane, thus, allowing access to the cytoplasm of the cell. Naturally, this toxin is produced by the bacteria streptococci. Commercially, it can either be extracted from supernatant of streptococci or can be produced by E coli as a recombinant product. It is water-soluble and binds to cholesterol-containing target membranes. The mechanism of pore formation is described in detail in chapter 3. Since the discovery that SLO can reversibly permeabilise the plasma membrane, it has been used successfully to deliver many types of

biomolecules, *e.g.*, antibodies, proteins, oligonucleotides and Si RNA into the cytoplasm of different cell lines^{119, 120} Reversible permeabilisation mainly depends on SLO dose or amount.

To the best of our knowledge, there is no report yet of using this toxin for bioconjugated gold nanoparticles delivery into the cells. Our objective was to achieve direct delivery of gold nanoparticles to the cytosol through the pores, thus avoiding endosomal entrapment. We obtained results indicating that SLO helps to increase the intracellular delivery of PEGylated gold nanoparticles. We assessed the different parameters, *e.g.*, concentration of gold NPs and surface chemistry of gold NPs, which could play a role or affect this enhanced intracellular delivery. This work is presented in chapter 3.

1.6.3 Hydrogel

Polymer nano carriers are the earliest type of nanomaterials, along with liposomes, tailored for the intracellular delivery of drugs. Biodegradable polymer nanoparticles (PACA and PLGA) were presented as favourable delivery vectors due to the efficient release of cargo from lysosomal vesicles.¹⁸ A comparative study of negatively and positively charged polymer nanoparticles of size range between 89-96 nm showed more uptake of positively charged particles by HeLa cells.¹²¹ Bayles *et al.* have used cationic polymeric nanoparticles, named as hydrogels of 160–200 nm size for endosomal disruption.²³ The cationic surface of these particles should act like a proton sponge at low pH, thus causing volume expansion of hydrogel, which in turn destabilizes the endosomes. These hydrogel nanoparticles were shown not only to break the vesicles, but were also capable to deliver the cargo (quantum dots) attached onto their surface. We have used peptide CALNN or CALNN and PEG-capped gold nanoparticles for functionalizing these hydrogels, received from Brett A Helm's group (NLBL, Berkely, USA) as a gift. The detailed results and discussion is given in chapter 4.

1.7 Bibliography

1. Sahoo, S.K. & Labhasetwar, V. Nanotech approaches to delivery and imaging drug. *Drug Discovery Today* **8**, 1112-1120 (2003).
2. Klostranec, J.M. & Chan, W.C.W. Quantum dots in biological and biomedical research: Recent progress and present challenges. *Advanced Materials* **18**, 1953-1964 (2006).
3. Lévy, R., Shaheen, U., Cesbron, Y. & Sée, V. Gold nanoparticles delivery in mammalian live cells: a critical review (2010).
4. Lewinski, N., Colvin, V. & Drezek, R. Cytotoxicity of nanoparticles. *Small* **4**, 26-49 (2008).
5. Park, S.J., Taton, T.A. & Mirkin, C.A. Array-based electrical detection of DNA with nanoparticle probes. *Science* **295**, 1503-1506 (2002).
6. Sandhu, K.K., McIntosh, C.M., Simard, J.M., Smith, S.W. & Rotello, V.M. Gold Nanoparticle-Mediated Transfection of Mammalian Cells. *Bioconjugate Chemistry* **13**, 3-6 (2001).
7. Chen, X. & Schluesener, H.J. Nanosilver: A nanoparticle in medical application. *Toxicology Letters* **176**, 1-12 (2008).
8. De Jong, W.H. & Borm, P.J.A. Drug delivery and nanoparticles: Applications and hazards. *International Journal of Nanomedicine* **3**, 133-149 (2008).
9. Drummond, D.C., Zignani, M. & Leroux, J.-C. Current status of pH-sensitive liposomes in drug delivery. *Progress in Lipid Research* **39**, 409-460 (2000).
10. Service, R.F. Nanoparticle Trojan Horses Gallop From the Lab Into the Clinic. *Science* **330**, 314-315 (2010).
11. Gupta, A.K. & Gupta, M. Synthesis and surface engineering of iron oxide nanoparticles for biomedical applications. *Biomaterials* **26**, 3995-4021 (2005).
12. Bianco, A., Kostarelos, K., Partidos, C.D. & Prato, M. Biomedical applications of functionalised carbon nanotubes. *Chemical Communications*, 571-577 (2005).
13. Shukla, R. et al. Biocompatibility of gold nanoparticles and their endocytotic fate inside the cellular compartment: A microscopic overview. *Langmuir* **21**, 10644-10654 (2005).
14. Elghanian, R., Storhoff, J.J., Mucic, R.C., Letsinger, R.L. & Mirkin, C.A. Selective colorimetric detection of polynucleotides based on the distance-dependent optical properties of gold nanoparticles. *Science* **277**, 1078-1081 (1997).
15. Rosi, N.L. & Mirkin, C.A. Nanostructures in biodiagnostics. *Chemical Reviews* **105**, 1547-1562 (2005).
16. Jain, P.K., Lee, K.S., El-Sayed, I.H. & El-Sayed, M.A. Calculated absorption and scattering properties of gold nanoparticles of different size, shape, and composition: Applications in biological imaging and biomedicine. *Journal of Physical Chemistry B* **110**, 7238-7248 (2006).
17. Zrazhevskiy, P., Sena, M. & Gao, X. Designing multifunctional quantum dots for bioimaging, detection, and drug delivery. *Chemical Society Reviews* **39**, 4326-4354 (2010).
18. Hillaireau, H. & Couvreur, P. Nanocarriers' entry into the cell: relevance to drug delivery. *Cellular and Molecular Life Sciences* **66**, 2873-2896 (2009).

19. Duncan, R. The dawning era of polymer therapeutics. *Nat Rev Drug Discov* **2**, 347-360 (2003).
20. Seymour, L.W., Duncan, R., Strohalm, J. & Kopecek, J. Effect of molecular-weight (MBARW) of n-(2-hydroxypropyl)methacrylamide copolymers on body distribution and rate of excretion after subcutaneous, intraperitoneal, and intravenous administration to rats. *Journal of Biomedical Materials Research* **21**, 1341-1358 (1987).
21. Won, Y.-W., Lim, K.S. & Kim, Y.-H. Intracellular organelle-targeted non-viral gene delivery systems. *Journal of Controlled Release* **152**, 99-109 (2011).
22. Ganta, S., Devalapally, H., Shahiwala, A. & Amiji, M. A review of stimuli-responsive nanocarriers for drug and gene delivery. *Journal of Controlled Release* **126**, 187-204 (2008).
23. Bayles, A.R. et al. Rapid Cytosolic Delivery of Luminescent Nanocrystals in Live Cells with Endosome-Disrupting Polymer Colloids. *Nano Letters* **10**, 4086-4092 (2010).
24. Lasic, D.D., Frederik, P.M., Stuart, M.C.A., Barenholz, Y. & McIntosh, T.J. Gelation of liposome interior A novel method for drug encapsulation. *FEBS Letters* **312**, 255-258 (1992).
25. Peer, D. et al. Nanocarriers as an emerging platform for cancer therapy. *Nat Nano* **2**, 751-760 (2007).
26. Allen, T.M. & Hansen, C. Pharmacokinetics of stealth versus conventional liposomes: effect of dose. *Biochimica et Biophysica Acta (BBA) - Biomembranes* **1068**, 133-141 (1991).
27. Torchilin, V.P. Recent advances with liposomes as pharmaceutical carriers. *Nat Rev Drug Discov* **4**, 145-160 (2005).
28. Fattal, E., Couvreur, P. & Dubernet, C. "Smart" delivery of antisense oligonucleotides by anionic pH-sensitive liposomes. *Advanced Drug Delivery Reviews* **56**, 931-946 (2004).
29. Johnston, A.P.R., Such, G.K., Ng, S.L. & Caruso, F. Challenges facing colloidal delivery systems: From synthesis to the clinic. *Current Opinion in Colloid & Interface Science* **16**, 171-181 (2011).
30. Khalil, I.A., Kogure, K., Akita, H. & Harashima, H. Uptake Pathways and Subsequent Intracellular Trafficking in Nonviral Gene Delivery. *Pharmacological Reviews* **58**, 32-45 (2006).
31. Wadia, J.S., Stan, R.V. & Dowdy, S.F. Transducible TAT-HA fusogenic peptide enhances escape of TAT-fusion proteins after lipid raft macropinocytosis. *Nat Med* **10**, 310-315 (2004).
32. El-Sayed, A., Khalil, I.A., Kogure, K., Futaki, S. & Harashima, H. Octaarginine- and Octalysine-modified Nanoparticles Have Different Modes of Endosomal Escape. *Journal of Biological Chemistry* **283**, 23450-23461 (2008).
33. Khalil, I.A., Kogure, K., Futaki, S. & Harashima, H. High Density of Octaarginine Stimulates Macropinocytosis Leading to Efficient Intracellular Trafficking for Gene Expression. *Journal of Biological Chemistry* **281**, 3544-3551 (2006).
34. Chan, W.C.W. et al. Luminescent quantum dots for multiplexed biological detection and imaging. *Current Opinion in Biotechnology* **13**, 40-46 (2002).
35. Murray, C.B., Norris, D.J. & Bawendi, M.G. Synthesis and characterization of nearly monodisperse CdE (E = sulfur, selenium, tellurium) semiconductor nanocrystallites. *Journal of the American Chemical Society* **115**, 8706-8715 (1993).

36. Michalet, X. et al. Quantum Dots for Live Cells, in Vivo Imaging, and Diagnostics. *Science* **307**, 538-544 (2005).
37. Kumar, C.S.S.R. Semiconductor nanomaterials (Wiley-VCH, Weinheim, 2010).
38. Nirmal, M. et al. Fluorescence intermittency in single cadmium selenide nanocrystals. *Nature* **383**, 802-804 (1996).
39. Ruan, G., Agrawal, A., Marcus, A.I. & Nie, S. Imaging and tracking of tat peptide-conjugated quantum dots in living cells: new insights into nanoparticle uptake, intracellular transport, and vesicle shedding. *Journal of the American Chemical Society* **129**, 14759-14766 (2007).
40. Shao, L., Gao, Y. & Yan, F. Semiconductor Quantum Dots for Biomedical Applications. *Sensors* **11**, 11736-11751 (2011).
41. Godly, E.W. & Taylor, R. Nomenclature and terminology of fullerenes: A preliminary survey. *Fullerene Science and Technology* **5**, 1667-1708 (1997).
42. Shvedova, A.A. et al. Mechanisms of pulmonary toxicity and medical applications of carbon nanotubes: Two faces of Janus? *Pharmacology & Therapeutics* **121**, 192-204 (2009).
43. Zhang, L.W., Zeng, L., Barron, A.R. & Monteiro-Riviere, N.A. Biological Interactions of Functionalized Single-Wall Carbon Nanotubes in Human Epidermal Keratinocytes. *International Journal of Toxicology* **26**, 103-113 (2007).
44. Goya, G.F., Berquo, T.S., Fonseca, F.C. & Morales, M.P. Static and dynamic magnetic properties of spherical magnetite nanoparticles. *Journal of Applied Physics* **94**, 3520-3528 (2003).
45. Krotz, F. et al. Magnetofection - A highly efficient tool for antisense oligonucleotide delivery in vitro and in vivo. *Molecular Therapy* **7**, 700-710 (2003).
46. Gupta, A.K. & Curtis, A.S.G. Lactoferrin and ceruloplasmin derivatized superparamagnetic iron oxide nanoparticles for targeting cell surface receptors. *Biomaterials* **25**, 3029-3040 (2004).
47. Mahmoudi, M., Sant, S., Wang, B., Laurent, S. & Sen, T. Superparamagnetic iron oxide nanoparticles (SPIONs): Development, surface modification and applications in chemotherapy. *Advanced Drug Delivery Reviews* **63**, 24-46 (2011).
48. Seoudi, R., Shabaka, A., El Sayed, Z.A. & Anis, B. Effect of stabilizing agent on the morphology and optical properties of silver nanoparticles. *Physica E: Low-dimensional Systems and Nanostructures* **44**, 440-447 (2011).
49. Sharma, V.K., Yngard, R.A. & Lin, Y. Silver nanoparticles: Green synthesis and their antimicrobial activities. *Advances in Colloid and Interface Science* **145**, 83-96 (2009).
50. Braydich-Stolle, L., Hussain, S., Schlager, J.J. & Hofmann, M.-C. In Vitro Cytotoxicity of Nanoparticles in Mammalian Germline Stem Cells. *Toxicological Sciences* **88**, 412-419 (2005).
51. Lee, Y. et al. Silver nanoparticles induce apoptosis and G2/M arrest via PKC ζ -dependent signaling in A549 lung cells. *Archives of Toxicology* **85**, 1529-1540 (2011).
52. Turkevich, J., Stevenson, P.C. & Hillier, J. A study of the nucleation and growth processes in the synthesis of colloidal gold. *Discussions of the Faraday Society*, 55-& (1951).
53. Shaw, C.P., Fernig, D.G. & Levy, R. Gold nanoparticles as advanced building blocks for nanoscale self-assembled systems. *Journal of Materials Chemistry* **21**, 12181-12187 (2011).

54. Han, G., Ghosh, P. & Rotello, V.M. Functionalized gold nanoparticles for drug delivery. *Nanomedicine* **2**, 113-123 (2007).
55. Daniel, M.C. & Astruc, D. Gold nanoparticles: Assembly, supramolecular chemistry, quantum-size-related properties, and applications toward biology, catalysis, and nanotechnology. *Chemical Reviews* **104**, 293-346 (2004).
56. Hostetler, M.J., Templeton, A.C. & Murray, R.W. Dynamics of Place-Exchange Reactions on Monolayer-Protected Gold Cluster Molecules. *Langmuir* **15**, 3782-3789 (1999).
57. Boal, A.K. & Rotello, V.M. Fabrication and Self-Optimization of Multivalent Receptors on Nanoparticle Scaffolds. *Journal of the American Chemical Society* **122**, 734-735 (2000).
58. El-Brolossy, T.A. et al. Shape and size dependence of the surface plasmon resonance of gold nanoparticles studied by Photoacoustic technique. *European Physical Journal-Special Topics* **153**, 361-364 (2008).
59. Niidome, T. et al. PEG-modified gold nanorods with a stealth character for in vivo applications. *Journal of Controlled Release* **114**, 343-347 (2006).
60. Connor, E.E., Mwamuka, J., Gole, A., Murphy, C.J. & Wyatt, M.D. Gold nanoparticles are taken up by human cells but do not cause acute cytotoxicity. *Small* **1**, 325-327 (2005).
61. Tkachenko, A.G. et al. Cellular Trajectories of Peptide-Modified Gold Particle Complexes: Comparison of Nuclear Localization Signals and Peptide Transduction Domains. *Bioconjugate Chemistry* **15**, 482-490 (2004).
62. Goodman, C.M., McCusker, C.D., Yilmaz, T. & Rotello, V.M. Toxicity of Gold Nanoparticles Functionalized with Cationic and Anionic Side Chains. *Bioconjugate Chemistry* **15**, 897-900 (2004).
63. Faulk, W.P. & Taylor, G.M. Immunocolloid method for electron microscope. *Immunochemistry* **8**, 1081-& (1971).
64. Zhang, J. et al. Aptamer-Based Multicolor Fluorescent Gold Nanoprobes for Multiplex Detection in Homogeneous Solution. *Small* **6**, 201-204 (2010).
65. Russ Algar, W., Massey, M. & Krull, U.J. The application of quantum dots, gold nanoparticles and molecular switches to optical nucleic-acid diagnostics. *TrAC Trends in Analytical Chemistry* **28**, 292-306 (2009).
66. Giljohann, D.A. et al. Gold Nanoparticles for Biology and Medicine. *Angewandte Chemie-International Edition* **49**, 3280-3294 (2010).
67. Pissuwan, D., Niidome, T. & Cortie, M.B. The forthcoming applications of gold nanoparticles in drug and gene delivery systems. *Journal of Controlled Release* **149**, 65-71 (2011).
68. Seferos, D.S., Prigodich, A.E., Giljohann, D.A., Patel, P.C. & Mirkin, C.A. Polyvalent DNA Nanoparticle Conjugates Stabilize Nucleic Acids. *Nano Letters* **9**, 308-311 (2008).
69. Pujals, S. et al. Shuttling Gold Nanoparticles into Tumoral Cells with an Amphipathic Proline-Rich Peptide. *ChemBiochem* **10**, 1025-1031 (2009).
70. Nativo, P., Prior, I.A. & Brust, M. Uptake and intracellular fate of surface-modified gold nanoparticles. *Acs Nano* **2**, 1639-1644 (2008).
71. Krpetic, Z. et al. Negotiation of Intracellular Membrane Barriers by TAT-Modified Gold Nanoparticles. *Acs Nano* **5**, 5195-5201 (2011).

72. Wadia, J.S., Stan, R.V. & Dowdy, S.F. Transducible TAT-HA fusogenic peptide enhances escape of TAT-fusion proteins after lipid raft macropinocytosis. *Nature Medicine* **10**, 310-315 (2004).
73. Cazenave, C., Chevrier, M., Thuong, N.T. & Helene, C. Rate of degradation of alpha - oligodeoxynucleotides and beta -oligodeoxynucleotides in xenopus oocytes - implications for anti-messenger strategies. *Nucleic Acids Research* **15**, 10507-10521 (1987).
74. See, V. et al. Cathepsin L Digestion of Nanobioconjugates upon Endocytosis. *ACS Nano* **3**, 2461-2468 (2009).
75. Thanh, N.T.K. & Green, L.A.W. Functionalisation of nanoparticles for biomedical applications. *Nano Today* **5**, 213-230 (2010).
76. Rosenthal, S.J., Chang, J.C., Kovtun, O., McBride, J.R. & Tomlinson, I.D. Biocompatible Quantum Dots for Biological Applications. *Chemistry & Biology* **18**, 10-24 (2011).
77. Duchesne, L., Gentili, D., Comes-Franchini, M. & Fernig, D.G. Robust Ligand Shells for Biological Applications of Gold Nanoparticles. *Langmuir* **24**, 13572-13580 (2008).
78. Chen, X. et al. Features of Thiolated Ligands Promoting Resistance to Ligand Exchange in Self-Assembled Monolayers on Gold Nanoparticles. *Australian Journal of Chemistry* **65**, 266-274 (2012).
79. Weakley, B.S. A beginner's handbook in biological transmission electron microscopy (Churchill Livingstone, Edinburgh, 1981).
80. Alan W. Agar, R.H.A.a.D.C. Principles and practice of electron microscope operation (North-Holland, Amsterdam, 1974).
81. Zinner, E.K., Moynier, F. & Stroud, R.M. Laboratory technology and cosmochemistry. *Proceedings of the National Academy of Sciences of the United States of America* **108**, 19135-19141 (2011).
82. Eskelinen, E.-L., Reggiori, F., Baba, M., Kovacs, A.L. & Seglen, P.O. Seeing is believing The impact of electron microscopy on autophagy research. *Autophagy* **7**, 935-956 (2011).
83. van Dijk, M.A. et al. Absorption and scattering microscopy of single metal nanoparticles. *Physical Chemistry Chemical Physics* **8**, 3486-3495 (2006).
84. Boyer, D., Tamarat, P., Maali, A., Lounis, B. & Orrit, M. Photothermal Imaging of Nanometer-Sized Metal Particles Among Scatterers. *Science* **297**, 1160-1163 (2002).
85. Berciaud, S., Cognet, L., Blab, G.A. & Lounis, B. Photothermal heterodyne imaging of individual nonfluorescent nanoclusters and nanocrystals. *Physical Review Letters* **93** (2004).
86. Cesbron, Y. (University of Liverpool, Liverpool, 2010).
87. Szelenyi, I. Nanomedicine: evolutionary and revolutionary developments in the treatment of certain inflammatory diseases. *Inflammation Research* **61**, 1-9 (2012).
88. Authier, F., Janicot, M., Lederer, F. & Desbuquois, B. Fate of injected glucagon taken up by rat liver in vivo. Degradation of internalized ligand in the endosomal compartment. *Biochem. J.* **272**, 703-712 (1990).
89. Chithrani, D.B., Dunne, M., Stewart, J., Allen, C. & Jaffray, D.A. Cellular uptake and transport of gold nanoparticles incorporated in a liposomal carrier'. *Nanomedicine-Nanotechnology Biology and Medicine* **6**, 161-169 (2010).
90. Mayor, S. & Pagano, R.E. Pathways of clathrin-independent endocytosis. *Nat Rev Mol Cell Biol* **8**, 603-612 (2007).

91. Lundmark, R. & Carlsson, S.R. Driving membrane curvature in clathrin-dependent and clathrin-independent endocytosis. *Seminars in Cell & Developmental Biology* **21**, 363-370 (2010).
92. Mellman, I. Endocytosis and molecular sorting. *Annual Review of Cell and Developmental Biology* **12**, 575-625 (1996).
93. Sahay, G., Alakhova, D.Y. & Kabanov, A.V. Endocytosis of nanomedicines. *Journal of Controlled Release* **145**, 182-195 (2010).
94. Champion, J.A., Katare, Y.K. & Mitragotri, S. Making polymeric micro- and nanoparticles of complex shapes. *Proceedings of the National Academy of Sciences* **104**, 11901-11904 (2007).
95. Zhang, M. et al. Variation in the internalization of differently sized nanoparticles induces different DNA-damaging effects on a macrophage cell line. *Archives of Toxicology* **85**, 1575-1588 (2011).
96. Sabharanjak, S., Sharma, P., Parton, R.G. & Mayor, S. GPI-anchored proteins are delivered to recycling endosomes via a distinct cdc42-regulated, clathrin-independent pinocytotic pathway. *Developmental Cell* **2**, 411-423 (2002).
97. Nakase, I., Kobayashi, S. & Futaki, S. Endosome-disruptive peptides for improving cytosolic delivery of bioactive macromolecules. *Peptide Science* **94**, 763-770 (2010).
98. Lee, S.H., Choi, S.H., Kim, S.H. & Park, T.G. Thermally sensitive cationic polymer nanocapsules for specific cytosolic delivery and efficient gene silencing of siRNA: Swelling induced physical disruption of endosome by cold shock. *Journal of Controlled Release* **125**, 25-32 (2008).
99. Endoh, T., Sisido, M. & Ohtsuki, T. Cellular siRNA delivery mediated by a cell-permeant RNA-Binding protein and photoinduced RNA interference. *Bioconjugate Chemistry* **19**, 1017-1024 (2008).
100. Veldhoen, S., Laufer, S.D. & Restle, T. Recent developments in peptide-based nucleic acid delivery. *International Journal of Molecular Sciences* **9**, 1276-1320 (2008).
101. Faria, M. et al. Phosphoramidate oligonucleotides as potent antisense molecules in cells and in vivo. *Nature Biotechnology* **19**, 40-44 (2001).
102. Stewart, S.E., D'Angelo, M.E. & Bird, P.I. Intercellular communication via the endo-lysosomal system: Translocation of granzymes through membrane barriers. *Biochimica et Biophysica Acta (BBA) - Proteins & Proteomics* **1824**, 59-67 (2012).
103. Idone, V. et al. Repair of injured plasma membrane by rapid Ca²⁺-dependent endocytosis. *The Journal of Cell Biology* **180**, 905-914 (2008).
104. Sandvig, K. & van Deurs, B. Delivery into cells: lessons learned from plant and bacterial toxins. *Gene Therapy* **12**, 865-872 (2005).
105. Provoda, C.J. & Lee, K.-D. Bacterial pore-forming hemolysins and their use in the cytosolic delivery of macromolecules. *Advanced Drug Delivery Reviews* **41**, 209-221 (2000).
106. Chou, L.Y.T., Ming, K. & Chan, W.C.W. Strategies for the intracellular delivery of nanoparticles. *Chemical Society Reviews* **40**, 233-245 (2011).
107. Kielian, M. & Rey, F.A. Virus membrane-fusion proteins: more than one way to make a hairpin. *Nature Reviews Microbiology* **4**, 67-76 (2006).
108. Nobusawa, E. et al. Comparison of complete amino-acid-sequences and receptor-binding properties among 13 serotypes of hemagglutinins of influenza A-viruses. *Virology* **182**, 475-485 (1991).

109. Cross, K.J., Langley, W.A., Russell, R.J., Skehel, J.J. & Steinhauer, D.A. Composition and Functions of the Influenza Fusion Peptide. *Protein and Peptide Letters* **16**, 766-778 (2009).
110. Han, X., Bushweller, J.H., Cafiso, D.S. & Tamm, L.K. Membrane structure and fusion-triggering conformational change of the fusion domain from influenza hemagglutinin. *Nature Structural Biology* **8**, 715-720 (2001).
111. Mastrobattista, E. et al. Functional characterization of an endosome-disruptive peptide and its application in cytosolic delivery of immunoliposome-entrapped proteins. *Journal of Biological Chemistry* **277**, 27135-27143 (2002).
112. Eckert, D.M. & Kim, P.S. Mechanisms of viral membrane fusion and its inhibition. *Annual Review of Biochemistry* **70**, 777-810 (2001).
113. Wagner, E., Plank, C., Zatloukal, K., Cotten, M. & Birnstiel, M.L. Influenza-virus hemagglutinin-HA-2N-terminal fusogenic peptides augment gene-transfer by transferring polylysine DNA complex- toward a synthetic virus-like gene-transfer vehicle. *Proceedings of the National Academy of Sciences of the United States of America* **89**, 7934-7938 (1992).
114. Wharton, S.A., Martin, S.R., Ruigrok, R.W.H., Skehel, J.J. & Wiley, D.C. Membrane-fusion by peptide analogs of influenza-virus hemagglutinin. *Journal of General Virology* **69**, 1847-1857 (1988).
115. Berry, C.C., de la Fuente, J.M., Mullin, M., Chu, S.W.L. & Curtis, A.S.G. Nuclear Localization of HIV-1 Tat Functionalized Gold Nanoparticles. *NanoBioscience, IEEE Transactions on* **6**, 262-269 (2007).
116. Heitz, F., Morris, M.C. & Divita, G. Twenty years of cell-penetrating peptides: from molecular mechanisms to therapeutics. *British Journal of Pharmacology* **157**, 195-206 (2009).
117. Duchardt, F., Fotin-Mleczek, M., Schwarz, H., Fischer, R. & Brock, R. A comprehensive model for the cellular uptake of cationic cell-penetrating peptides. *Traffic* **8**, 848-866 (2007).
118. Sugita, T. et al. Improved cytosolic translocation and tumor-killing activity of Tat-shepherdin conjugates mediated by co-treatment with Tat-fused endosome-disruptive HA2 peptide. *Biochemical and Biophysical Research Communications* **363**, 1027-1032 (2007).
119. Bhakdi, S. et al. A guide to the use of pore-forming toxins for controlled permeabilization of cell-membranes. *Medical Microbiology and Immunology* **182**, 167-175 (1993).
120. Walev, I. et al. Delivery of proteins into living cells by reversible membrane permeabilization with streptolysin-O. *Proceedings of the National Academy of Sciences of the United States of America* **98**, 3185-3190 (2001).
121. Harush-Frenkel, O., Debotton, N., Benita, S. & Altschuler, Y. Targeting of nanoparticles to the clathrin-mediated endocytic pathway. *Biochemical and Biophysical Research Communications* **353**, 26-32 (2007).

CHAPTER 2

2. Intracellular delivery of gold nanoparticles using viral peptides

2.1 Viral peptides: Haemagglutinin subunit 2 (HA2)

In nature, Influenza virus takes over its host cell machinery by disrupting the endosomes at low pH. For this purpose it uses a glycoprotein, haemagglutinin complex HA0 present on its envelope. HA0 is a precursor polypeptide, which after proteolysis converts into the pH sensitive HA polypeptide. The HA consists of two subunits, HA1 and HA2, linked together by a disulfide bond. The HA1 subunit helps the virus to bind to the cell membrane while, in a second step, the HA2 subunit disrupts the endosomal vesicles at low pH by destabilizing the endosomal membrane, leaving the virus free in the cytosol.¹

HA2 peptide either having 23 amino acid residues (wild type) or 20 amino acids and its analogues have been tested *in vitro* to evaluate the fusion activity.^{2,3} The fusion activity of HA2 peptide has been used for cytosolic delivery of proteins.⁴ On entering the cell via receptor mediated endocytosis, the low pH of endolysosomes triggers conformational changes, causing the fusogenic HA2 peptide to get inserted into the lipid bilayer membrane of the endosome resulting in membrane destabilization, which in turn can cause the leakage of endosomal vesicles.^{3, 5, 6} Cross *et al.* recently published a review on the structure and function of the HA2 peptide.⁷

The exact process by which irreversible conformational changes in the HA2 peptide structure lead to lipid membrane fusion is not fully understood. However, Han *et al.* have used the NMR modelling supported by EPR (electron paramagnetic resonance) and circular dichroism spectra data, for showing the interaction of HA2 peptide with dodecylphosphocholine (DPC) micelles and with synthetic lipid bilayers at different pH values. It was concluded that at pH 5, the N-terminal part of HA2 peptide forms an α -helix that penetrates into the detergent micelle core.⁸ Esbjörner *et al.* compared the fusion

activity of wild type HA2 peptide and a glutamic acid rich HA2 analogue, INF7, with lipid vesicles. The data suggest that introduction of glutamic acid residues in the N-terminal part of HA2 peptides has an effect on pH sensitivity. It was found that despite of 100% leakage activity by both types of HA2, none of the vesicles were burst. The kinetics of peptide and lipid interaction was also found to be slower.⁹

2.2 Viral peptides: Trans-activator of transcription (TAT)

TAT is a viral protein consisting of 86-101 amino acids derived from the human immunodeficiency virus 1 (HIV-1). The virus uses this protein to increase the transcription of its genes. TAT protein also acts like a toxin to invade and infect the host cells. It contains a protein transduction domain that explains why it is classified as a CPP, *i.e.*, a peptide, which can directly translocate the plasma membrane of cells. Examples of other naturally occurring CPPs are transportan and penetratin.¹⁰

CPPs are typically short cationic or amphipathic peptide sequences derived from natural sources or *de novo* designed. Due to their cationic/amphipathic nature they were presumed to be capable of direct penetration into the plasma membrane without disrupting it, especially when present at high concentrations.^{11, 12} Derrosi *et al.* suggested that the direct translocation of antennapedia homeodomain peptide (CPP derived from the genome of a fly, *Drosophila species*) occurs through the plasma membrane in a temperature independent manner.¹³ The ability of TAT to penetrate the cell membrane is highly controversial. It was found that CPPs utilizes more than one mechanism of endocytosis to translocate through the plasma membrane.^{14, 15} Direct observation for cellular uptake of CPPs at a single molecular level using real-time microscopy also suggested multimechanistic cellular uptake of CPPs.¹⁶ Green *et al.* have regarded the direct penetration phenomenon as an artefact due to the cationic nature of the peptide, which causes it to associate closely to the cell membrane and subsequently be taken in by endocytosis.¹⁷ Ruan *et al.* have shown the endocytic uptake of TAT-functionalized Qdots by HeLa cells and found that the endosomal vesicles containing Qdots, further moved in the perinuclear region.¹⁸ The limitations in the use of CPPs include endosomal entrapment of cargos and several measures to overcome this limitation have been reviewed in details.¹⁹

2.3 HA2 and TAT assisted gold nanoparticles delivery

Gold nanoparticles (2.8 nm approximate size) functionalized with TAT peptides, were shown to be localized in the nucleus and in the cytoplasm.²⁰ In another study, it was showed that TAT or penetratin (Pntn) functionalized gold nanoparticles were not able to escape endosomes, but a combination of both peptides and PEG in the SAM of gold nanoparticles led to some delivery into the cytoplasm²¹ although nearly 100% of the particles were in the endosomal compartments (private communication cited by Iversen et al).²² This parallel endosomal uptake was also observed by Berry *et al* for TAT peptide functionalized nanoparticles.^{15, 23}

Michiue *et al.* compared the transcription activity of polyarginine-fused p53 protein (p53-11R) and polyarginine-fused p53 conjugated with HA2 (HA2-p53-9R) in living malignant glioma cells. The data showed that HA2 conjugation with p53-9R caused an enhancement of the transcriptional activity and consequently of the antitumor activity of the p53 protein.²⁴ Wadia *et al.* have used HA2-fused TAT peptide (dTAT-HA2) to improve the escape of TAT-Cre from macropinosomes.²⁵

Kumar *et al.* reported an efficient labelling of actin filaments by using 20 nm gold nanoparticle multi-functionalised with anti-actin targeting antibodies, anti-biotin antibodies, biotinylated TAT-HA2 peptide and PEG. It was shown that lacking of any of the functional moiety resulted in failure of targeting. For example nanoparticles having all other functional moieties, but lacking TAT-HA2 peptide showed no actin labelling. The same was true for TAT peptide alone.²⁶

Here we explore the potential of HA2 and TAT peptides and their analogues for cytosolic delivery of gold nanoparticles. In particular, we have tested the role of HA2 orientation on fusogenic activity, the effect of PEGylation and the effect of free *versus* nanoparticle-bound peptides. The gold nanoparticles (size ranges from 5-15 nm) functionalized with viral peptides were co-incubated with HeLa cells for various times. Photothermal imaging and transmission electron microscopy have been employed to elucidate the extent of internalisation and localization of nanoparticles. To measure the entry of free peptide, a peptide labelled with FITC instead of gold nanoparticles was used and imaged by fluorescence microscopy.

The names and sequences of the peptides are given in the table below (table 2.1)

Table 2.1: Viral peptide HA2, TAT and derivatives

No.	Name	Sequence	No. of amino acid residues
1	dCCALNN-HA2	ccalnnGdimGewGneifGaiaGfIG-amide	6+ 20= 26
2	HA2-NNLACC	*GLFEAIEGFIENGWEGMIDGWYGGGGNNLACC	6+ 3+ 23= 32
3	CCALNN-HA2	CCALNNGGGGLFEAIEGFIENGWEGMIDGWYGG	6+ 3+ 23= 32
4	HA2 fused TAT	GLFEAIEGFIENGWEGMIDGWYGYGRKKRRQRRR	11+ 23= 34
5	CALNN-TAT	CALNNAAGRKKRRQRRR	5+ 11= 16
6	FITC-TAT fused fluorescein isothiocyanate	YGRKKRRQRRRK-FITC	12
7	CALNN	CALNN	5
8	CCALNN-PEG	CCALNN-(EG) ₆ -ol	6
9	PEG or SH-C11-(EG) ₄ -ol	11-mercaptoundecyl-tetra(ethylene glycol) or SH-(CH ₂) ₁₁ -EG ₄ -OH	

*Green: anchor peptide; blue: linker residues; yellow: HA2 peptide

2.4 Results

2.4.1 Nanoparticle-bound HA2 increases cellular uptake of gold nanoparticles

In early experiments, Cesbron *et al.* showed at least two fold increase in cellular uptake of gold nanoparticles in the presence of dCCALNN-HA2 in the SAM of gold nanoparticles compared to the gold nanoparticles without dCCALNN-HA2. They compared the cellular uptake of 10% dCCALNN-HA2 20% CCALNN-PEG and 70% (all mole/mole) CALNN-capped gold nanoparticles with 20% CCALNN-PEG 80% (all mole/mole) CALNN-capped gold nanoparticles (5 nm). Although they did not do a detailed localization study, the photothermal microscopy images are showing predominantly vesicular localization of gold nanoparticles (reproduced in Fig. 2.1).²⁷

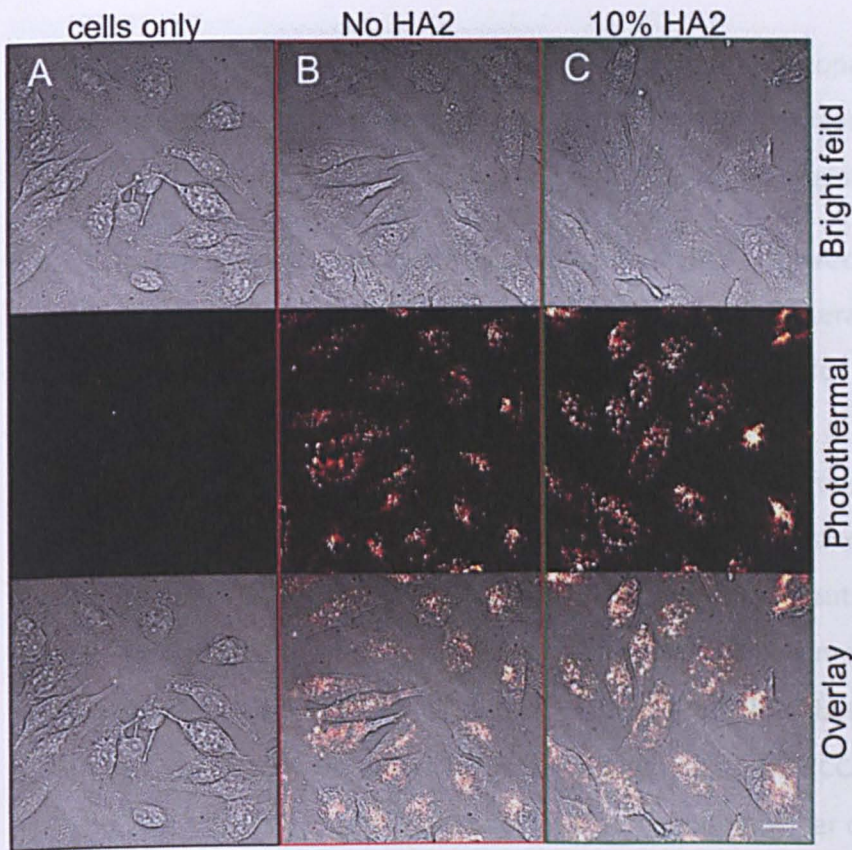


Fig. 2.1

HA2 peptide increases cellular uptake of gold nanoparticles

(HeLa cells treated with or without gold nanoparticles, images A – C)

A) Cells only. B) 80% CALNN 20% (all mole/mole) CCALNN-PEG-capped gold nanoparticles. C) 10% dCCALNN-HA2 70% CALNN 20% (mole/mole) CCALNN-PEG-capped gold nanoparticles. For all conditions, HeLa cells were incubated with or without 5 nm diameter gold nanoparticles (500 nM) for 3 h and fixed prior to photothermal imaging. Scale bar represents 20 μ m. The graph D shows the quantification of gold nanoparticles for different conditions (mentioned above) based on photothermal signal. The mean photothermal intensities for each condition were calculated by whole field method. Error bars represent SE (Fig. modified and adapted from Cesbron's PhD thesis, 2010).

To understand the cellular localization of HA2-capped gold nanoparticles and to investigate further the potential of HA2 analogue peptides for cytosolic delivery of gold nanoparticles, it was decided to have a closer look inside the cells using transmission electron microscopy.

2.4.2 Effect of PEGylation on the localization of HA2- capped gold nanoparticles

It is well known fact that PEG reduces the non-specific interaction of molecules with cellsmembrane. It has been used in SAM of gold nanoparticles for targeted cellular delivery.^{21, 28} The idea of using PEG in SAM was to reduce the stickiness of gold nanoparticles to the endosomal membranes, which is an ultimate outcome of HA2 peptide interaction with the membrane. With PEG in SAM along with HA2 peptide, gold nanoparticles may be flexible enough not only to interact with vesicular membrane components, but also able to release from them. To see the effect of PEGylation, two types of 10 nm gold nanoparticles were functionalized; one coated with 10% dCCALANN-HA2 and 90% (both mole/mole) CALNN and the other type of gold nanoparticles were capped with 10% dCCALNN-HA2, 20% CCALNN-PEG and 70% (all mole/mole) CALNN. It was the same monolayer composition mentioned in the experiments discussed above (Fig. 2.1, C). The HeLa cells were incubated with the gold nanoparticles for 4 h and then observed under the EM to investigate the intracellular localization.

In terms of vesicular membrane interaction, it was found that both types of particles were interacting with the vesicular membranes (Fig. 2.2). As far as cellular localization is concerned, both types of particles were found either inside the vesicles, just around the vesicles or at the brim of ruptured vesicular membrane. There were very few particles that were present freely in cytoplasm in both samples. This cytosolic presence was negligible (Fig. 2.2).

Based on this observation it can be concluded that in terms of cellular localization CCALNN-PEG has no influence on localization as the particles were mainly showing vesicular entrapment. However, apparently the number of gold nanoparticles per vesicle is lower for CCALNN-PEG containing sample compared to the sample without CCALNN-PEG. The effect of PEG on reduction for overall uptake of gold nanoparticles was not quantified here, as the main interest was the localization.

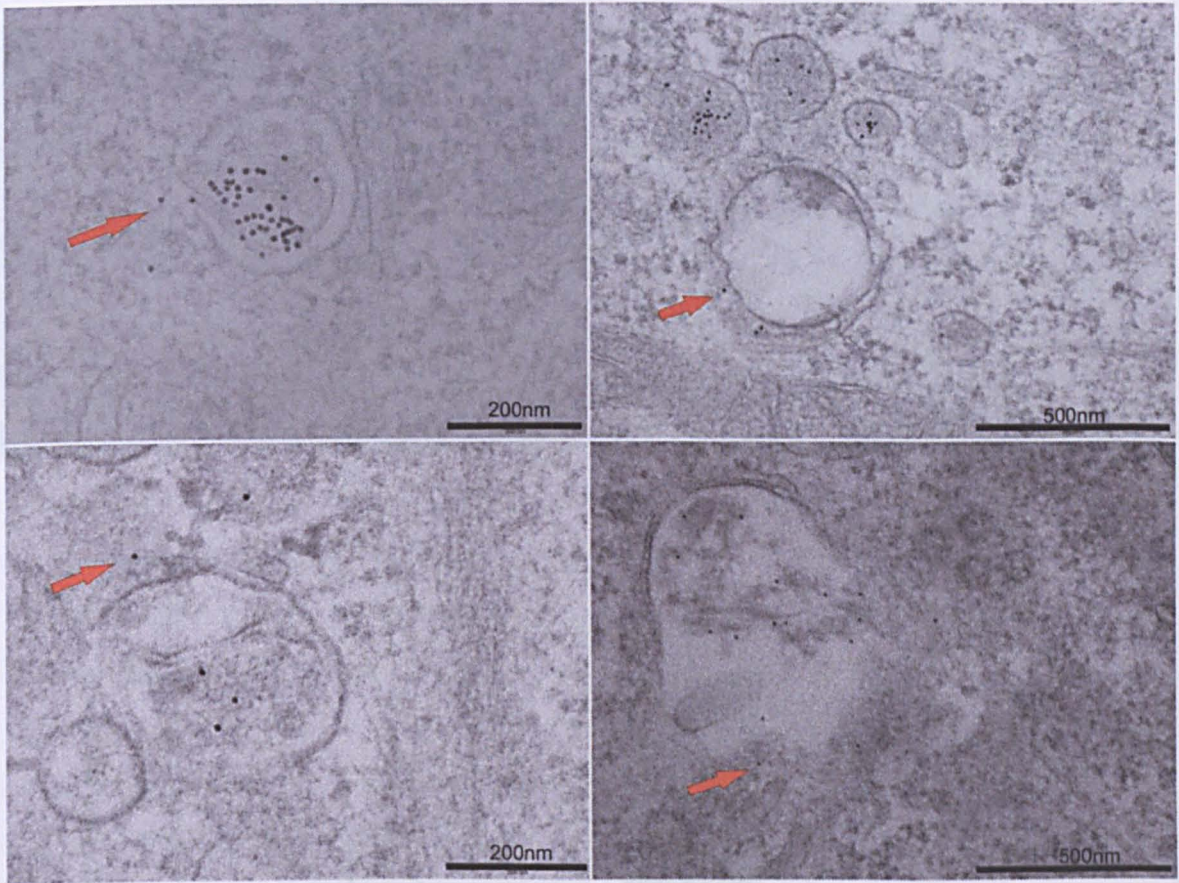


Fig. 2.2 Intracellular localization of HA2 functionalized gold nanoparticles: effect of PEG.

Top panel) 10% dCCALNN-HA2 and 90% (both mole/mole) CALNN gold nanoparticles (No PEG).
 Bottom panel) 10% dCCALNN-HA2, 20% CCALNN-PEG and 70% (all mole/mole) CALNN-capped gold nanoparticles (with PEG).

HeLa cells incubated with gold nanoparticles 10 nm (6 nm) for 4 h were then washed thoroughly with 1 x PBS and fixed for electron microscopy. Arrows are pointing toward gold nanoparticles either interacting with vesicular membranes or present around endosomes.

2.4.3 Increasing percentage of HA2 in SAM increases the cellular uptake

At the surface of the influenza virus, many HA2 peptides are displayed in close proximity and it is, therefore, possible that a cooperative effect is necessary to disrupt the endosomal membrane. To test whether increasing the proportion of HA2 peptide in the SAM on gold nanoparticles could improve cytosolic delivery an experiment was done with 100% (mole/mole) dCCALNN-HA2-capped gold nanoparticles and 50% dCCALNN-HA2 50% 9both mole/mole) CALNN-capped gold nanoparticles. The 6 nm diameter gold nanoparticles were incubated with the HeLa cells for 4 h.

Analysis of the TEM images of cells with 50% dCCALNN-HA2 50% (mole/mole) CALNN-capped gold NPs or with 100% (mole/mole) dCCALNN-HA2-capped gold nanoparticles reveals

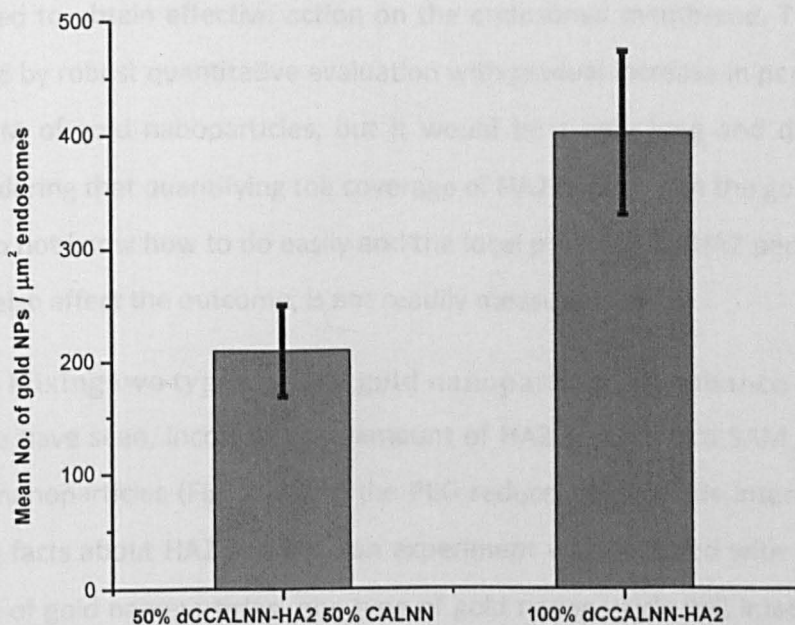
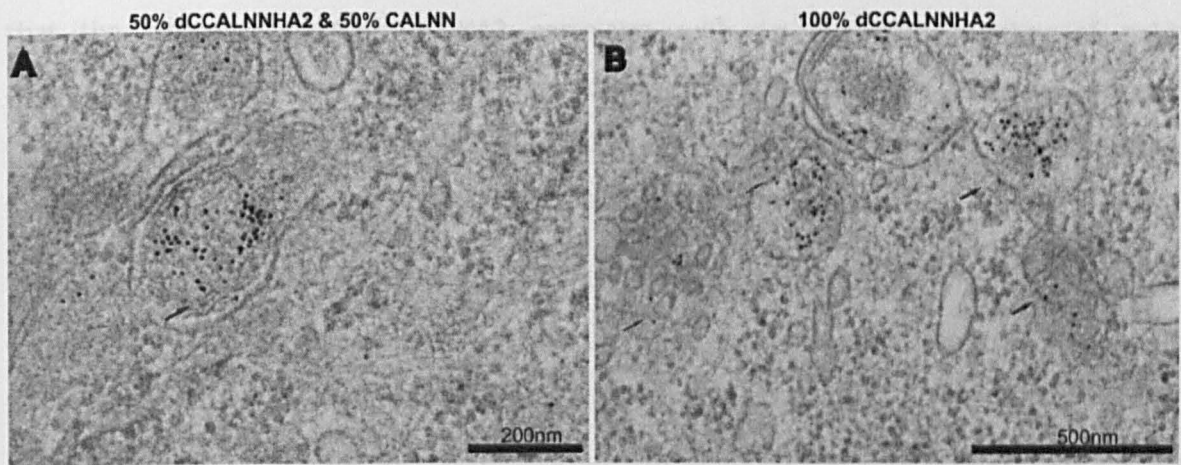


Fig. 2.3 Increasing the proportion of dCCALNN-HA2 in the monolayer of gold nanoparticles increases cellular uptake.

A) 50% dCCALNN-HA2 and 50% (both mole/mole) CALNN-capped gold NPs 6 nm (6 nM) for 4 h. B) 100% (mole/mole) dCCALNN-HA2 – capped gold NPs. In both conditions, HeLa cells were incubated with gold NPs (6nM) for 4 h and fixed for EM imaging. Arrows are pointing toward gold NPs interacting with vesicular membranes. The graph is showing mean gold nanoparticles count/vesicle for each condition. The quantification is based on selecting 15-20 random EM images and counting the number of gold nanoparticles per unit area (in μm^2) of endosome. The error bars show the standard error of mean.

Analysis of the TEM images of cells with 50% dCCALNN-HA2 50% (mole/mole) CALNN-capped gold NPs or with 100% (mole/mole) ccalnnHA2-capped gold nanoparticles reveals

that the higher percentage of HA2 correlates with an increased number of gold nanoparticles per vesicle compared to that shown by 10% cCALNN-HA2 90% (both mole/mole) CALNN-capped gold nanoparticles (Fig. 2.3, A & B and Fig. 2.2, top panel). The localization of gold nanoparticles was mainly vesicular as was observed in the previous set of experiments.

When the 50% dCCALNN-HA2 50% CALNN and 100% dCCALNN-HA2 conditions were compared for overall gold nanoparticle uptake, there was almost a two-fold increase in cellular uptake for the latter condition. This suggests a positive effect of the density of HA2 peptide in the SAM of gold nanoparticles on cellular interaction, but no significant difference in intracellular interaction. It may be that a very precise HA2 surface coverage is needed to obtain effective action on the endosomal membrane. This hypothesis could be tested by robust quantitative evaluation with gradual increase in percentage of HA2 peptide in SAM of gold nanoparticles, but it would be a very long and difficult study. Especially considering that quantifying the coverage of HA2 peptides on the gold core is still something we do not know how to do easily and the local proximity of HA2 peptides in the SAM, which may also affect the outcome, is not readily measured.

2.4.4 Mixing two types of HA2 gold nanoparticles to enhance cytosolic delivery

As we have seen, increasing the amount of HA2 peptide in a SAM increases the uptake of gold nanoparticles (Fig. 2.3) and the PEG reduces nonspecific interaction. Keeping in mind these facts about HA2 and PEG, an experiment was designed with the combination of two types of gold nanoparticles. one type of gold nanoparticle will interact more with vesicular membranes because it possess more HA2, but no PEG While, the other type of gold nanoparticle will reduce binding to membranes through PEG functionalization. This delivery system would work in two steps, first the gold nanoparticles having more HA2 peptide and no PEG in their SAM will interact more with vesicular membranes at low pH, hence would be able to destabilize the membranes, then the gold nanoparticles with PEG and HA2 peptide in SAM may be able to pass through the destabilized vesicular membranes, owing to their reduced adhesion to membranes, and will enter into the cytosol. A new 23 amino acid residue peptide containing HA2, (CCALNN-HA2 sequence is showed in table 2.1, 3), was used to see if this dual nanoparticle delivery system enhanced access to the cytosol.

Two types of gold nanoparticles were functionalized as; PEGylated 9 nm, and non-PEGylated 15 nm. The PEGylated gold nanoparticles of 9 nm coated with 10% CCALNN-HA2, 20% CCALNN-PEG and 70% (all mole/mole) CALNN and non-PEGylated gold NPs of 15 nm were capped with 50% CCALNN-HA2 and 50% (all mole/mole) CALNN. They were mixed together in equal concentration (6 nM). The size difference between the two types of gold nanoparticles was chosen in order to allow them to be distinguished and so observe clearly, which gold nanoparticles were localized where and how they interacted with membranes.

The EM images showed that few PEGylated CCALNN-HA2 gold nanoparticles were present inside the cells, thus their interaction with the vesicular membranes was difficult to establish quantitatively (Fig. 2.4, C, D). In contrast, gold nanoparticles capped with 50 % CCALNN-HA2, 50 % CALNN showed interaction with vesicular membranes regardless of the absence or presence of PEGylated CCALNN-HA2 gold nanoparticles (Fig 2.4, A & B and E-H). Importantly, the presence of large numbers of HA2 containing nanoparticles did not appear to have any effect on the passenger PEGylated nanoparticles. Whether this is simply because of the very low number of PEGylated nanoparticles taken up by the cells or is an invalidation of the hypothesis, cannot be determined from these data.

Based on these results, it was concluded that although the PEGylation was clearly reducing the overall cellular uptake of gold nanoparticles and consequently the interaction with the vesicular membranes. However, the vesicular localization of the gold nanoparticles was probably not affected by CCALNN-PEG (Fig. 2.4) The CCALNN-HA2 peptide, which was different from the dCCALNN-HA2 (sequences given in table 2.1), but showed a similar type of interaction with the endosomal membranes. In both conditions, the gold nanoparticles seemed to interact with vesicular membranes and appeared stuck at this stage (Fig. 2.3, A and Fig. 2.4, A, B or E-H). For 50% CCALNN-HA2 50% (both mole/mole) CALNN-capped gold nanoparticles, the arrangement of gold nanoparticles along the periphery of endosomes can be visualized easily due to their large size (15 nm) compared to 50% dCCALNN-HA2 50% (both mole/mole) CALNN-capped gold nanoparticles (9 nm). Few gold nanoparticles can be seen at the borders of vesicles (Fig. 2.4, A, B and E-H). The TEM results indicate that the enantiomeric form of HA2 peptide, or the difference in the number of amino acid residues, did not measurably affect the ability of peptides to interact with the membranes and subsequent endosomal uptake. This hypothesis can be probed further by quantifying

cellular uptake of gold nanoparticles using different techniques parallel with TEM for example ICP-AES (inductively coupled plasma-atomic emission spectroscopy) and photothermal microscopy.

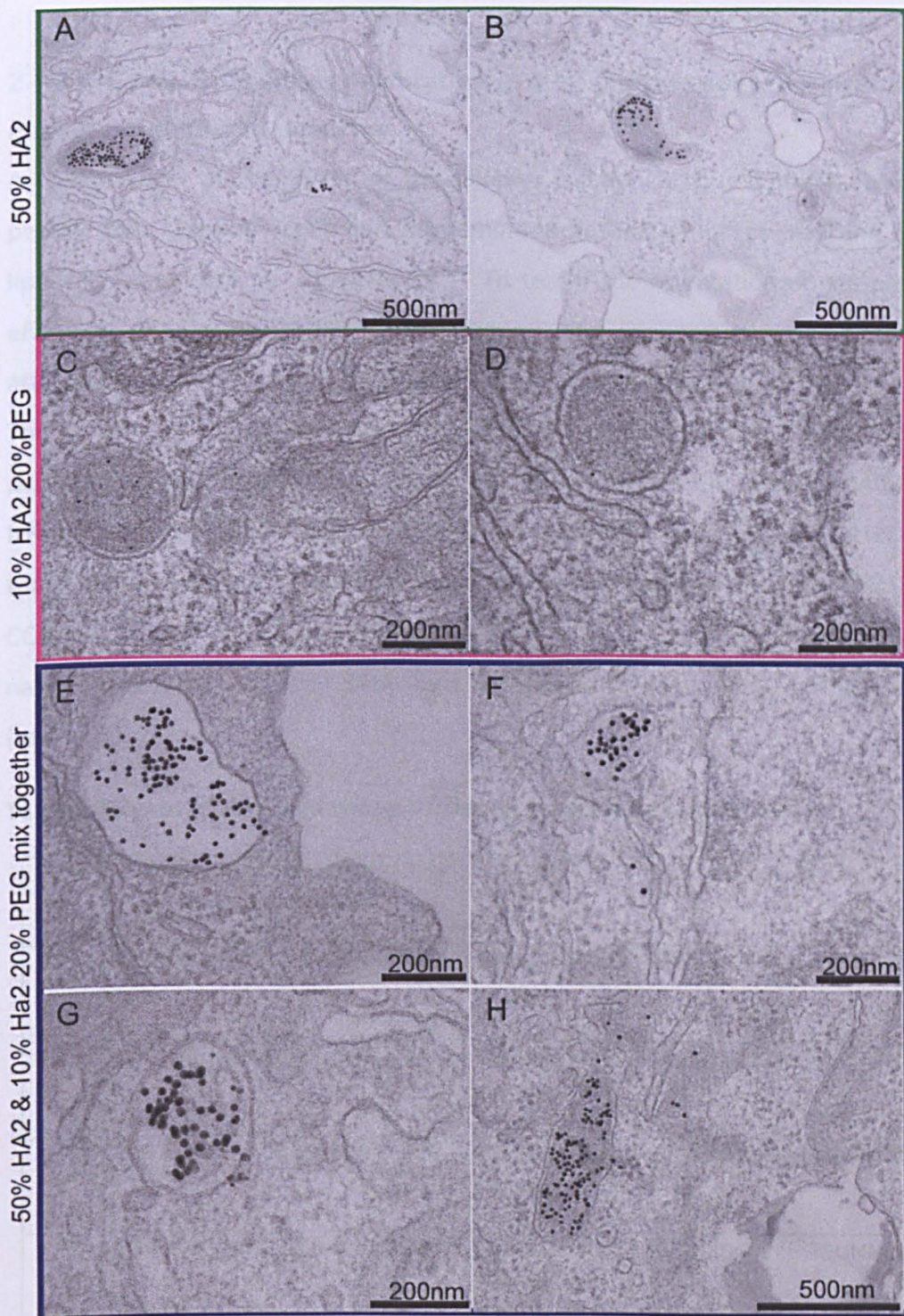


Fig. 2.4 (PEGylated vs none PEGylated) Mixing two types of CCALNN-HA2 gold NPs to enhance cytosolic delivery of HA2 peptide.

A,B) 50% CCALNN-HA2-50% CALNN-capped Gold NP (15 nm) **C,D)** 10% CCALNN-HA2, 20% CCALNN-PEG and 70% (mole/mole) CALNN-capped gold NPs (9 nm). **E-H)** 50% CCALNN-HA2-50% (mole/mole) CALNN-capped Gold NPs (15 nm) mixed with 10% CCALNN-HA2, 20% CCALNN-PEG and 70% 9mole/mole) CALNN-capped gold NPs (9 nm). HeLa cells incubated with gold NPs (6 nM) for 3 h and fixed afterward for EM imaging.

2.4.5 N-C or C-N terminus orientation of HA2 peptide does not alter the cytosolic delivery of gold nanoparticles

As discussed in the beginning of this chapter (section 2.1), it is the N terminus of HA2 peptide that takes an active part in membrane destabilization by inserting itself into the lipid bilayer of vesicular membranes.^{7, 8} To test if the orientation of the peptide had an effect on cellular localization of HA2-capped gold nanoparticles, the HA2 peptide was attached to the gold nanoparticles with a linker connected either to the C- or N- terminus. The 23 amino acid residues containing the HA2 peptide sequence was attached to the peptide CCALNN via both orientations, *i.e.*, from N to C (CCALNN-HA2) and C to N (HA2-NNLACC). The anchor peptide CCALNN and a linker peptide (GGG), the latter consisting of three residues to offer flexibility, were incorporated along with the HA2 peptide. The CCALNN peptide has a cysteine residue, which forms the covalent bond with the gold nanoparticles. Four types of SAM were being used to coat the 10 nm gold nanoparticles (table 2.2).

Table 2.2 Types of HA2 gold nanoparticles with N-C or C-N orientations

Serial No.	% (mole/mole) of peptides in SAM of gold nanoparticles	Sequence orientation
1	20% CCALNN-HA2 and 80% CALNN	CCALNNGGGGLFEAIEGFIENGWEGMIDGWYG and CALNN
2	50% CCALNN-HA2 and 50% CALNN	CCALNNGGGGLFEAIEGFIENGWEGMIDGWYG and CALNN
3	20% HA2-NNLACC and 80% CALNN	GLFEAIEGFIENGWEGMIDGWYGGGGNNLACC and CALNN
4	50% HA2-NNLACC and 50% CALNN	GLFEAIEGFIENGWEGMIDGWYGGGGNNLACC and CALNN

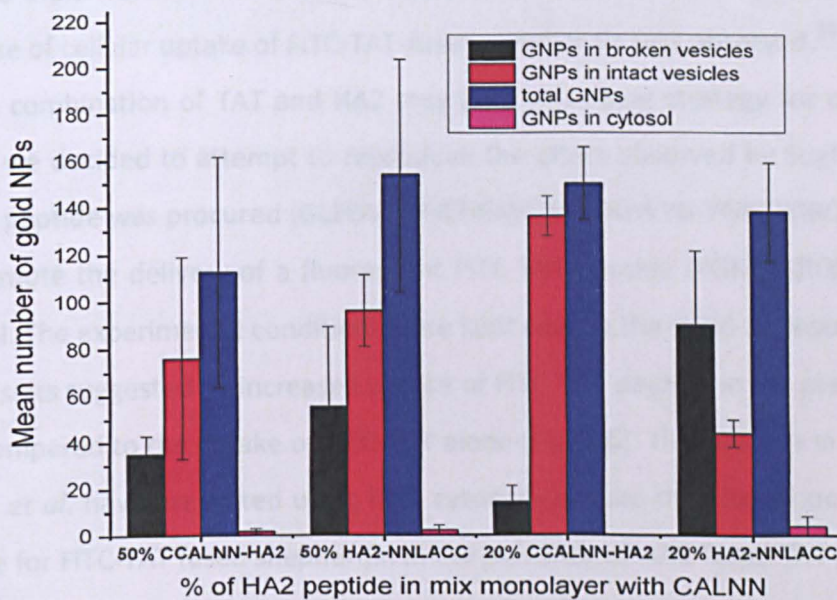
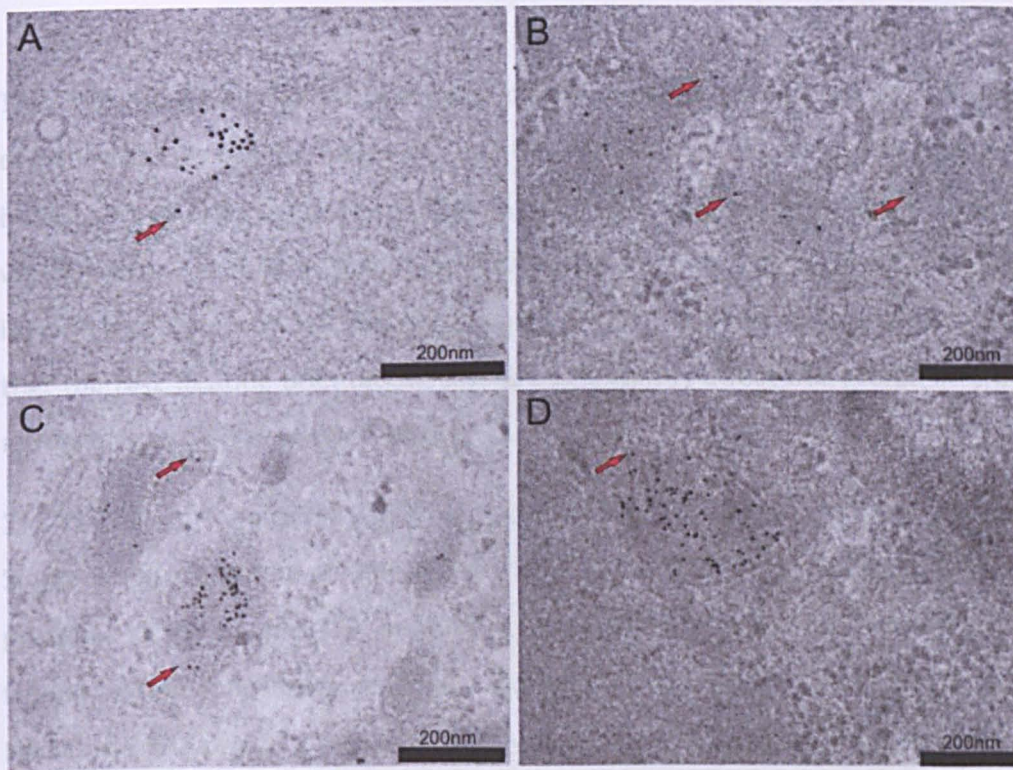


Fig. 2.5 Attaching HA2 via the C-terminus versus N-terminus: effect of HA2 orientation on cellular localization

In all conditions, HeLa cells were incubated with gold nanoparticles 10 nm (6 nM) for 4 h. (A) 20% CCALNN-HA2 80% CALNN (B) 50% CCALNN-HA2 50% CALNN (C) 20% HA2-NNLACC 80% CALNN (D) 50% HA2-NNLACC 50% (all mole/mole) CALNN gold NPs. Arrows indicating the particles around or outside the endosomes. Bar graph is showing gold nanoparticles quantification based on TEM. Total number of gold nanoparticles/cell section was counted in 3 to 5 cell sections/condition. Error bars represent the standard deviation.

The TEM images revealed that orientation difference or percentage of HA2 peptide in SAM of nanoparticles did not help releasing the endosomally localized gold nanoparticles. With both types of orientations, the gold nanoparticles were seen inside or at the brim of the vesicles (Fig. 2.5, A-D). A quantified estimation showed that in terms of overall uptake or localization there was not different among all four conditions (Fig. 2.5). It was concluded that the HA2 peptide orientations did not significantly affect the overall interaction of gold nanoparticles with vesicular membranes.

2.4.6 FITC- TAT peptide and HA2 fused TAT peptide for cytosolic delivery

Sugita *et al.* reported an enhanced activity of the anti-cancer drug shepherdin in the presence of HA2-fused TAT peptide. It was shown that FITC-TAT fused shepherdin was trapped inside endosomes of tumour cells (HeLa and A549 cell lines), but in the presence of HA2-fused TAT peptide, cytosolic fluorescence signal was detected in the tumour cells. The flow cytometry data were interpreted to suggest that co-incubation with HA2-fused TAT peptide enhances the anti-cancer activity of FITC-TAT-fused shepherdin, even though no increase of cellular uptake of FITC-TAT-fused shepherdin was observed.²⁹

As the combination of TAT and HA2 may be a promising strategy for cytosolic delivery of cargo, we decided to attempt to reproduce the effect observed by Sugita *et al.* A HA2-TAT fusion peptide was procured (GLFEAIEGFIENGWEGMIDGWYG-YGRKKRRQRRR) and was used to promote the delivery of a fluorescent FITC-TAT peptide (YGRKKRRQRRRK-FITC) into the cytosol. The experimental conditions were kept exactly the same as described in the study.²⁹ The results suggested an increased uptake of FITC-TAT peptide in the presence of HA2-fused TAT compared to the uptake of FITC-TAT alone (Fig. 2.6). This result is in disagreement what Sugita *et al.* have presented using flow cytometry, since they found no increase in cellular uptake for FITC-TAT fused shepherdin in the presence of HA2-fused TAT peptide.

In terms of cellular localization, there were 2-3 cells that showed either nuclear or cytosolic localization of FITC-TAT in the presence of HA2-TAT (Fig. 2.6, E). Sugita *et al.* have presented fluorescence image of only one HeLa cell as evidence of cytosolic localization of FITC-TAT fused shepherdin in the presence of HA2-TAT. However, our results are in agreement with what Cesbron *et al.* have showed by using the HA2 and TAT peptides separately and in

combination, while probing the potential of these peptides for cytosolic delivery of gold. The results from this study are summarized in the next section.

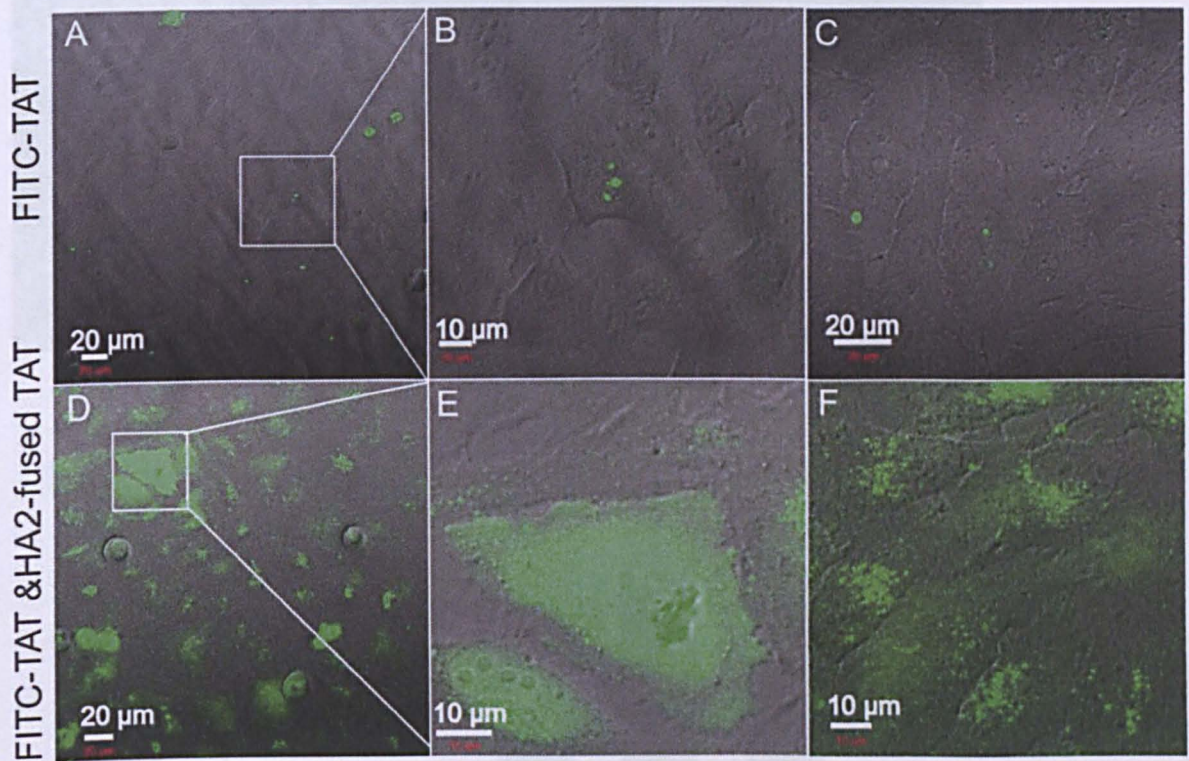


Fig. 2.6 HA2-fused TAT peptide for intracellular delivery of FITC-TAT peptide

A-C) FITC-TAT (fluorescein isothiocyanate fused-TAT) 10 μ M. D-F) FITC-TAT peptide (10 μ M) with HA2-fused-TAT (2 μ M). HeLa Cells were incubated with peptide/ peptides for 4-5 h and washed with fresh medium before confocal fluorescence microscopy. (Contrast set at 40-47 for all images).

2.4.7 TAT and HA2 increases cellular uptake of gold nanoparticles

Cesbron *et al.* found that the addition of HA2 and TAT peptides in the SAM of nanoparticles increased the cellular uptake of gold nanoparticles. The effect of TAT was pronounced, but HA2 did also improve the uptake even in the presence of TAT in SAM of nanoparticles (Fig. 2.7, C, D). However, the localization of gold nanoparticles was not altered for the different conditions, *i.e.*, a punctate photothermal signal, which is an indication of vesicular sequestration of gold nanoparticles, was observed. A proposed interpretation was the effect of PEG in monolayers of gold nanoparticles, which might have reduced the interaction of peptides with vesicular membranes. However, further study to clearly establish the potential of this monolayer functionalization was proposed.²⁷ So the behaviour of TAT in the presence of PEG was further investigated (following paragraph, 2.2.8).

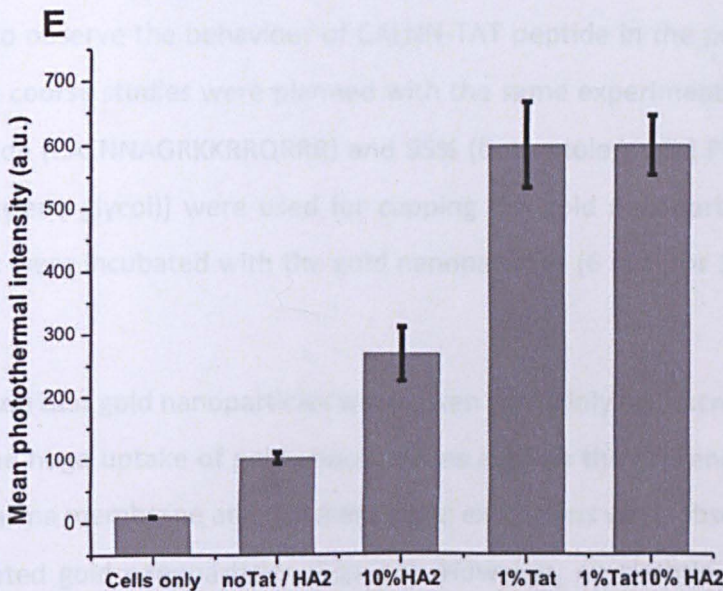
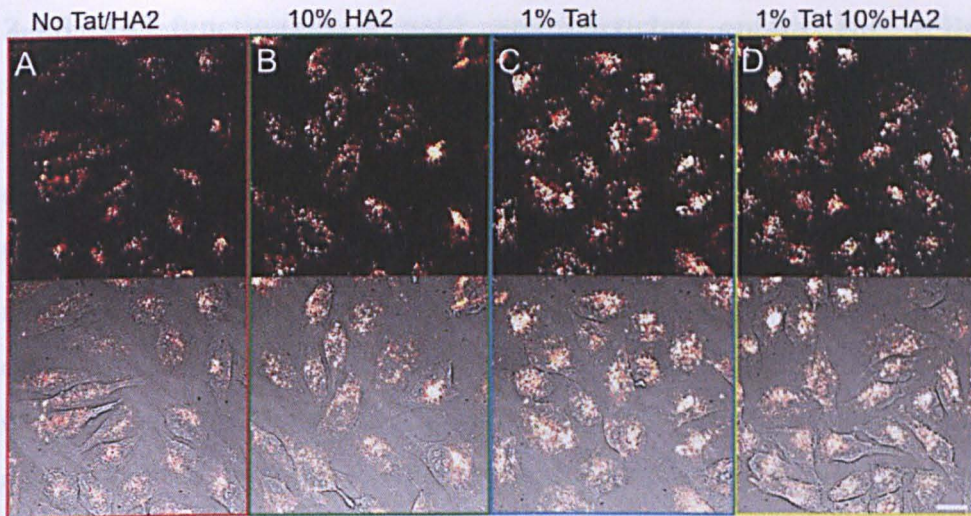


Fig. 2.7 Intracellular delivery and Quantification of CALNN-HA2/CALNN-TAT assisted delivery of gold nanoparticles.

Top: photothermal image; bottom: overlay of the bright field and photothermal images. A) 80% CALNN 20% CCALNN-PEG-gold nanoparticles. B) 10% dCCALNN-HA2 70% CALNN 20% CCALNN-PEG-gold nanoparticles. C) 1% CALNN-TAT 79% CALNN 20% CCALNN-PEG-gold nanoparticles. D) 10% dCALNN-HA2 1% CALNN-TAT 69% CALNN 20% (all mole/mole) CCALNN-PEG-gold nanoparticles. In all conditions, HeLa cells were incubated with 5 nm nanoparticles for 3 h (final concentration 500 nM), fixed and imaged by photothermal microscopy. Scale bar represents 20 μ m.

For quantification, three or four fields of view were analysed per condition to produce whole field mean photothermal intensities for each condition (average of 53 cells per condition) and a mean photothermal intensity was generated by taking the average of the fields mean values (weighted by the number of cells per field). Error bars represent the SE. (Fig. reproduced from Cesbron's PhD thesis, 2010).

2.4.8 TAT-functionalized gold nanoparticles enters the cells mainly via macropinocytosis

Krpetic *et al.* showed cytosolic, nuclear, mitochondrial and endosomal localizations of CALNN-TAT and PEG functionalized gold nanoparticles after 2 h incubation with HeLa cells.²⁸ For cellular entry mechanism, the direct translocation or rapid endocytosis or both mechanisms were proposed. The gold nanoparticles present in organelles and in the cytoplasm were shown to be cleared after 24 h. The endosomes became densely packed with gold nanoparticles at this time. It was also shown that gold nanoparticles were able to escape from the endosomes either through membrane rupture or by direct translocation through the vesicular membrane.²⁸

In order to observe the behaviour of CALNN-TAT peptide in the presence of PEG, the same TEM time course studies were planned with the same experimental conditions. 5% CALNN-TAT peptide (CALNNAGRKKRRQRRR) and 95% (both mole/mole) PEG (11-mercaptopoundecyl-tetra (ethylene glycol)) were used for capping the gold nanoparticles of 15 nm diameter. HeLa cells were incubated with the gold nanoparticles (6 nM) for 10 minutes, 2 h, 24 h and 48 h.

It was found that gold nanoparticles were taken up mainly by macropinocytosis, which could explain the huge uptake of gold nanoparticles even in the presence of PEG. In the images, ruffled plasma membrane and cell membrane extensions were observed with large numbers of associated gold nanoparticles (Fig. 2.8). However, no clathrin-mediated endocytosis of gold nanoparticles was observed. Interestingly, under the TEM approximately 3-7 macropinosomes were seen per section of a cell, with large number of 5% CALNN-TAT 95% (both mole/mole) PEG-capped gold nanoparticles, while most of the cell area was clear (Fig. 2.8 and 2.9). The cellular uptake at different time points was not quantified, but EM images indicate a trend in gold nanoparticles uptake, which was maximum at 2 h and gradually decreasing after 24 h and 48 h incubation with CALNN-TAT and PEG-capped gold nanoparticles. Macropinosomes were seen densely packed with the gold nanoparticles after 2 h incubation, which is in agreement with Krpetic *et al.* (Fig. 2.9).²⁸ In many instances the gold nanoparticles in the vesicles appeared to be clustered and exhibit some sort of ordered pattern (Fig. 2.9, A and Fig. 2.10, C, D). Such ordering would be due to the underlying order of the molecules the nanoparticles are attached to. However, without knowledge of the

identity of these molecules and because of the highly variable presentation of the gold nanoparticles between samples, no statistical analysis was performed to determine whether such distributions may have arisen by chance or represented a real phenomenon. As stated before, the gold nanoparticles have shown a close association with the cell membrane and in some images appeared as entering by direct translocation (Fig. 2.9, A). Clearly this was not the case, as the gold nanoparticles were not seen to penetrate far inside the cytoplasm. Moreover, macropinosomes were present on the borders of the cells, especially after 2 h incubation (Fig. 2.9). Thus, the latter is the likely means of uptake of the nanoparticles in this instance.

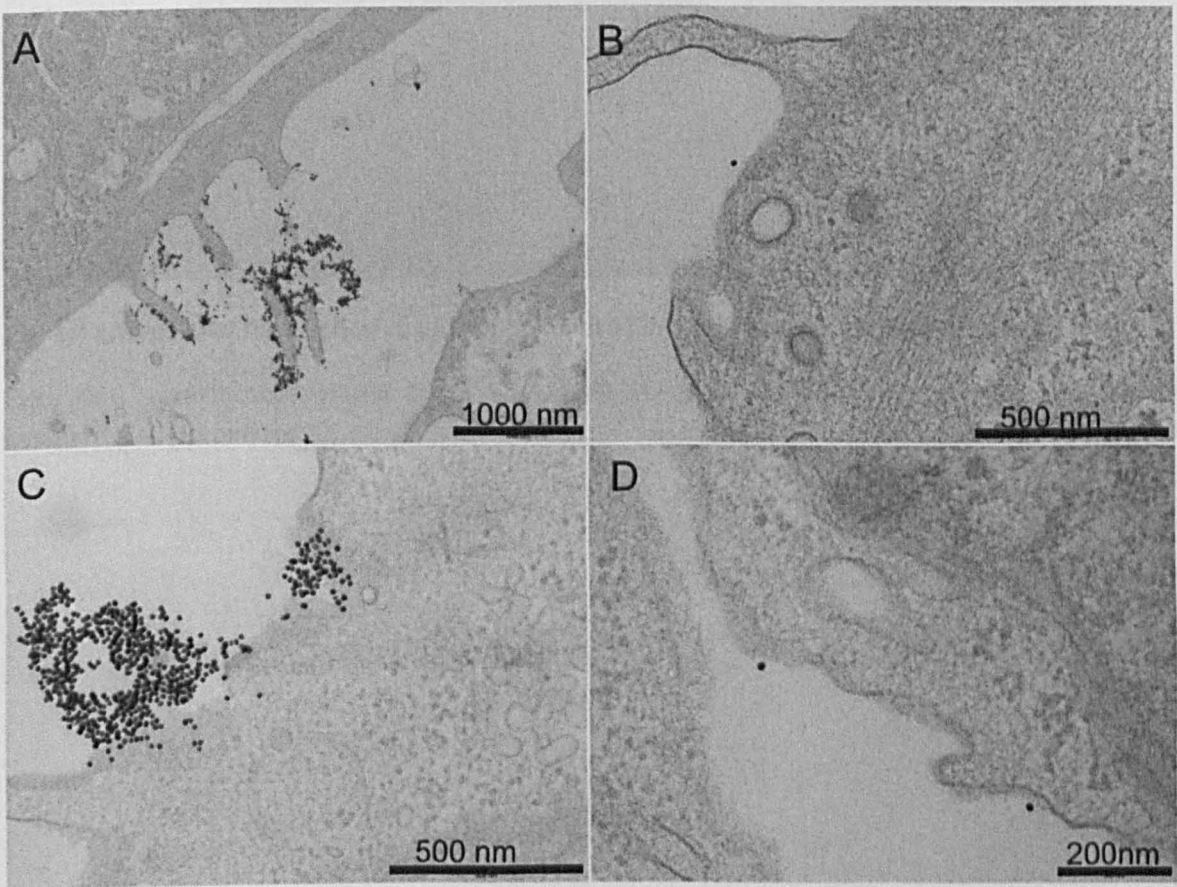


Fig. 2.8 Entry mechanism of CALNN-TAT PEG-capped gold nanoparticles; macropinocytosis

HeLa cells were incubated with 6 nM 5% CALNN-TAT 95% (both mole/mole) PEG-capped gold nanoparticles (15 nm) for A, B) 10 minutes, C,D) 2 h.

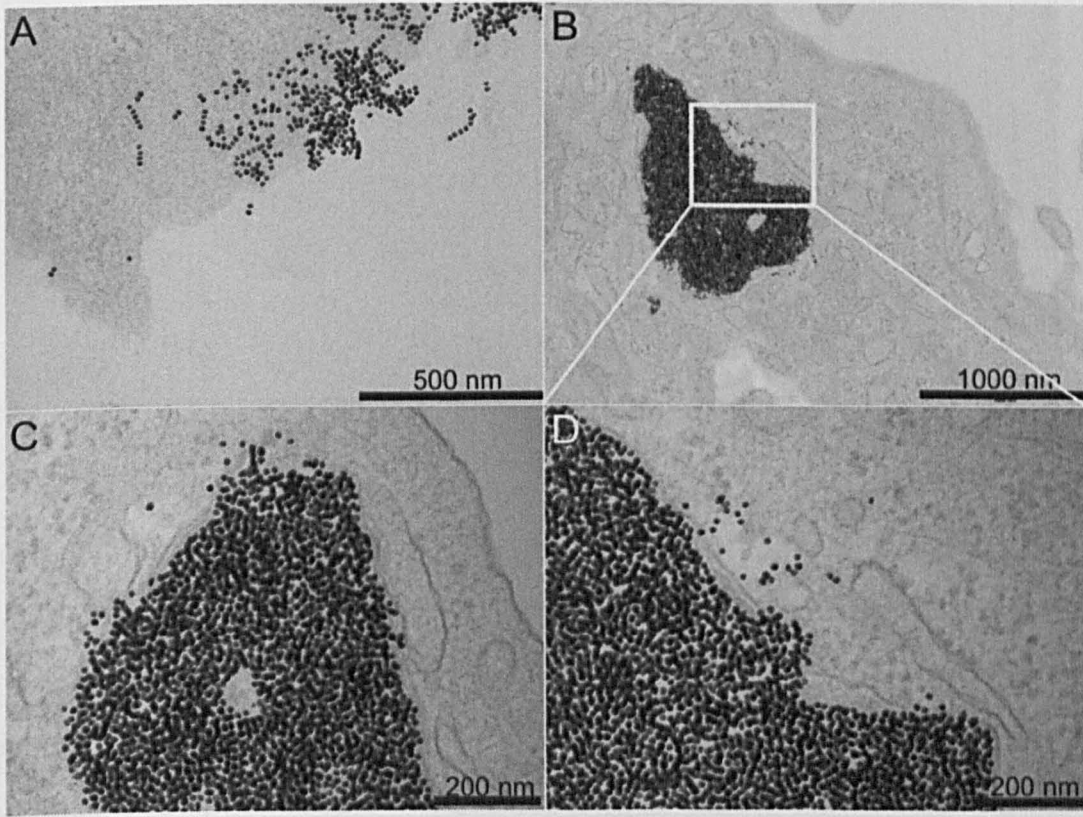


Fig. 2.9 Intracellular localization of CALNN-TAT and PEG-capped gold nanoparticles after 2 h

HeLa cells were incubated with 6 nM 5% CALNN-TAT 95% (both mole/mole) PEG-capped gold nanoparticles (15 nm) for 2 h.

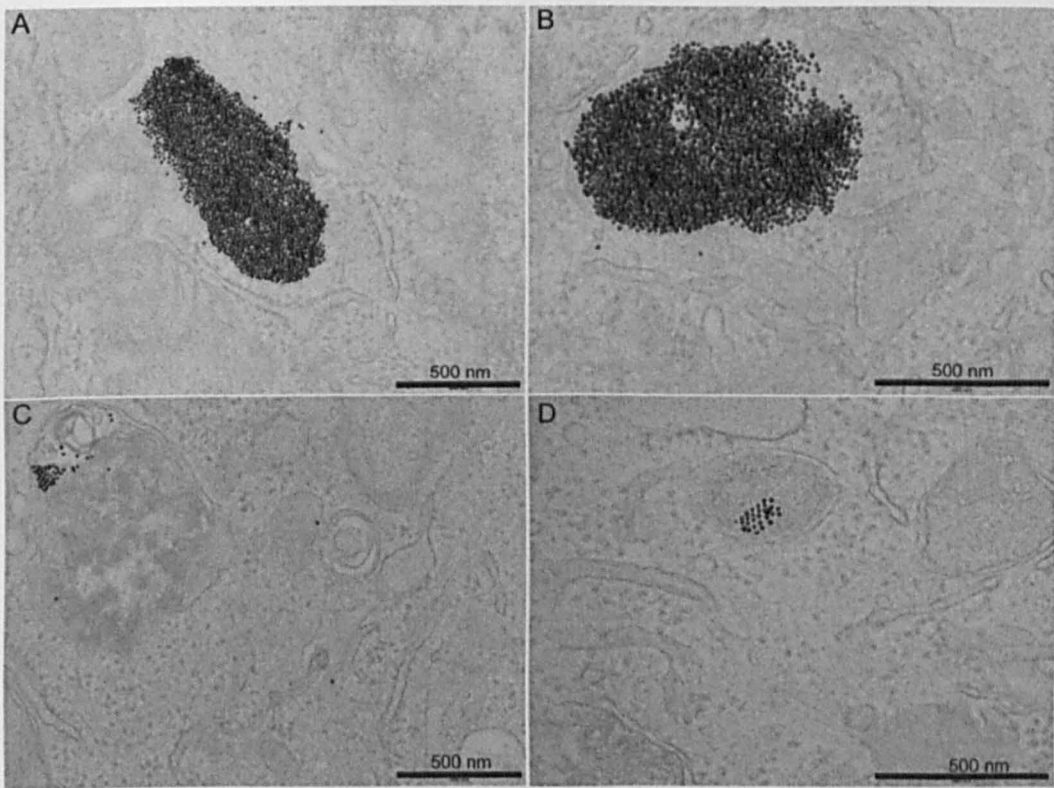


Fig. 2.10 Intracellular localization of CALNN-TAT and PEG-capped gold nanoparticles after 24 h

HeLa cells were incubated with 6 nM 5% CALNN-TAT 95% (both mole/mole) PEG-capped gold nanoparticles (15 nm) for 24 h.

2.5 Discussion

2.5.1 HA2 facilitates cellular uptake of gold nanoparticles

The increase of sCALNN-HA2 nanoparticles from 5% to 50% or 100% resulted in a higher cellular uptake. This effect of increased uptake related to the conjugation of HA2 to the nanoparticles was reported by Wang et al., who showed a dependence of cellular uptake of sCALNN-HA2 on the concentration of HA2. However, we reported no quantitative increase in sCALNN-HA2 uptake by HeLa cells, but we have observed an increase in cellular uptake of HA2-coated TAT peptide (Fig. 2.5).²⁸ Our observation of an increase in uptake of our HA2-coated nanoparticles may be due to the presence of HA2 on the surface of the nanoparticles, which may facilitate their uptake by the cells.

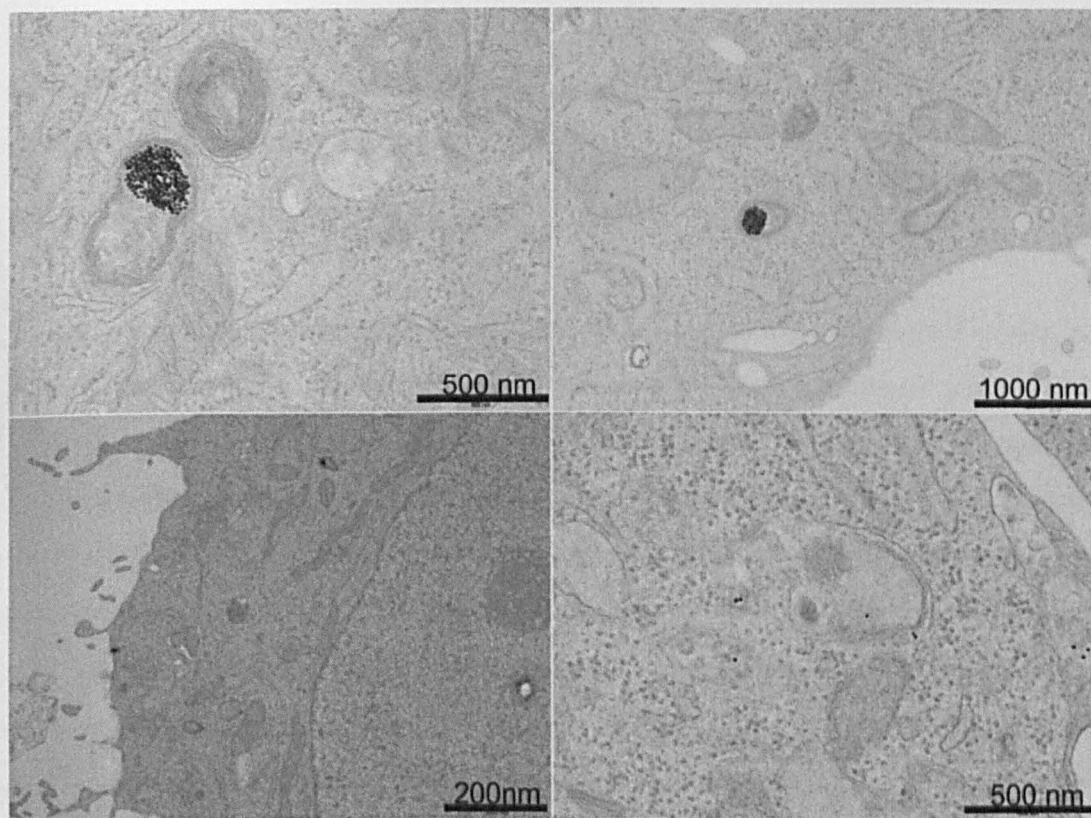


Fig. 2.11 Intracellular localization of CALNN-TAT and PEG-capped gold nanoparticles after 48 h

HeLa cells were incubated with 6 nM 5% CALNN-TAT 95% (both mole/mole) PEG-capped gold nanoparticles (15 nm) for 48 h.

2.5 Discussion

2.5.1 HA2 increases cellular uptake of gold nanoparticles

The increase of dCCALNN-HA2 mole percentage in the SAM of gold nanoparticles from 10% to 50% or 100% resulted in a higher cellular uptake of gold nanoparticles (Fig. 2.3). A similar effect of increased uptake related to the coverage in functional group was reported by Giljohann *et al.*, who showed a dependence of nanoparticles cellular uptake on the density of oligonucleotide loading on the nanoparticles surface.³⁰ For free peptides, Sugita *et al.* reported no quantitative increase in FITC-TAT cellular uptake in the presence of HA2-fused TAT, but we have observed increased cellular uptake for FITC-TAT in the presence of HA2-fused TAT peptide (Fig. 2.6).²⁹ Our observation is corroborated by Wadia *et al.* who reported an increased uptake of dextran–Texas red fluid-phase marker in the presence of dTAT or

dTAT-HA2 peptides.²⁵ The present results are also in agreement with those reported by Cesbron *et al.* for increased uptake of HA2-containing gold nanoparticles, using photothermal imaging based quantification (Fig. 2.1).²⁷

2.5.2 Cytosolic delivery of gold nanoparticles?

As far as cellular localization is concerned, no statistically significant (test) cytosolic distribution has been observed for gold nanoparticles functionalized with HA2 and its derivatives. We found that the presence or absence of CCALNN-PEG in SAMs did not have a significant (test) effect on vesicular localization of ccalnnHA2-containing gold nanoparticles (Fig. 2.2). Similarly, no effect of the HA2 orientation could be observed on the localization of gold nanoparticles (Fig. 2.4). Although we have observed the interaction of gold nanoparticles with the vesicular membranes characterized with typical arrangement of HA2-capped gold nanoparticles along the borders of endosomes (Fig. 2.3, 2.4,) and then a few gold nanoparticles were found around the endosomes (Fig. 2.2, 2.4) , but not a single image has been seen with evenly dispersed cytosolic localization of HA2-containing gold nanoparticles. It seemed that HA2-containing gold nanoparticles were able to destabilize the endosomal membrane, but would not further disperse in the cytoplasm. Esbjörner *et al.* showed a similar effect, while comparing the fusion activity of two types of HA2 peptides with lipid vesicles. Despite a 100% leakage activity by both types of HA2, vesicles did not burst.⁹

Recently, Lee *et al.* showed that HA2 fused proteins were not able to release from the endosomes despite endosomal lysis.³¹ A HA2 analog E5 (GLFEAIAEFIENGWEGLIEGWYG) fused with TAT and a model fluorescent protein mCherry (E5-TAT-mCherry) was used for delivery of TAT-mCherry, mCherry and fluorescent dextrans. It was concluded that E5-TAT-mCherry in the presence of E5-TAT was able to deliver fluorescent dextran, mCherry or TAT-mCherry into the cytosol, but itself was stuck inside endosomes. The proposed mechanism responsible for endocytic localization of E5-TAT-mCherry was the strong interaction of E5 with lipid bilayers. The data further suggest that introduction of a disulfide linkage between the E5-TAT and protein cargo (E5-TAT-S-S-mCherry) can lead to cytosolic delivery of protein cargo.³¹

2.5.3 TAT: entry mechanism and cytosolic delivery

Wadia *et al.* had shown the macropinocytotic uptake of TAT peptide by blocking all other types of endocytosis.²⁵ We have found that, even in the absence of any endocytic inhibitors for receptor mediated endocytosis, 5%CCALNN-TAT and 95% (both mole/mole) PEG-capped gold nanoparticles showed macropinocytosis as the main entry mechanism. The present result is supported by a recent review about the interaction of protein transduction domains (PTNs) or CPPs *in vivo* and *in vitro* where macropinocytosis has been regarded as main endocytic uptake mechanism for CPPs.³²

We found that intracellular uptake of FITC-TAT peptide alone was far less than when it was co-incubated with HA2 fused TAT peptide. We further observed that in the presence of HA2-fused TAT peptide, there were two or three cells out of at least 30 with clearly diffused cytosolic and nuclear fluorescence signal (Fig. 2.6, D & E).

Kumar *et al.* showed that TAT alone was not enough for targeted cytosolic delivery, but TAT-HA2 in the presence of the targeted moiety, in this case actin antibodies, were found successful to achieve the goal of cytosolic delivery. Kumar *et al.* had shown targeted cytosolic localization of 20 nm gold nanoparticles functionalized with TAT-HA2, actin antibodies and PEG.²⁶

Sugita *et al.* used the HA2-fused TAT peptide for FITC-TAT fused shepherdin delivery and showed the cytosolic localization of FITC-TAT-fused shepherdin. Shepherdin is an anti-cancer drug, which kills the cancer cells. As an evidence for cytosolic localization, fluorescence image of one cell has been shown.²⁹ Another study has represented only a single electron microscopic image for demonstrating nuclear localization of TAT-functionalized gold nanoparticles of around 3 nm size.²⁰ In a follow up study by the same group, the cellular uptake mechanisms were compared for TAT and non TAT-containing gold nanoparticles of 5 nm diameter and again the TAT-functionalized gold nanoparticles were showed in nucleus. However, the represented TEM image for nuclear localization was the same (see the paper published by group in 2007) as shown in the previous study (see the paper published by same group in 2005).^{20, 23}

As discussed in the above paragraph, it is necessary that future studies in this field should critically consider the weight of the evidence provided to support a hypothesis. In many

published reports conclusions are drawn on the basis of only one or two TEM or fluorescence images or flow cytometry results which may not be representative of the localization of molecular cargos inside the cells. Recently, Krpetic et al. observed 5% CALNN-TAT and 95% (both mole/mole) PEG capped gold nanoparticles leaking out of vesicles, although no clear explanation for the mechanism has been proposed.²⁸ We also observed endosomal vesicles full of 5% CALNN-TAT and 95% (both mole/mole) PEG-functionalized gold nanoparticles, but no significant leakage was observed. Under the TEM, there were very few particles found just on the brim or around the macropinosomes, but most of the 5% CALNN-TAT and 95% (both mole/mole) PEG functionalized gold nanoparticles remained confined inside the vesicles at different length of incubation varying from 10 min to 48 h.

Comparing our results those of Krpetic *et al.* results, one possible explanation for the discrepancy could be that a particular density of TAT peptide in the SAM of gold nanoparticles is responsible for breakage of endosomal membrane. A higher TAT peptide proportion in the SAM means a larger proton sponge effect, because of the cationic nature of the peptide. As the density of TAT peptide on the gold nanoparticles cannot be controlled robustly, this variability may be taken as an explanation for the discrepancy. Even in the same laboratory the gold nanoparticles capped with the same TAT peptide and PEG, but with different protocols have given different results. Using the first method described in material and methods, section 2.4.2, gold nanoparticles did not show cellular uptake at all (TEM data not shown) which clearly means that the % molar amount of CALNN-TAT was too low in the SAM of gold nanoparticles. The method of preparing SAM was then modified and all the TEM images presented in this chapter, for 5% CALNN-TAT, 95% PEG (both mole/mole) functionalized gold nanoparticles, are based on second preparation method (material and methods, section 2.4.2). Cesbron *et al.* showed endosomal localization of gold nanoparticles with 1% (mole/mole) TAT in SAM along with PEG and CALNN (Fig. 2.7).²⁷ This result further strengthens the hypothesis of TAT peptide density as responsible factor for cytosolic delivery of gold nanoparticles after destabilizing the endosomes.

The quantitative results of localization studies for 5% CALNN-TAT 95% (mole/mole) PEG-capped gold nanoparticles presented by Krpetic *et al.*, based on TEM images, showed clusters of gold nanoparticles along with freely dispersed gold nanoparticles in the cytosol. The photothermal based quantitative studies for the same experiment can be helpful by

providing a clearer picture about the localization at a larger scale, where gold nanoparticles can be seen in several cells at a time.

2.6 Conclusion and future perspective

We examined the role of different sequences of HA2 peptide or HA2-fused TAT and TAT peptides for delivery of gold nanoparticles. We did not add any other functionality to gold nanoparticles except some PEG in order to reduce the non-specific interaction of gold nanoparticles with the cellular membranes. We also used the gold nanoparticles free labelling system and observed the HA2-fused TAT peptide assisted delivery of FITC-TAT.

In terms of the localization of gold nanoparticles functionalized with HA2 peptide, our results were not different from the already available research findings discussed above. Observing events under the electron microscope, where HA2-functionalized gold nanoparticles were found interacting with vesicular membranes, was never reported before. The cytosolic localization of HA2-functionalized gold nanoparticles was a rare and insignificant event, regardless of absence or presence of PEG and also regardless of the type of sequence of HA2 used, *i.e.*, wild type having 23 amino acid residues and truncated peptide having 20 amino acids residues). Same vesicular localization was observed for fluorescent FITC-TAT when incubated with cells, but in the presence of HA2-TAT peptide a few cells showed a fluorescence signal localized in nucleus and in cytosol.

In terms of quantitative cellular uptake, we found that the interaction of HA2-capped gold nanoparticles with the cellular membranes increases uptake of gold nanoparticles. An increased uptake was also observed for fluorescent TAT peptide (FITC-TAT) in the presence of HA2-TAT peptide. We identified macropinocytosis as a major endocytic mechanism for cellular uptake of 5% CALNN-TAT and 95% (both mole/mole) PEG-capped gold nanoparticles, in agreement with most other studies.

Based on the results discussed in this chapter, it seems that there is limited prospect in the use of HA2 for cytosolic delivery of gold nanoparticles, since it seems that HA2 can destabilize the endosomal membrane by interacting with it, but then would not be able to detach from the membrane. To check this hypothesis, further investigations are required. These could include experiments where the HA2 peptide is attached to the particle via a

disulphide containing linker that could be cleaved in the reducing environment following the destabilization of the membrane.

In order to check the hypothesis that the density of TAT peptide in SAM of gold nanoparticles is causing macropinosome bursting, there is a need for a detailed TEM and photothermal microscopy studies where the mole % of TAT peptide in the SAM of gold nanoparticles is titrated in the presence of PEG ligands.

2.7 Bibliography

1. Skehel, J.J. & Wiley, D.C. Receptor binding and membrane fusion in virus entry: The influenza hemagglutinin. *Annual Review of Biochemistry* **69**, 531-569 (2000).
2. Wagner, E., Plank, C., Zatloukal, K., Cotten, M. & Birnstiel, M.L. Influenza Virus Hemagglutinin HA-2 N-Terminal Fusogenic Peptides Augment Gene Transfer by Transferrin-Polylysine-DNA Complexes: Toward a Synthetic Virus-Like Gene-Transfer Vehicle. *Proceedings of the National Academy of Sciences of the United States of America* **89**, 7934-7938 (1992).
3. Wharton, S.A., Martin, S.R., Ruigrok, R.W.H., Skehel, J.J. & Wiley, D.C. Membrane Fusion by Peptide Analogues of Influenza Virus Haemagglutinin. *Journal of General Virology* **69**, 1847-1857 (1988).
4. Mastrobattista, E. et al. Functional characterization of an endosome-disruptive peptide and its application in cytosolic delivery of immunoliposome-entrapped proteins. *Journal of Biological Chemistry* **277**, 27135-27143 (2002).
5. Bullough, P.A., Hughson, F.M., Skehel, J.J. & Wiley, D.C. Structure of influenza haemagglutinin at the pH of membrane fusion. *Nature* **371**, 37-43 (1994).
6. Cross, K.J., Wharton, S.A., Skehel, J.J., Wiley, D.C. & Steinhauer, D.A. Studies on influenza haemagglutinin fusion peptide mutants generated by reverse genetics. *Embo Journal* **20**, 4432-4442 (2001).
7. Cross, K.J., Langley, W.A., Russell, R.J., Skehel, J.J. & Steinhauer, D.A. Composition and Functions of the Influenza Fusion Peptide. *Protein and Peptide Letters* **16**, 766-778 (2009).
8. Han, X., Bushweller, J.H., Cafiso, D.S. & Tamm, L.K. Membrane structure and fusion-triggering conformational change of the fusion domain from influenza hemagglutinin. *Nature Structural Biology* **8**, 715-720 (2001).
9. Esbjörner, E.K., Oglęcka, K., Lincoln, P., Gräslund, A. & Nordén, B. Membrane Binding of pH-Sensitive Influenza Fusion Peptides. Positioning, Configuration, and Induced Leakage in a Lipid Vesicle Model†. *Biochemistry* **46**, 13490-13504 (2007).
10. Veldhoen, S., Laufer, S.D. & Restle, T. Recent developments in peptide-based nucleic acid delivery. *International Journal of Molecular Sciences* **9**, 1276-1320 (2008).
11. Vives, E., Brodin, P. & Lebleu, B. A truncated HIV-1 Tat protein basic domain rapidly translocates through the plasma membrane and accumulates in the cell nucleus. *Journal of Biological Chemistry* **272**, 16010-16017 (1997).
12. Fischer, R., Fotin-Mleczek, M., Hufnagel, H. & Brock, R. Break on through to the other side - Biophysics and cell biology shed light on cell-penetrating peptides. *ChemBiochem* **6**, 2126-2142 (2005).
13. Derossi, D. et al. Cell internalization of the third helix of the antennapedia homeodomain is receptor-independent. *Journal of Biological Chemistry* **271**, 18188-18193 (1996).
14. Duchardt, F., Fotin-Mleczek, M., Schwarz, H., Fischer, R. & Brock, R. A comprehensive model for the cellular uptake of cationic cell-penetrating peptides. *Traffic* **8**, 848-866 (2007).
15. Berry, C.C. Intracellular delivery of nanopartides via the HIV-1 tat peptide. *Nanomedicine* **3**, 357-365 (2008).

16. Liu, C.J. et al. Enhanced x-ray irradiation-induced cancer cell damage by gold nanoparticles treated by a new synthesis method of polyethylene glycol modification. *Nanotechnology* **19** (2008).
17. Green, I., Christison, R., Voyce, C.J., Bundell, K.R. & Lindsay, M.A. Protein transduction domains: are they delivering? *Trends in Pharmacological Sciences* **24**, 213-215 (2003).
18. Ruan, G., Agrawal, A., Marcus, A.I. & Nie, S. Imaging and tracking of tat peptide-conjugated quantum dots in living cells: new insights into nanoparticle uptake, intracellular transport, and vesicle shedding. *Journal of the American Chemical Society* **129**, 14759-14766 (2007).
19. Fonseca, S.B., Pereira, M.P. & Kelley, S.O. Recent advances in the use of cell-penetrating peptides for medical and biological applications. *Advanced Drug Delivery Reviews* **61**, 953-964 (2009).
20. de la Fuente, J.M. & Berry, C.C. Tat peptide as an efficient molecule to translocate gold nanoparticles into the cell nucleus. *Bioconjugate Chemistry* **16**, 1176-1180 (2005).
21. Nativo, P., Prior, I.A. & Brust, M. Uptake and intracellular fate of surface-modified gold nanoparticles. *Acs Nano* **2**, 1639-1644 (2008).
22. Iversen, T.-G., Skotland, T. & Sandvig, K. Endocytosis and intracellular transport of nanoparticles: Present knowledge and need for future studies. *Nano Today* **6**, 176-185 (2011).
23. Berry, C.C., de la Fuente, J.M., Mullin, M., Chu, S.W.L. & Curtis, A.S.G. Nuclear localization of HIV-1 tat functionalized gold nanoparticles. *Ieee Transactions on Nanobioscience* **6**, 262-269 (2007).
24. Michiue, H. et al. The NH2 terminus of influenza virus hemagglutinin-2 subunit peptides enhances the antitumor potency of polyarginine-mediated p53 protein transduction. *Journal of Biological Chemistry* **280**, 8285-8289 (2005).
25. Wadia, J.S., Stan, R.V. & Dowdy, S.F. Transducible TAT-HA fusogenic peptide enhances escape of TAT-fusion proteins after lipid raft macropinocytosis. *Nature Medicine* **10**, 310-315 (2004).
26. Kumar, S., Harrison, N., Richards-Kortum, R. & Sokolov, K. Plasmonic nanosensors for imaging intracellular biomarkers in live cells. *Nano Letters* **7**, 1338-1343 (2007).
27. Cesbron, Y. (University of Liverpool, Liverpool, 2010).
28. Krpetic, Z. et al. Negotiation of Intracellular Membrane Barriers by TAT-Modified Gold Nanoparticles. *Acs Nano* **5**, 5195-5201 (2011).
29. Sugita, T. et al. Improved cytosolic translocation and tumor-killing activity of Tat-shepherdin conjugates mediated by co-treatment with Tat-fused endosome-disruptive HA2 peptide. *Biochemical and Biophysical Research Communications* **363**, 1027-1032 (2007).
30. Giljohann, D.A. et al. Gold Nanoparticles for Biology and Medicine. *Angewandte Chemie-International Edition* **49**, 3280-3294 (2010).
31. Lee, Y.-J., Johnson, G., Peltier, G.C. & Pellois, J.-P. A HA2-Fusion tag limits the endosomal release of its protein cargo despite causing endosomal lysis. *Biochimica et Biophysica Acta (BBA) - General Subjects* **1810**, 752-758 (2011).
32. Noguchi, H., Matsushita, M., Kobayashi, N., Levy, M.F. & Matsumoto, S. Recent Advances in Protein Transduction Technology. *Cell Transplantation* **19**, 649-654 (2010).

CHAPTER 3

3. Bacterial toxin assisted delivery of capped gold nanoparticles

3.1 Streptolysin O: Mechanism of pore formation

Streptolysin O (SLO) is a 541 amino acid residues bacterial exotoxin secreted by most strains of streptococci bacteria.¹ It can reversibly damage the cytoplasmic cell membrane by forming pores. Bacteria use this naturally acquired mechanism of pore formation to get entry into the cytoplasm of the host cell.²⁻⁴

There are approximately fifteen exotoxins produced by gram positive bacteria of group A streptococci, which can be categorized together due to their similar properties, *e.g.*, water solubility, thiol-activation, oxygen liability and single polypeptide chain structure. Representatives of these toxins include listeriolysin O, perfringolysin O and streptolysin O. SLO is commercially available and it is either extracted from supernatant of streptococci or produced by *E coli* as a recombinant product.³

Sekiya *et al* have done electron microscopy studies to probe streptolysin O pore structure and estimated the internal and external diameters of the pore in an intact cell membrane as 24 nm and 34 nm respectively.¹ Bhakdi *et al.* analyzed the properties of SLO and SLO-induced pore by electron microscopy and gel electrophoresis and proposed a mechanism for pore formation. Essentially, the thiol-activated toxin monomer binds to cholesterol-containing cell membranes and starts to oligomerize by binding more toxin molecules. This oligomerized toxin chain gets inserted into the cell membrane, first forming an arc shape structure, which then completes into a ring shape transmembrane pore/channel with an internal diameter of 24-30 nm. The binding of toxin monomers to cell membrane is a temperature independent process whereas pore formation requires 37°C. There is evidence that arc shape transmembrane slits with free membrane on opposite side can also act as transit channels. Events of the fusion of two arcs were also observed. It was concluded that cholesterol plays a vital role in the initial binding of the toxin molecules to the cell membrane, but doesn't have any role in the further process of pore formation.^{3,5}

The lesions or pores in cell membrane can be resealed by adding fetal calf serum (FCS) as a source of exogenous cholesterol.^{6, 7} Idone *et al.* showed Ca^{2+} and cholesterol dependent repair of SLO induced lesions. Ca^{2+} dependent endocytosis was recognized as the mechanism for membrane resealing and it was shown that cells use the same mechanism for pore lesion resealing and for repairing any mechanical injury to the cell membrane. Kinetics of membrane resealing was also shown to be very fast (seconds) compare to previously reported times for toxin induced pore resealing (minutes to hours).⁸

3.2 Streptolysin O assisted intracellular delivery

Since the discovery that SLO can reversibly permeabilize the plasma membrane, it has been used successfully to deliver many types of biomolecules, *e.g.*, antibodies, proteins, oligonucleotides and Si RNA into the cytoplasm/ nucleus of different cell lines.^{6, 9}

Streptolysin O forms pores wide enough to allow the passage of a molecule with approximately 15- 30 nm diameter.³ To find out the maximum size of molecule, which could enter through the SLO pores, Walev, Bhakdi *et al.* have delivered FITC-labeled dextran of varying molecular weights (4, 80, 150, 260, 500 kDa) and FITC-labeled albumin to the three different cell lines. The cut off value, for SLO-assisted delivery of FITC- albumin and FITC-dextran, was found approximately in the range of 100-150 kDa by flow cytometry and fluorescence microscopy studies respectively.¹⁰

Similarly, Fawcett *et al.* reported the cytosolic localization of 11 kDa, 38 kDa, 148 kDa FITC-dextran and 67 kDa FITC-labeled bovine serum albumin complexes when cells were incubated in the presence of SLO.¹¹

Spiller *et al.* and Berry *et al.* have successfully transfected the mammalian cells with the help of streptolysin O to introduce antisense oligonucleotides into the cytoplasm/nucleus.^{7, 12}

To the best of our knowledge, there is no report of using this toxin for the delivery of nanoparticles inside cells. Our objective was to achieve direct delivery of gold nanoparticles into the cytosol through the pores on the cell membrane thus, avoiding endosomal entrapment.

3.3 Choosing the right conditions

3.3.1 Optimization of SLO amount

Insufficient amount of SLO does not lead to membrane permeabilization and excessive amount leads to cell death. The SLO amount needs to be optimized with particular conditions of experiment for example cell line, temperature, condition of cells (suspended or adherent), medium type and concentration of cells. The amount of SLO also needs to be optimized each time before proceeding to actual experiment, as the toxin activity reduces due to oxidation with the passage of time, even at -80°C . We optimized the SLO amount for both suspended and adherent cells (Fig. 3.1). The procedure and conditions for optimization are given in detail in the material and methods, section 2.8. Briefly the cells were incubated with SLO for 10 min at 37°C in serum-free medium and in the presence of propidium iodide dye (PI). For resealing, pre-warmed serum-containing medium was added to the cells and incubated for 20-30 minutes. Later the medium was replaced with fluorescein-di-acetate-containing fresh medium and cells were imaged under a confocal fluorescence microscope. The amount of SLO, which showed at least 40-50% permeabilized and resealed cells with least overall cytotoxicity was chosen for further permeabilization experiments with gold nanoparticles for each particular experimental condition. Remember, here, the amount of SLO is used not the concentration. However, in figure 3.1 the concentrations were calculated from the amount of SLO used for this particular set of experiments, where the optimum concentration of SLO for suspended cells was 114 nM and for adherent cell, it was 190 nM (Fig. 3.1, B and G). The reasons for optimizing the amount of SLO each time, before performing an actual experiment are that the activity of SLO may change with storage of SLO, temperature and time of incubation, density of cells per unit area (for adherent cells), concentration of cells, batch of SLO and so on.

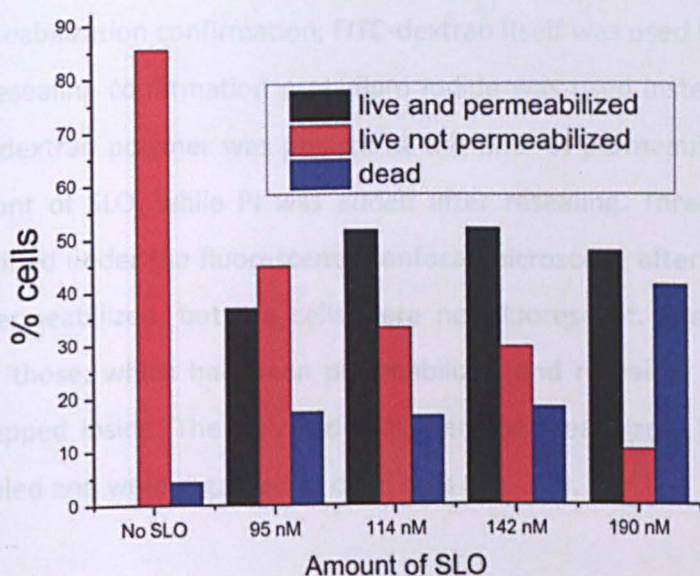
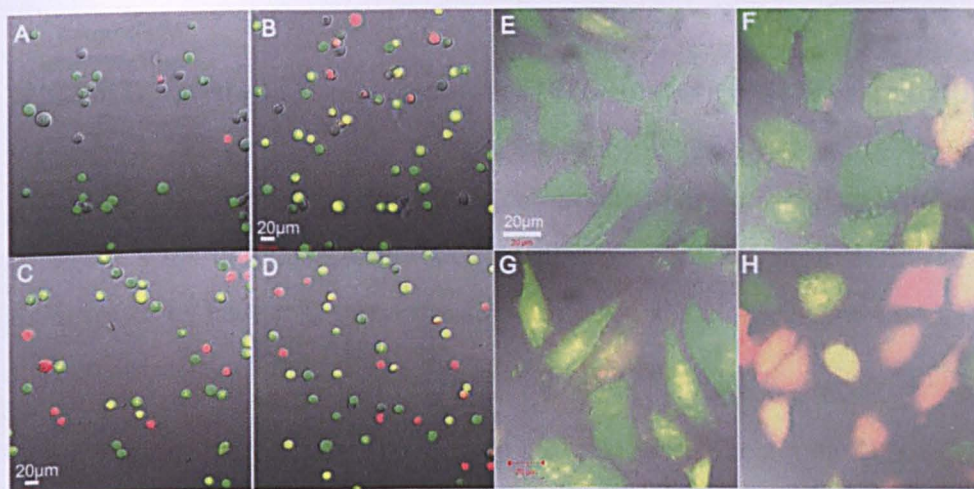


Fig. 3.1: Permeabilization of cells with Streptolysin O.

A-D) Optimized SLO concentration for suspended cells; HeLa cells (4×10^5 cells/condition) treated with or without SLO ($3.8 \mu\text{M}$ (60 kDa); A) no SLO B) SLO (114 nM), C) SLO (142 nM), D) SLO (190 nM). E-H) Optimized SLO concentration for adherent cells: Cells (3.6×10^5 cells/condition) treated with and without SLO E) no SLO, F) SLO 171 nM, G) SLO 190 nM, H) SLO 247 nM. Red colour dye, Propidium iodide (PI) $4 \mu\text{L}$ (1 mg/mL), which can stain only permeabilized cells. Green dye is fluorescein-di-acetate (FDA) $3 \mu\text{L}$ (2 $\mu\text{g}/\text{mL}$), which can stain only live cells. Cells showing yellow color are live and permeabilized. Cells showing only red colour are permeabilized, but not resealed. Cells showing green colour only are live, but not permeabilized.

Bar graph shows the quantified screening for suitable concentration of SLO for maximum permeabilization. Data based on 4 kDa FITC-dextran cellular uptake by the cells in suspension. Percentage of live, dead or permeabilized and live cells was calculated with increasing amount of SLO in the presence of 4 kDa FITC-dextran. For each SLO concentrations, at least 4-5 microscopy fields were analyzed (each field containing 15-20 cells). Unfocused cells in case of suspended cells were not taken into account.

3.3.2 SLO-assisted cellular uptake of FITC-dextran (proof of principle)

In order to confirm the SLO-assisted cell permeabilization and to estimate the pore size, different sizes of fluorescently labeled dextran polymer were delivered into HeLa cells. Scherrer *et al.* have measured the approximate sizes of 4 kDa and 60 kDa dextran as 3 nm and 10 nm, respectively.^{5,13}

The FITC-dextran of 4 kDa, 70 kDa and 150 kDa were chosen for SLO-assisted delivery into HeLa cells both in adherent and suspended cells. The protocol described in material and methods, section 2.12, was used for SLO-assisted delivery of FITC-dextran. For permeabilization confirmation, FITC-dextran itself was used instead of propidium iodide and for resealing confirmation propidium iodide was used instead of fluorescein-di-acetate. The FITC-dextran polymer was present at the time of permeabilization with already optimized amount of SLO, while PI was added after resealing. Three different kinds of cells were identified under the fluorescence confocal microscope after completion of experiment. The un-permeabilized, but live cells were not fluorescent. The cells with green fluorescence were those, which had been permeabilized and resealed, essentially having FITC-dextran entrapped inside. The only red cells were permeabilized, but have not been successfully resealed and were regarded as dead cells (Fig. 3.2).

3.4 Gold nanoparticles co-incubation with SLO

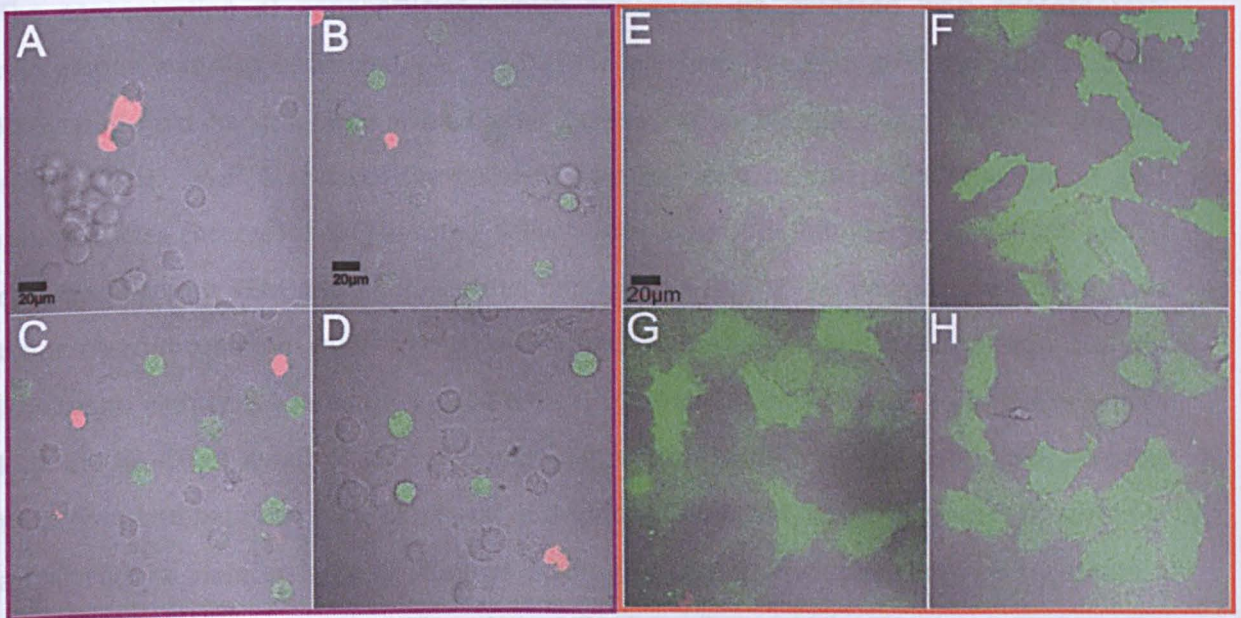


Fig. 3.2 SLO assisted delivery of fluorescein-conjugated dextran of increasing MW (Permeabilization confirmation). (B, F) 4 kDa, (C, G) 70 kDa and (D, H) 150 kDa FITC-Dextran treated cells in the presence of SLO. A, E) 4 kDa FITC-dextran-treated cells in the absence of SLO. 4×10^5 cells/condition for cells in suspension have been used. For adherent cells, 3.6×10^5 cells were incubated overnight before $-/+$ SLO treatment. The amount of SLO is already optimized. Here red cells (PI-stained) are dead cells and green cells are permeabilized and resealed cells. Colourless cells are live, but not permeabilized. Final concentration of FITC-dextran in all conditions is 0.8% (w/v) except for A & B, it is 0.4% (w/v).

FITC-dextran molecules (4 kDa, 70 kDa, 150 kDa) were able to enter both in adherent and in suspended HeLa cells (Fig. 3.2). This is in agreement what Walev *et al.* had found, while delivering the FITC-dextran in three different cell lines, although fluorescence images were shown only for suspended cells.¹⁰ Walev *et al.* have also reported changes in morphology of adherent cells from flat to rounding up, while permeablized with SLO. However, no morphological change was observed in permeabilized and resealed adherent HeLa cells.

of the time HeLa cells require to settle and attach on the dish, the cells were fixed 4 h after SLO treatment and imaged under phase-contrast and transmission electron microscope.

3.5 Effect of PEGylation (Adding the nanoparticles surface properties to avoid endocytosis)

Keeping in mind the well-known fact that PEG reduces the non-specific interaction of gold nanoparticles with cells, it was hypothesized that increasing the percentage of PEG in the

3.4 Gold nanoparticles co-incubation with SLO

The concentration of nanoparticles, which can easily be detected with photothermal microscope was also optimized, *i.e.*, 60-100 nM or above for 5nm gold nanoparticles. For PEGylated gold nanoparticles even higher concentration 600nM was chosen to see the effect of SLO, as PEG reduces the cellular uptake of gold nanoparticles. The size of gold nanoparticles chosen for SLO-assisted delivery was 5 nm, the minimum size, which can be detected by both TEM and photothermal microscopy. During the course of this work, two types of co-incubation were considered: co-incubation with cells in suspension and co-incubation with cells spread on a culture dish. The motivation to use adherent cells was to look at the direct event of gold nanoparticles entry inside the cells, potentially allowing to differentiate between pore entry and endocytosis. However, to work on cells attached in a cell culture plate, a large amount of 5 nm gold nanoparticles is required to obtain a concentration as high as 600 nM in at least 1.5 mL medium, which is necessary to cover the whole 35 mm glass coverslip cell culture dish. Attempts to further minimize the amount of gold use led to large inhomogeneities on the plate presumably due to drying effects.

Therefore, only the suspended cells were being focused, which were co-incubated with the gold nanoparticles and SLO according to the protocol described in material and methods, section 2.11.1. The suspended cells were first incubated with already optimized amount of SLO and gold nanoparticles for 10 minutes at 37⁰C/5% (v/v) CO₂ supply in serum-free medium. In the second step, serum-containing medium was added to the cells to inactivate the toxin and to induce resealing of pores for 20-30 minutes. The gold nanoparticles present in the medium were then removed by centrifugation to avoid further endocytic cellular uptake. The cells were then seeded on either glass cell culture dishes for photothermal microscopy or on Corning cell culture dishes for transmission electron microscopy. Because of the time HeLa cells require to settle and attach on the dish, the cells were fixed 4 h after SLO treatment and imaged under photothermal and transmission electron microscope.

3.5 Effect of PEGylation (tailoring the nanoparticles surface properties to avoid endocytosis)

Keeping in mind the well known fact that PEG reduces the non-specific interaction of gold nanoparticles with cells, it was hypothesized that increasing the percentage of PEG in the

SAM of gold nanoparticles would reduce the cellular uptake of gold nanoparticles via endocytosis, which is essentially the only way of cellular uptake in the absence of any transfection agent. The introduction of CCALNN-PEG in SAM will thus, help to control the surface properties of gold nanoparticles and consequently the interaction of nanoparticles with the cell surface. On the other hand, control on endocytotic uptake of nanoparticles will help to see the SLO effect. To confirm this hypothesis, optimization of CCALNN-PEG amount in composition of SAM of gold nanoparticles was required in order to find out the limit where PEG reduces the non-specific interaction of nanoparticles with the cell membrane moderately. Too much PEG can stop interaction of nanoparticles with membrane altogether, which is not favourable for any delivery system. Four SAMs have been tested (Table 3.1).

Table 3.1 Monolayers of gold nanoparticles for PEG titration

No.	% (mole) of peptides in SAM of gold nanoparticles	Short name
1	0% CCALNN-PEG, 100% CALNN	0% CCALNN-PEG or 0% PEG
2	10% CCALNN-PEG, 90% CALNN	10% CCALNN-PEG or 10% PEG
3	20% CCALNN-PEG, 80% CALNN	20% CCALNN-PEG or 20% PEG
4	30% CCALNN-PEG, 70% CALNN	30% CCALNN-PEG or 30% PEG

CCALNN-PEG and/or CALNN-capped gold nanoparticles (5 nm, 100 nm) were incubated with cells following the same procedure described in material and methods (section 2.11.1), but in the absence of SLO. The quantification of cellular uptake based on photothermal images shows a clear reduction of the endocytotic cellular uptake with the increasing proportion of CCALNN-PEG in the capping layer (Fig. 3.3). 0-20% CCALNN-PEG conditions were chosen for further experiments to evaluate the effect of SLO.

3.6 Streptolysin O-assisted delivery; increased cellular uptake of gold

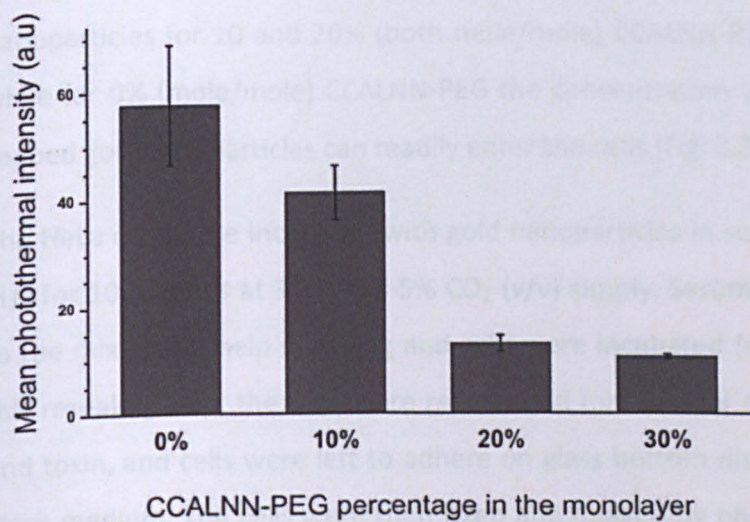
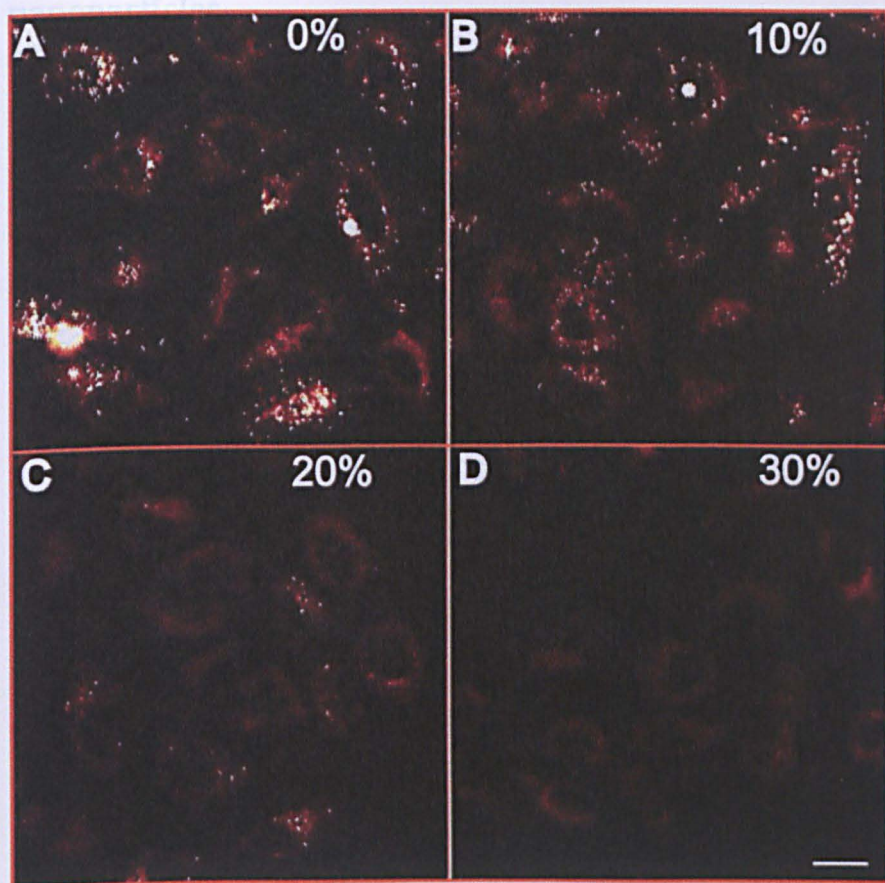


Fig. 3.3 Tuning surface chemistry to control endocytotic uptake (PEG effect)

HeLa cells in suspension were incubated with 5 nm gold nanoparticles (100 nM) coated with CALNN and 0% (A), 10% (B), 20% (C), 30% (all mole/mole) (D) of CCALNN-PEG peptides in the absence of SLO. Gold nanoparticles were removed and cells were incubated in fresh medium for 4 h before fixation for photothermal imaging. Scale bar represent 20 μm . The graph shows a quantification of ~ 50 single cells mean photothermal intensities for the conditions indicated as 0%, 10%, 20% and 30% (all mole/mole) for CCALNN-PEG in SAM of gold nanoparticles. Error bars represent the SE.

3.6 Streptolysin O-assisted delivery; increased cellular uptake of gold nanoparticles

After optimizing the SLO amount for given experimental conditions and knowing the PEG effect on cellular uptake, the suspended HeLa cells were incubated with 5 nm gold nanoparticles capped with CALNN and varying amount of CCALNN-PEG, in the presence (or absence) of SLO. The following SAMs (all mole %) were chosen to passivate the gold nanoparticles:

0% CCALNN-PEG, 100% CALNN (0% PEG)

10% CCALNN-PEG, 90% CALNN (10% PEG)

20% CCALNN-PEG, 80% CALNN (20% PEG)

The goal of using SLO as transfection agent was to achieve cytosolic delivery of gold nanoparticles. It was thought that SLO effect will be maximized for 10 and 20% (mole/mole) CCALNN-PEG as endocytosis with these conditions is either moderate or very low. It was hypothesized that in the case of limited endocytic uptake, the gold nanoparticles present in high concentration outside the cells, will be driven toward the pores (which are formed in cell membrane by toxin) thus, will enter into the cytosol directly. The concentration of gold nanoparticles for 10 and 20% (both mole/mole) CCALNN-PEG was kept high, *i.e.*, 600 nM, while for 0% (mole/mole) CCALNN-PEG the concentration was kept at 100 nM, as CALNN-capped gold nanoparticles can readily enter the cells (Fig. 3.3).

The HeLa cells were incubated with gold nanoparticles in serum-free medium with/without SLO for 10 minutes at 37°C and 5% CO₂ (v/v) supply. Serum-containing medium was added to the mixture to help resealing and cells were incubated for another 20-30 minutes. After this resealing step, the cells were centrifuged for removal of the excess gold nanoparticles and toxin, and cells were left to adhere on glass bottom dishes for 4 h in serum-containing fresh medium. The cells were then fixed and imaged by photothermal microscopy for gold nanoparticles quantification.

In the case of 0% (mole/mole) CCALNN-PEG there was no observable difference between cells incubated with or without SLO (Fig. 3.5). A substantial effect of SLO on cellular uptake of gold nanoparticles was seen with 10% (mole/mole) CCALNN-PEG condition for which

there was a clear difference between cellular uptake of gold nanoparticles with and without SLO. The difference is confirmed by quantitative image analysis (Fig. 3.5; graph B & C, Fig. 3.4; images C & D). With 20% (mole/mole) CCALNN-PEG ligand, which showed quite low endocytic uptake of gold nanoparticles previously in the absence of SLO (Fig. 3.3), the situation was not much different even at 6 times higher concentration in the absence of SLO, but with SLO, a moderate and statistically significant increased cellular uptake of gold nanoparticles was observed (Fig. 3.5; graph A & C, Fig. 3.4; images E&F).

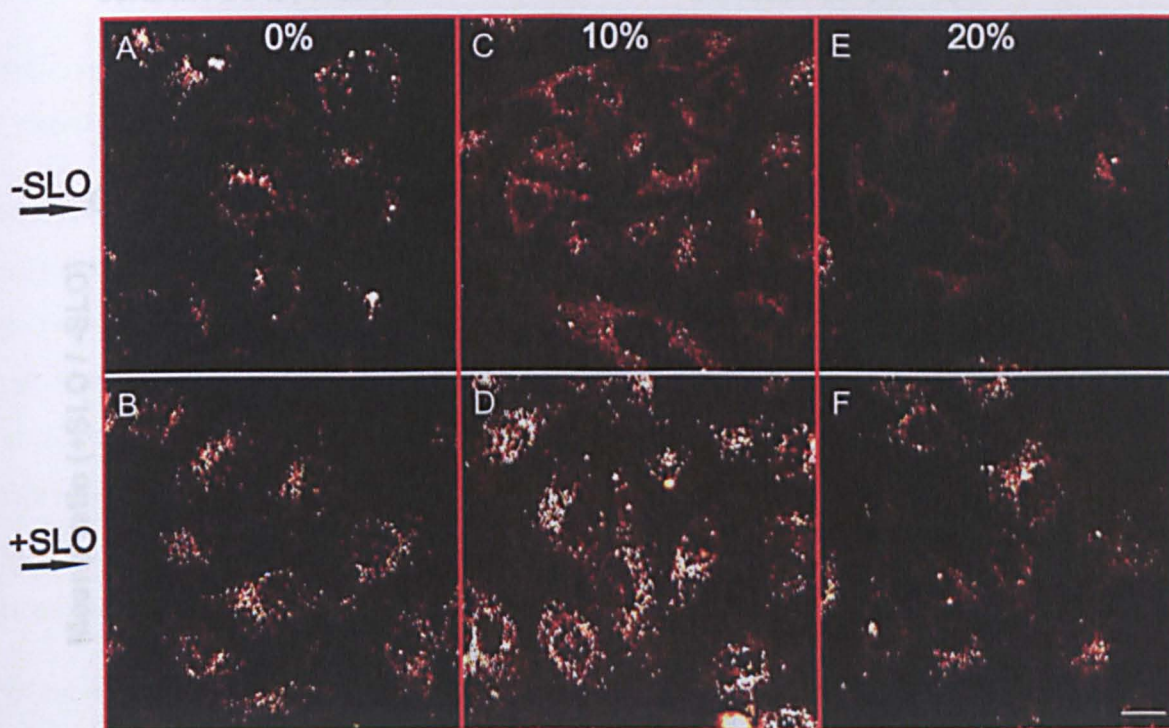


Fig. 3.4 Streptolysin O induced increase cellular uptake of CALNN or/and CCALNN-PEG functionalised gold nanoparticles.

HeLa cells were incubated in suspension with 5 nm gold nanoparticles (100 nM for 0%, 600 nM for 10% and 20% (all mole/mole)) coated with CALNN peptide or CALNN and 10% or 20% (all mole/mole) of CCALNN-PEG peptides in the presence (or absence) of the membrane pore forming toxin SLO. (A, B) Photothermal images of cells incubated with nanoparticles containing 0% (mole/mole) CCALNN-PEG in SAM, in absence or presence of SLO. (C, D) Photothermal images of cells incubated with nanoparticles containing 10% (mole/mole) CCALNN-PEG in SAM, in absence or presence of SLO. (E, F) Photothermal images of cells incubated with nanoparticles containing 20% (mole/mole) CCALNN-PEG in the SAM, in the absence or presence of SLO. Scale bars represent 20 μm .

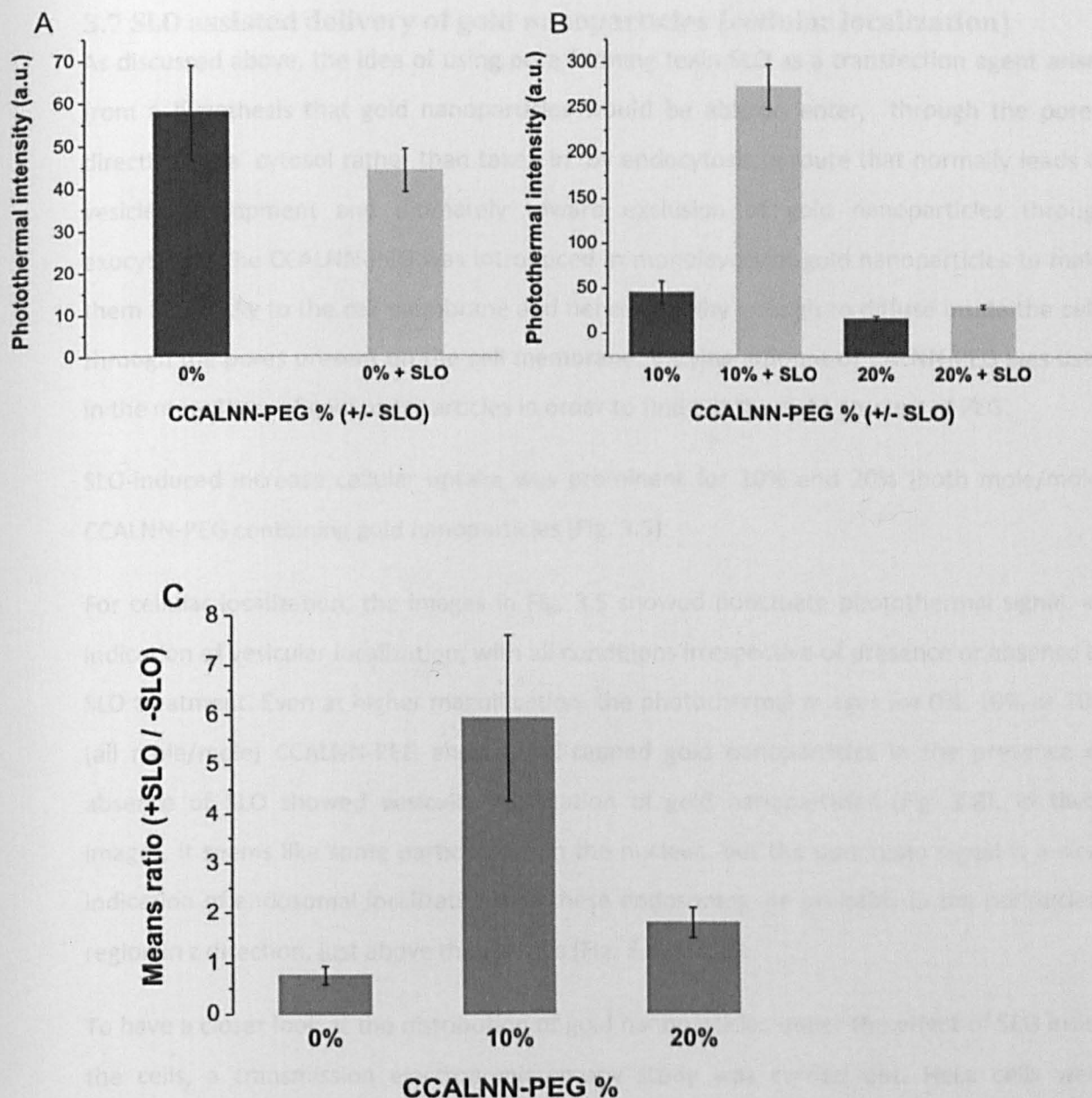


Fig. 3.5 SLO effect: Quantification based on mean photothermal intensities for 0%, 10% and 20% (all mole/mole) CCALNN-PEG conditions with/without SLO. A) Quantification of 64 and 50 single cells mean photothermal intensities for the 0% (mole/mole) condition with/without SLO. The means were not found significantly different (one-way ANOVA test). B) Quantification of approximately 50 single cells mean photothermal intensities for the 10% and 20% (all mole/mole) CCALNN-PEG conditions. Statistically, the means were found significantly different ($p < 0.01$, one-way ANOVA). (C) Same data, which is presented in graph A and B was normalized by +SLO/-SLO. Quantification based on normalized mean photothermal signal intensities for the conditions 0%, 10% and 20% (all mole/mole) CCALNN-PEG. For all six conditions, the mean amount of nanoparticle uptake per cell was appraised by the analysis of 50-60 single cells mean photothermal intensities in each condition. Error bars represent the SE. (graphs adapted from Cesbron's PhD thesis, 2010)

3.7 SLO assisted delivery of gold nanoparticles (cellular localization)

As discussed above, the idea of using pore forming toxin SLO as a transfection agent arises from a hypothesis that gold nanoparticles would be able to enter, through the pores, directly in the cytosol rather than taken in by endocytosis, a route that normally leads to vesicles entrapment and ultimately toward exclusion of gold nanoparticles through exocytosis. The CCALNN-PEG was introduced in monolayers of gold nanoparticles to make them less sticky to the cell membrane and hence stealthy enough to diffuse inside the cells through the pores present on the cell membrane. Varying amount of CALNN-PEG was used in the monolayer of gold nanoparticles in order to find out the right amount of PEG.

SLO-induced increase cellular uptake was prominent for 10% and 20% (both mole/mole) CCALNN-PEG containing gold nanoparticles (Fig. 3.5).

For cellular localization, the images in Fig. 3.5 showed punctuate photothermal signal, an indication of vesicular localization, with all conditions irrespective of presence or absence of SLO treatment. Even at higher magnification, the photothermal images for 0%, 10% or 20% (all mole/mole) CCALNN-PEG and CALNN-capped gold nanoparticles in the presence or absence of SLO showed vesicular localization of gold nanoparticles (Fig. 3.8). In these images, it seems like some particles are in the nucleus, but the punctuate signal is a clear indication of endosomal localization and these endosomes are probably in the perinuclear region in z direction, just above the nucleus (Fig. 3.8, B & D).

To have a closer look at the distribution of gold nanoparticles under the effect of SLO inside the cells, a transmission electron microscopy study was carried out. HeLa cells were incubated with 0%, 10% or 20% (all mole/mole) CCALNN-PEG and CALNN-capped gold nanoparticles in the presence of SLO. EM images for all conditions showed endosomal localization of gold nanoparticles (Fig. 3.7). Due to the difference in the time of incubation between 0% (mole/mole) PEG (15 h) and 10%/20% CCALNN-PEG conditions (4 h), these data were not entirely comparable, but still the difference in the number of gold nanoparticles per endosome among the different (mole %) CCALNN-PEG conditions can be correlated to the photothermal quantification data (Fig. 3.4 and Fig. 3.7). 0% (mole/mole) CCALNN-PEG condition, even at 2 times lower concentration of gold nanoparticles and at least 2 times

longer incubation time showed more gold nanoparticles per endosome than the corresponding 10% or 20% (both mole/mole) CCALNN-PEG conditions.

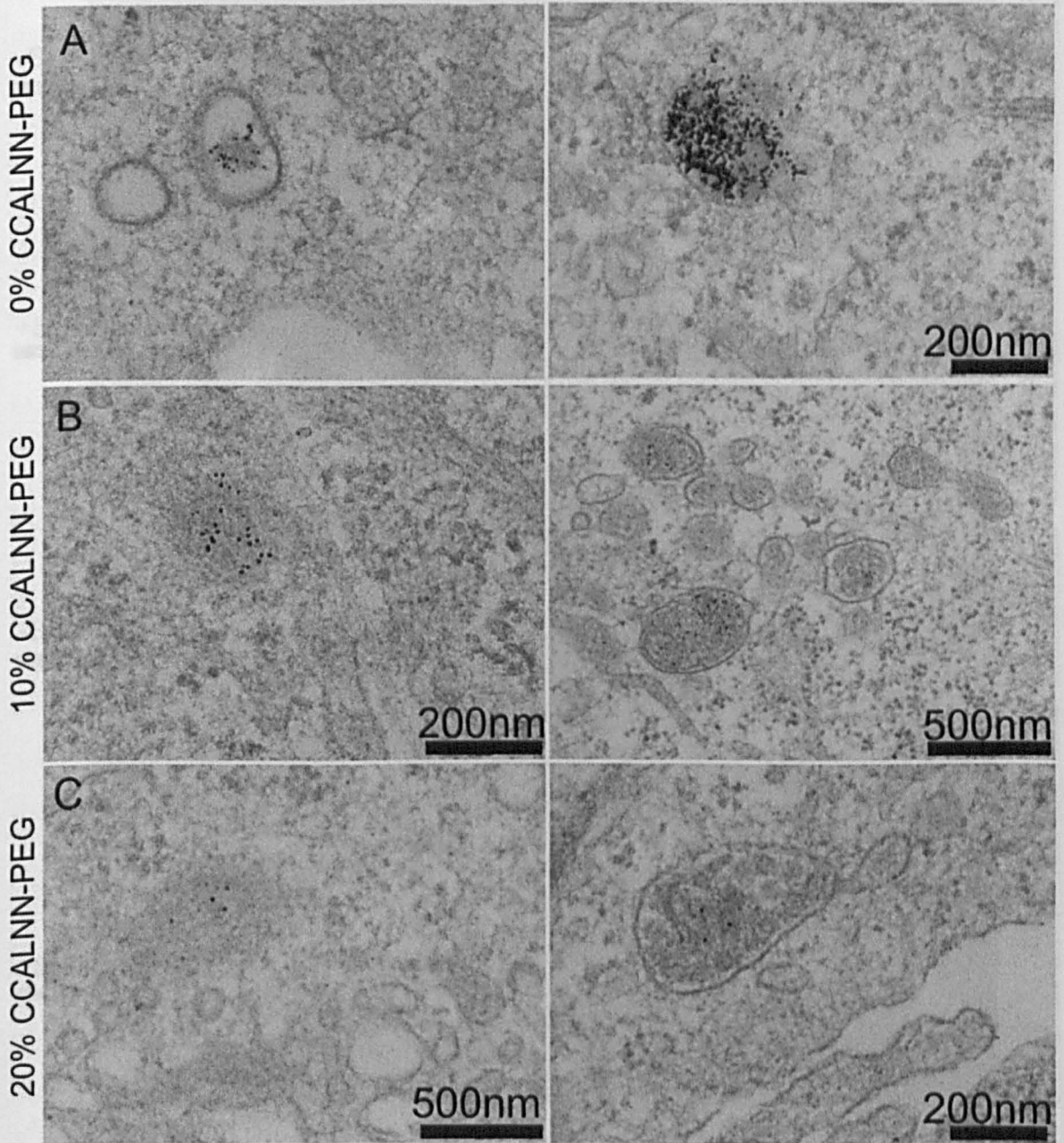


Fig. 3.6 Localization of gold nanoparticles in SLO treated HeLa cells (electron microscopy study)

HeLa cells in suspension were co-incubated with SLO and gold nanoparticles. The cells were then resealed and gold nanoparticles-containing medium was removed. The cells were left to adhere at the dish bottom. For 10% or 20% (both mole/mole) CCALNN-PEG (600 nM), cells were left to adhere in Corning dishes for 4 h and fixed and processed for electron microscopy. For 0% (mole/mole) CCALNN-PEG (400 nM), cells were left to adhere for 15 h before fixation for EM.

3.8 Discussion

Successful stripping of assisted cytoskeletons of antisense oligonucleotides through

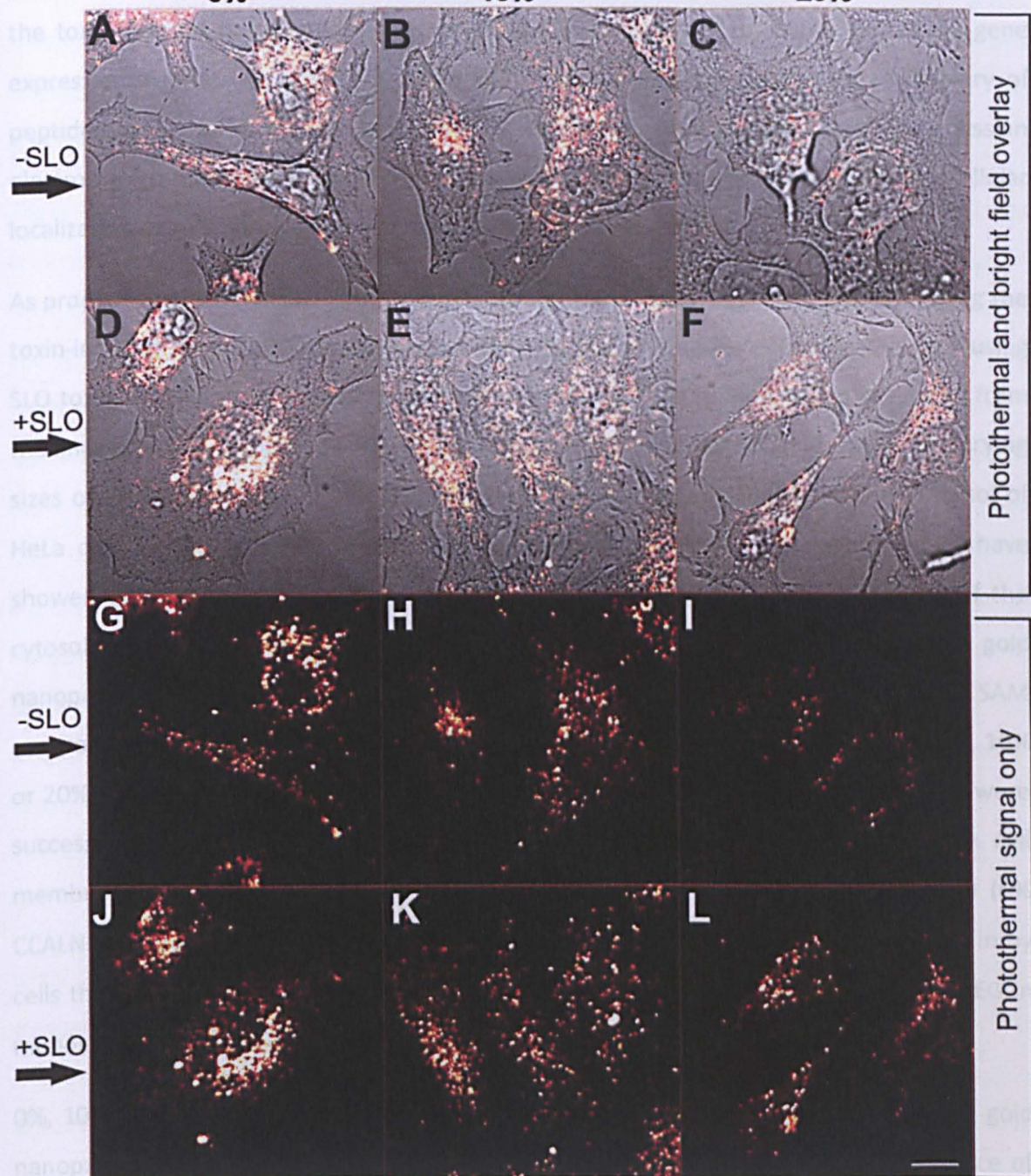


Fig. 3.7 Localization of gold nanoparticles in +/- SLO samples (photothermal microscopy)

HeLa cells incubated with 0% (A, G) or 10% (B, H) or 20% (all mole/mole) (C, I) CCALNN-PEG in SAM of CALNN-capped gold nanoparticles (5 nm) in the absence of SLO. HeLa cells incubated with 0% (D, J) or 10% (E, K) or 20% (all mole/mole) (F, L) CCALNN-PEG in the SAM of CALNN-capped 5 nm gold nanoparticles (300 nM) in the presence of SLO. The images were taken at 2 times higher magnification than Fig. 3.5. Scale bar represent 10 μm .

3.8 Discussion

Successful streptolysin O assisted cytosolic deliveries of antisense oligonucleotides, through the toxin-induced pores present on membrane, was reported to silence or reduce gene expression in different cancerous cell lines.^{6, 7} In this chapter, toxin-assisted delivery of peptide-capped gold nanoparticles was investigated. Photothermal and transmission electron microscopy were employed to assess the overall cellular uptake and intracellular localization of gold nanoparticles in the presence or absence of SLO.

As proof of principle for SLO activity as a cytosolic transfection agent and for estimating the toxin-induced pore size, fluorescent-dextran polymer was delivered inside the cells using SLO toxin. Normally, dextran polymer cannot enter the cells readily, which is evident from the images of cells incubated with FITC-dextran in the absence of SLO (Fig. 3.2, A, E). Varying sizes of FITC-dextran (4, 70 or 150 kDa) were delivered successfully inside the cytosol of HeLa cells in the presence of SLO. The cells co-incubated with polymer and SLO have showed diffused green fluorescent signal all over the cells, which is an indication of the cytosolic localization of the polymer (Fig. 3.2). Next, SLO-assisted delivery of gold nanoparticles with systematic variations in their capping layer was attempted. The SAM composition was modified to include varying proportion (mole %) of CCALNN-PEG (0%, 10% or 20%) and CALNN (100%, 90% or 80%). The surface properties of gold nanoparticles were successfully tuned using CCALNN-PEG for controlling their cellular interaction with cell membrane so that the SLO effect on cell uptake could be identified. 100% CALNN (0% CCALNN-PEG) and 90% CALNN (10% CCALNN-PEG) (all mole/mole) were readily taken in by cells through endocytosis. On the contrary, 20% or 30% (both mole/mole) CCALNN-PEG in monolayer reduced the cellular interaction of nanoparticles dramatically.

0%, 10% and 20% (all mole/mole) CCALNN-PEG monolayers were chosen for capping gold nanoparticles. The cells were incubated with nanoparticles in the presence or absence of SLO. Figure 3.5, graph C shows that when the results are normalized to remove the effect of concentration, no influence of SLO on amount of uptake can be seen for the particles capped only with CALNN, whereas there was a significant increase when particles included a proportion of PEG in their SAMs.

In the presence of toxin-induced pores on cell membrane, a natural hypothesis is that the increased cellular uptake of PEGylated nanoparticles is due to direct entry of nanoparticles through the pores. However, photothermal and electron microscopy studies displayed vesicular localization for all three types of monolayers of gold nanoparticles (Fig. 3.5, 3.6 and 3.7).

There are a number of studies reporting efficient toxin-assisted cytosolic delivery of cargos by flow cytometry measurements, cytosolic fluorescence localization, gene knock down or RNA interference. However, obtaining direct evidence of pore-mediated entry of cargo into the cytosol remains highly challenging because of the difficulties related to the use of a toxin transfection agent. The treatment leads to highly variable levels of transfection and/or distribution of pores. Only 40-50% cells were able to survive after successful permeabilization, while a considerable proportion of cells were live, but unpermeabilized (Fig. 3.2). This makes the visualization of entry events impractical since at the time of transfection there is no certainty whether the cell is going to die or survive. In spite of those difficulties, direct imaging of toxin-mediated entry would be a great progress towards the understanding of permeation. Most of the present information/data about structure of SLO pore are largely based on electron microscopy studies. Looking at the interaction of nanoparticles with pore will be a challenge due to all the limitations stated above plus limitations and artifacts associated with electron microscopy itself.

In a recent study by Chen *et al.*, SLO, electroporation/microporation and TAT peptide have been compared as cytosolic delivery agents for delivery of NeutrAvidin conjugated 2'-O-methyl-modified molecular beacons (MBs) into NIH/3T3 cells.¹⁴ With all three strategies, the MBs were observed in endolysosomes. When the MBs were PEGylated, microporation led to uniformly spread fluorescent signal in the cytosol along with some punctate spots, but the other two strategies showed cells with punctate fluorescent signal.

Specifically with SLO, firstly, the fluorescent signal was detectable at relatively high concentrations of MBs (20 times more than required for microporation) and secondly the authors found great variation not only in total fluorescence signal from cell to cell but also in of the localization of the signal with a small proportion of cells showing cytosolic localization. Images just after resealing (1.5 h) showed few cells both with cytosolic as well

as endosomal localization of fluorescence, but most of the cells showed endosomal localization of fluorescence. After 24 h, all cells showed lysosomal localization of MBs. PEGylation was found not improving overall cellular uptake of MBs with any of the strategies.¹⁴

Chen *et al.* observations about endocytic uptake and variation in fluorescence signal from cell to cell are in accordance to what we observed in HeLa cells co-incubated with SLO and peptide or/and CCALNN-PEG-capped gold nanoparticles imaged with photothermal microscopy.

The results reported in this chapter raise a first question: why peptide-capped gold nanoparticles do not pass through SLO-induced pores, while dextran polymer, oligonucleotides, or proteins (albumin or antibodies) of similar or comparatively bigger physical dimension than 5-8 nm nanoparticles, do enter into the cytosol in the presence of SLO? Possible explanations or hypotheses include differences in the way of interaction, due to the type or charge of cargo, or, impact of the concentration of cargo required to exert an osmotic pressure driving pore-mediated entry:

- a. First, there are very few papers available where SLO has been used for successful cytosolic delivery of proteins or oligonucleotides and secondly, as discussed above, no direct proteins/cargo and toxin-pores interaction has been documented. In such instance it can only be hypothesized that biomolecules interact with the pore in a way, which is different than when they are present on surface of gold nanoparticles.
- b. Charge of biomolecules cannot be taken solely as responsible factor for endocytotic cellular uptake of gold nanoparticles in the presence of SLO. As CALNN peptide has overall negative charge like oligonucleotides and albumin protein for which cytosolic delivery had been shown in the presence of SLO, while CCALNN-PEG is neutral.
- c. It can also be hypothesized that it is the high concentration of cargo, which drives some of the PEGylated molecules into the pores along with parallel endocytic uptake. This hypothesis is reinforced by the observation of Chen *et al.* who found cytosolic and endosomal localization of fluorescent PEGylated neutravidin conjugated 2'-O-methyl-modified molecular beacons (PEGylated-MBs) in the presence of SLO. The concentration of PEGylated-MPs optimized to see the fluorescence signal in the presence of SLO was really

high (3.6 μM).¹⁴ Gold nanoparticles of 5 nm cannot be used in μM concentrations for practical reasons and this was not necessary since even at 0.6 μM concentration of peptide-capped gold nanoparticles, intense photothermal signal was observed (Fig. 3.4).

Given our conclusion that all nanoparticles entry is through endocytosis, a second puzzling question is why an increased uptake is observed in the presence of SLO. We propose that this can be explained by a cellular wound healing response due to calcium influx as has been reported in perforin treated cells and SLO treated cells.^{15 8} This can explain our observation of enhanced uptake of gold nanoparticles induced in SLO treated cells, *i.e.*, an increased endocytosis is induced by the membrane repair mechanism.

3.9 Conclusion and future perspective

To summarize the above discussion, it can be concluded that in the absence of a detailed mechanistic and extent of interaction between the peptide-capped gold nanoparticles and toxin-pore, it is hard to propose any explanation for behaviour where polymer, oligonucleotides, albumin *etc.* were located in cytosol, while peptide-capped gold nanoparticles and non-PEGylated MBs were located in endosomes. May be it is the globular, hard and solid dimensions of the gold nanoparticles, with peptides all around, which is causing them interact/entangle with meshwork of proteins and glycoproteins outside the cell membrane and consequent trapping in endosomes, but this phenomenon alone cannot explain all the results mentioned in this chapter. Further work will be needed to clarify the mechanisms of nanoparticle cell entry in the presence of toxins.

3.10 Bibliography

1. Sekiya, K., Satoh, R., Danbara, H. & Futaesaku, Y. A ring-shaped structure with a crown formed by Streptolysin-O on the erythrocyte-membrane. *Journal of Bacteriology* **175**, 5953-5961 (1993).
2. Alouf, J.E. Streptococcal toxins (Streptolysin-O, Streptolysin-S, Erythrogenic toxin). *Pharmacology & Therapeutics* **11**, 661-717 (1980).
3. Bhakdi, S., Tranumjensen, J. & Sziegoleit, A. Mechanism of membrane damage by Streptolysin-O. *Infection and Immunity* **47**, 52-60 (1985).
4. Bhakdi, S. et al. Staphylococcal alpha-toxin, streptolysin-O, and Escherichia coli hemolysin: prototypes of pore-forming bacterial cytolysins. *Archives of Microbiology* **165**, 73-79 (1996).
5. Palmer, M. et al. Assembly mechanism of the oligomeric streptolysin O pore: the early membrane lesion is lined by a free edge of the lipid membrane and is extended gradually during oligomerization. *Embo Journal* **17**, 1598-1605 (1998).
6. Brito, J.L.R., Davies, F.E., Gonzalez, D. & Morgan, G.J. Streptolysin-O reversible permeabilisation is an effective method to transfect siRNAs into myeloma cells. *Journal of Immunological Methods* **333**, 147-155 (2008).
7. Spiller, D.G. & Tidd, D.M. Nuclear delivery of antisense oligodeoxynucleotides through reversible permeabilization of human leukemia-cells with Streptolysin-O. *Antisense Research and Development* **5**, 13-21 (1995).
8. Idone, V. et al. Repair of injured plasma membrane by rapid Ca²⁺-dependent endocytosis. *The Journal of Cell Biology* **180**, 905-914 (2008).
9. Bhakdi, S. et al. A guide to the use of pore-forming toxins for controlled permeabilization of cell-membranes. *Medical Microbiology and Immunology* **182**, 167-175 (1993).
10. Walev, I. et al. Delivery of proteins into living cells by reversible membrane permeabilization with streptolysin-O. *Proceedings of the National Academy of Sciences of the United States of America* **98**, 3185-3190 (2001).
11. Fawcett, J.M., Harrison, S.M. & Orchard, C.H. A method for reversible permeabilization of isolated rat ventricular myocytes. *Experimental Physiology* **83**, 293-303 (1998).
12. Barry, E.L.R., Gesek, F.A. & Friedman, P.A. Introduction of antisense oligonucleotides into cells by permeabilization with Streptolysin-O. *Biotechniques* **15**, 1016-& (1993).
13. Scherrer, R. & Gerhardt, P. Molecular sieving by bacillus-megaterium cell wall and protoplast. *Journal of Bacteriology* **107**, 718-& (1971).
14. Chen, A.K., Behlke, M.A. & Tsourkas, A. Efficient cytosolic delivery of molecular beacon conjugates and flow cytometric analysis of target RNA. *Nucleic Acids Research* **36** (2008).
15. Stewart, S.E., D'Angelo, M.E. & Bird, P.I. Intercellular communication via the endo-lysosomal system: Translocation of granzymes through membrane barriers. *Biochimica et Biophysica Acta (BBA) - Proteins & Proteomics* **1824**, 59-67 (2012).

CHAPTER 4

4. Intracellular delivery of gold nanoparticles using polymer nanoparticles

4.1 Polymer nanoparticles

Polymers are large macromolecules composed of repeating structural units connected with one another by covalent bonds. Some examples of polymers out of many are plastics, rubber, PVC, polystyrene, polyethylene glycol and biopolymers like DNA, polysaccharides and proteins. As discussed in the introduction (Chapter 1, section 1.2.1) polymeric nanoparticles were the first choice for delivering different types of molecular cargos *in vitro* or *in vivo*, because of the availability of a wide choice of polymeric materials (synthetic or natural), ease of synthesis at large scale and carrying efficiency for virtually all different types of cargos.^{1, 2} The potential of naturally occurring polymers with stimuli-responsive properties has been reviewed for gene delivery to the cytosol and concluded that only few successful efficient endosomal release of the cargo have been reported.³

Destabilizing endosomal membranes using cationic polymers, cationic peptides or pH sensitive polymers or liposomes, has been previously used as one of the possible strategies for cargo delivery to the cytosol, but the efficiency of this system is very low and need further improvement in the design of delivery systems.⁴⁻⁶

Kievit *et al.* have shown successful DNA transfection in a mouse model using polyethyleneimine (PEI). PEI is a cationic polymer capable of inducing vesicular membrane permeability due to the proton sponge effect, thus it has been widely investigated for DNA transfection. The issues related to the use of PEI, *i.e.*, cytotoxicity and poor stability in culture medium, have been overcome by introducing PEG and chitosan grafting with PEI, now called copolymer-PEI (CP-PEI). This CP-PEI complex has been loaded with plasmid DNA and attached to SPIONS to form a NP-CP-PEI complex. PEG has been used to increase the stability and reduced the toxicity of PEI. Chitosan has served as coating for stabilizing SPIONS and they also have increased the binding capability of PEI with DNA. These NP-CP-PEI have shown successful non toxic *in vivo* and *in vitro* delivery of DNA.⁷

Kim *et al.* have encapsulated the actin-antibody functionalized Qdots and MitoTrack Red simultaneously within a pH sensitive biodegradable polymer nanosphere (poly D,L-lactide-co-glycolide) termed a Qdots nanocomposite (QDNCs). Qdots nanocomposites exhibited a high endocytic cellular uptake along with cytosolic localization (104 nm size). The mechanism proposed for cytosolic delivery was the conversion of surface charge of the Qdots nanocomposites to a highly positive one, once inside the acidic environment of lysosomes due to the proton sponge effect. The result was the destabilization of the vesicle and delivery of the Qdots within 3 h of incubation with cells. Qdots containing-polystyrene nanospheres of same size, which had negative charge at all pH values, were used as a control and showed vesicular localization.⁸

The same proton sponge strategy for breaking endosome membranes was used for cytosolic delivery of Qdots attached with PEG grafted hyper branched-polyethyleneimine (PEI-g-PEG).⁹ Two types of grafting densities of PEG with PEI were used, PEG₂, a PEI molecule grafted with 2 PEG chains (PEI-g-PEG₂) and PEG₄, a PEI molecule with 4 PEG chains (PEI-g-PEG₄). It was claimed that PEI-g-PEG₂-coated Qdots have more capability to translocate into the cytosol by breaking vesicles than PEI-g-PEG₄-coated Qdots. However, critical examination of the fluorescence images of HeLa cells after 2 h incubation with PEI-g-PEG₂-coated Qdots or PEI-g-PEG₄-coated Qdots clearly showed a punctate fluorescence, characteristic of vesicular or endosomal localization for both types of Qdots. Two colour co-localization studies for PEI-g-PEG-coated Qdots (red colour) with green DiO (a lipophilic dye, commonly used to stain endosomal vesicles in living cells) have revealed many green punctate fluorescence signals along with one or two red punctate signal for both types of Qdots (PEI-g-PEG₂-coated Qdots and PEI-g-PEG₄-coated Qdots). Furthermore, the red fluorescence signal for PEI-g-PEG₂-coated Qdots in the cytosol was almost indistinguishable from the background. On the other hand, cell viability assay has showed that PEI-g-PEG₂-coated Qdots were more cytotoxic than PEI-g-PEG₄-coated Qdots.⁹

Hu *et al.* used a pH sensitive PDEAEMA-core/PAEMA-shell nanoparticle (CSPs) of 205-208 nm diameter for showing successful cytosolic delivery of many different types of cargos in primary dendritic and endothelial cell lines. These cargos were either adsorbed on the PDEAEMA-core/PAEMA-shell nanoparticle surface via electrostatic interaction or co-incubated with PDEAEMA-core/PAEMA-shell nanoparticle for simultaneous endocytic

uptake. With both types of delivery strategy, the cargos were found to be released into the cytosol due to destabilization of endosomes. The destabilization of endosomes was explained on the basis of cationic proton sponge effect.¹⁰ A detailed model to elucidate proton sponge effect was presented by Hu *et al.* as follows:

“(1) protons and counter ions such as chloride are pumped into the endosomal vesicle to acidify the compartment, (2) the DEAEMA groups (core) in the particles absorb protons, becoming ionized, (3) association of counter ions with now charged DEAEMA groups in the particle core drives osmotic swelling of the particle, and the endosome is disrupted either due to the osmotically driven uptake of water into the endosome caused by counterion build up in the gel particle and the concomitant mechanical pressure of particle swelling.”¹¹

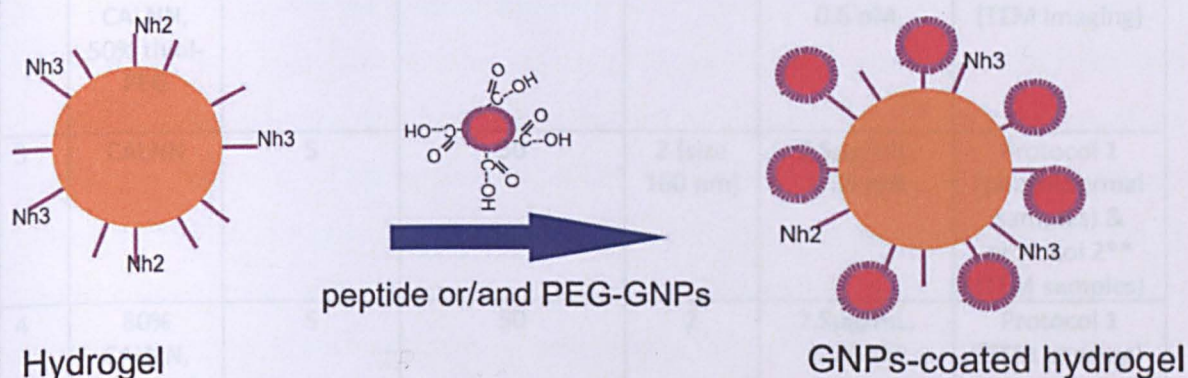
Bayles *et al.* have adopted a similar design, described for PDEAEMA-core/PAEMA-shell nanoparticle, while preparing pH sensitive core-shell cationic polymer colloids (hydrogels), which were able to destabilize endosomal vesicles at low pH because of the cationic core. These hydrogels consisted of a pH sensitive core, poly (2 (diethylamino) ethyl methacrylate) (PDEAEMA) cross-linked via poly (ethylene glycol) dimethacrylate (PEGDMA) to a shell, made up of poly(2-aminoethyl methacrylate) (PAEMA). The hydrogels were claimed to be temperature insensitive and were able to expand 50 times to their original volume at a pH below 6.¹² The volume expansion of hydrogels due to charged solvated core at low pH was regarded as the key factor for destabilizing endosomal membrane.¹²

Negatively charged streptavidin-coated Qdots were attached with the cationic surface of hydrogels due to electrostatic interaction and successful cytosolic delivery of streptavidin-coated Qdots-containing hydrogels was visualized within 4 h of incubation with HeLa cells.¹²

To the best of our knowledge no cationic core-shell polymeric pH sensitive delivery systems have been used so far for targeted intracellular delivery of gold nanoparticles. As the hydrogels are cationic in nature they can carry through unspecific electrostatic interaction virtually any cargo (biomolecules or nanoparticles) that has negative surface charge. I have used CALNN peptide, which leads to negatively charged capped gold nanoparticles and these nanoparticles were adsorbed on hydrogels. Hydrogels were received as a gift from Brett A Helms (Lawrence Berkeley National Laboratory, California).

4.2 Polymer nanoparticles for delivery of gold nanoparticles

I have used these hydrogel for the intracellular delivery of peptide-capped and PEG-capped gold nanoparticles. The basic theme for functionalizing hydrogels with peptide or peptide and thiol-PEG-capped gold nanoparticles is illustrated in scheme 4.1. This scheme is adapted and modified from Bayles *et al.* for streptavidin-capped Qdots-containing hydrogels. The differences include replacement of Qdots with peptide-capped or mix monolayer of peptide and PEG-capped gold nanoparticles.



Scheme 4.1 Functionalization of hydrogels with gold nanoparticles

To elucidate the effect of surface properties of gold nanoparticles on interaction with the hydrogel surface, different monolayers for capping gold nanoparticles have been designed with varying amount of CALNN peptide and PEG (HS-C₁₁-(EG)₄OH). The suitable monolayer should make gold nanoparticles evenly and sparsely distributed on the hydrogel surface. It will leave the cationic moieties to produce maximum proton sponge effect at low pH inside vesicles, allowing the hydrogel to expand and destabilize the vesicle. The gold nanoparticle concentration was also been varied to determine suitable working conditions. The monolayer composition and experimental conditions are summarized in table 4.1. Gold nanoparticles of either 9 nm (batch HB06) or 8 nm (BBI) were used. The synthesis procedure for 9 nm gold nanoparticles is given in materials and methods (section 2.2). For functionalizing hydrogels with peptide or peptide and PEG-capped gold nanoparticles, gold nanoparticles and hydrogels were co-incubated in Dulbecco's PBS (D-PBS) for 12 h at 4°C on rotating carousel (scheme 4.1). Photothermal and transmission electron microscopy (TEM) have been used to visualize the entry and intracellular localization of nanoparticles.

Table 4.1 Experimental conditions for gold nanoparticles functionalized hydrogels

No.	Hydrogel-nanoparticle assembly				Cell uptake	
	Monolayer	Nanoparticle (nM)	Hydrogel($\mu\text{g}/\text{mL}$)	Hydrogel batch	Hydrogel/gold nanoparticles	Incubation protocol
1	CALNN	15.5	10	1 (size 225 nm)	1 $\mu\text{g}/\text{mL}$, 1.55 nM	10 h incubation with hydrogels in medium (TEM imaging)
2	50% CALNN, 50% thiol-PEG	5	50	1	5 $\mu\text{g}/\text{mL}$, 0.5 nM	Protocol 1* (TEM imaging)
3	CALNN	5	50	2 (size 160 nm)	2.5 $\mu\text{g}/\text{mL}$, 0.25 nM	Protocol 1 (photothermal samples) & protocol 2** (TEM samples)
4	80% CALNN, 20% thiol-PEG	5	50	2	2.5 $\mu\text{g}/\text{mL}$, 0.25 nM	Protocol 1 (TEM imaging)
5	50% CALNN, 50% thiol-PEG	5	50	2	2.5 $\mu\text{g}/\text{mL}$, 0.25 nM	Protocol 1 & 2 sets of samples (TEM imaging)

*Protocol 1= Cells were co-incubated with hydrogels and medium for 4 h then incubated in fresh medium for another 2 h.

** Protocol 2 = Cells were co-incubated with hydrogels and medium for 4 h then incubated in fresh medium for another 10 h.

In the following results section, the behaviour of gold nanoparticle-containing hydrogels has been compared mainly for experimental conditions 1, 2 and 3, given in table 4.1 or discussed below in section 4.3.1. The interactions of peptide-capped or peptide and PEG-capped gold nanoparticles containing hydrogels with the cell membrane have been compared for probing the uptake mechanisms adapted by the hydrogels with varying concentration and type of gold nanoparticles. Then the fate of hydrogels inside the cells, whether localized in cytosol, in endosomes or in both have been discussed with the support of TEM images. Furthermore, the potential of hydrogels for breaking the endosomes have been estimated based on TEM observations and finally the cellular localization status of gold nanoparticles present on hydrogel surface have been observed that whether they were able to translocate inside the cytosol.

4.3 Results

4.3.1 Effect of PEGylation and concentration of gold nanoparticles on the interaction with hydrogel

Initially, hydrogels were functionalized with an excess of CALNN-capped gold nanoparticles (table 4.1, number 1), which resulted in aggregated CALNN-capped gold nanoparticles, present in patches on the hydrogel surface (Fig. 4.1, B). This result established clearly the interaction of the hydrogel with the negatively charged CALNN-capped gold nanoparticles. In an attempt to control the gold nanoparticle distribution in hydrogels, the concentration of CALNN-capped gold nanoparticles was reduced and the hydrogel concentration was increased (table 4.1, row 3). The images showed less CALNN-capped gold nanoparticles present per hydrogel, which was expected due to the large change in the ratio between reagents (Fig. 4.1, compare B & C). One concern was that the electrostatic adsorption of CALNN-capped gold nanoparticles might be irreversible, even after endosomal breakage, thereby preventing the detachment of gold nanoparticles from the hydrogel. In order to control the intensity of electrostatic interaction of gold nanoparticles with the surface of hydrogels, alkanethiol-PEG ligands were introduced into the nanoparticle ligand shell. It was hypothesized that as PEG (HS-C₁₁-(EG)₄-ol) is a neutral molecule, *i.e.*, does not have any charge, 50% (mole/mole) PEG in a monolayer of CALNN-capped gold nanoparticles will present 50% neutral and 50% charged surface to the hydrogel, so the electrostatic attachment can be established along with enough flexibility to detach from the hydrogel after coming out of a broken endosome. The electron microscopy imaging showed an even distribution of 50% PEG 50% CALNN-capped gold nanoparticles on hydrogel surface, which can be explained on the basis of steric hindrance experienced by the gold nanoparticles, due to the presence of PEG. On contrary CALNN gold nanoparticles whether present at low concentration or at high concentration on the hydrogel surface, showed patchy appearance (Fig. 4.1).

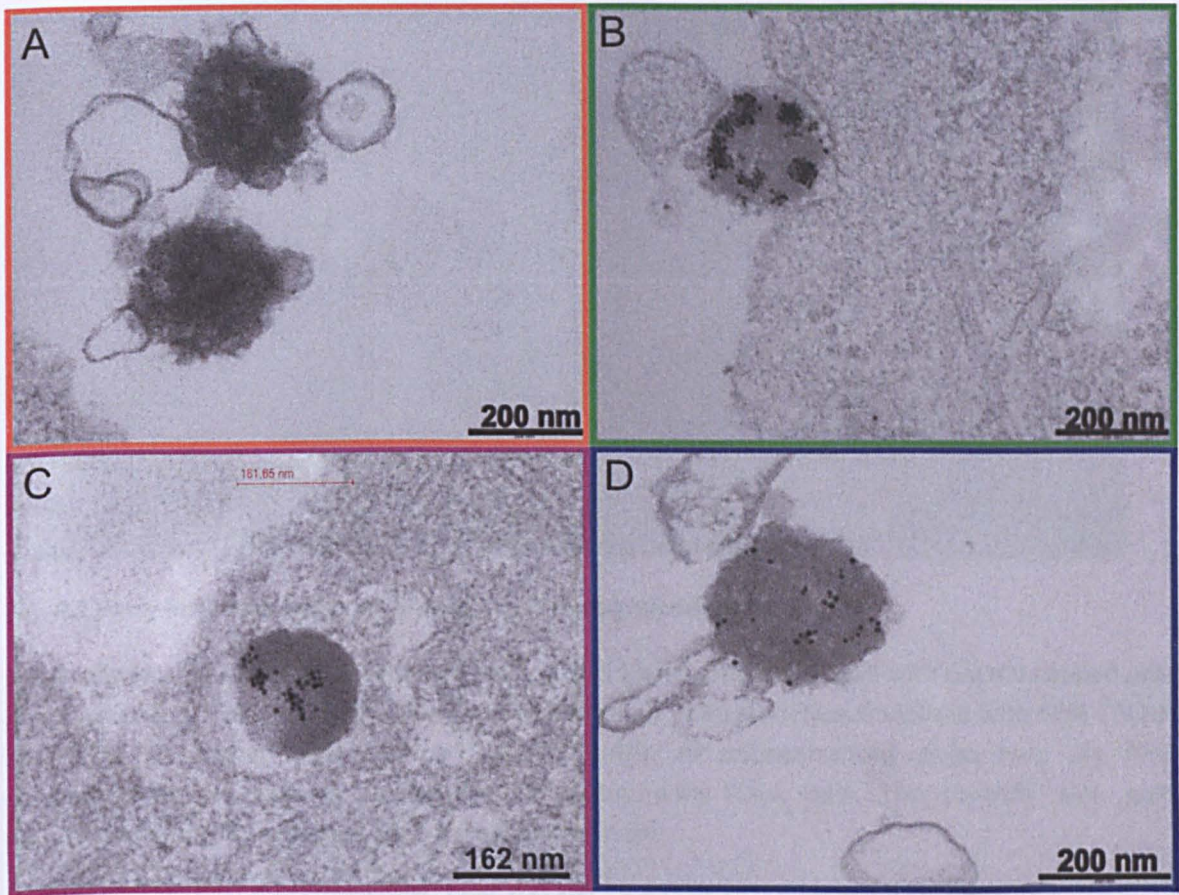


Fig. 4.1 Gold nanoparticles distribution on hydrogel surface HeLa cells (5×10^5 /dish) were cultured overnight and then incubated with A) hydrogels only B) hydrogels (1 $\mu\text{g}/\text{mL}$) functionalized with CALNN-capped gold nanoparticles (1.5 nM) C) hydrogel (2.5 $\mu\text{g}/\text{mL}$) functionalized with 9 nm CALNN-capped gold nanoparticles (0.25 nM), D) hydrogels (4.5 $\mu\text{g}/\text{mL}$) functionalized with 9 nm 50% CALNN 50% PEG-capped gold nanoparticles (0.5 nM). The ratios of hydrogel to gold nanoparticles, for C and D, were identical.

4.3.2 Interaction of hydrogels with the cell membrane

An electron microscopy based investigation was performed to discover the entry mechanism of gold nanoparticles functionalized hydrogels of 160-225 nm size. The hydrogels with densely packed patches of CALNN-capped gold nanoparticles on their surface were found to be taken up mainly by phagocytosis, which is in line with the literature for particles in this size range (Fig. 4.2, upper panel).¹

PEG-capped gold nanoparticles have showed cytosolic localization, as well as an unusual localization (Fig. 4.3, A, B and Fig. 4.4, E, F). The cytosolic localization is unlikely to be an artefact since the hydrogels preserved in the cytosol were found intact spherical, while hydrogels trapped inside vesicles have lost their integrity (Fig. 4.3 and Fig. 4.4). A similar observation was made for the hydrogels without any gold on their surface (Fig. 4.3, C-E). The hydrogels with

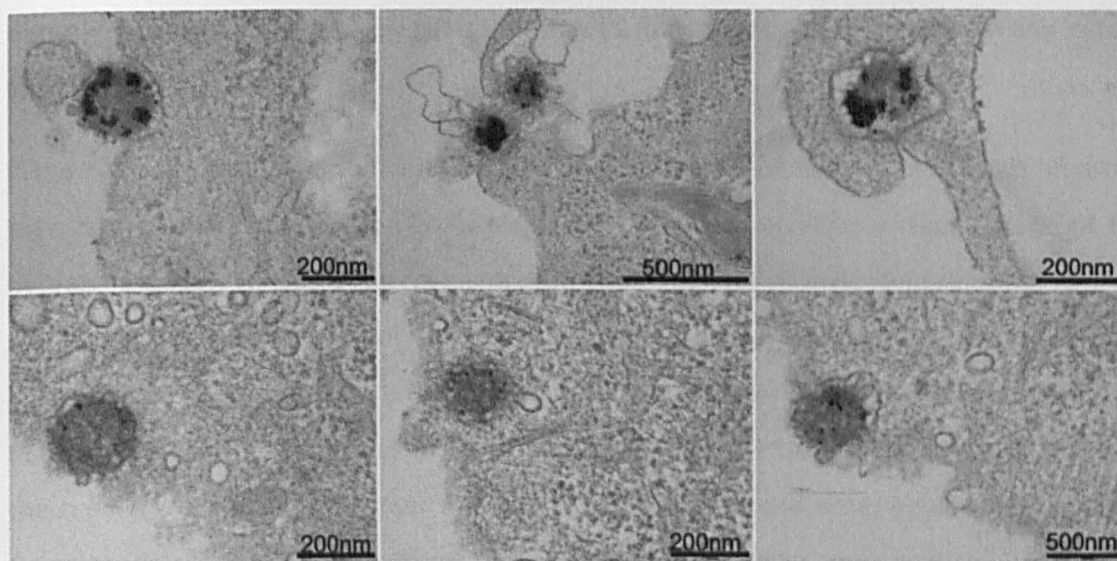


Fig. 4.2 Entry inside the cells: via phagocytosis/direct translocation

HeLa cells incubated with (upper panel) hydrogels (1 $\mu\text{g}/\text{mL}$) functionalized with CALNN-capped gold nanoparticles (1.5 nM) for 10 h, (lower panel) hydrogels (4.5 $\mu\text{g}/\text{mL}$) functionalized with 50% CALNN and 50% PEG-capped gold nanoparticles (0.5 nM). All concentrations given here are final concentrations of reagents during the incubation with HeLa cells. The controls with gold nanoparticles only or hydrogels only are not shown here.

The hydrogels functionalized with 50% CALNN and 50% (both mole/mole) PEG-capped gold nanoparticles on their surface, also showed a mainly phagocytic uptake. However, many events were observed where hydrogels seemed to enter the cells by direct translocation through the plasma membrane through a limited membrane adjacent to the hydrogel (Fig. 4.2, lower panel). The images indicate a strong interaction of cationic hydrogels with the cell membrane and suggest translocation through the membrane. To confirm this scenario, in the next section, the localization of those hydrogel particles after internalization, *i.e.*, further away from the membrane, was examined.

4.3.3 Cytosolic localization of hydrogels: direct translocation through cell membrane

Hydrogels functionalized with 50% CALNN, 50% (both mole/mole) PEG-capped gold nanoparticles have showed cytosolic localization, as well as endosomal localization (Fig. 4.3, A, B and Fig. 4.4, E, F). The cytosolic localization is unlikely to be an artefact since the hydrogels observed in the cytosol were found intact spherical, while hydrogels trapped inside vesicles have lost their integrity (Fig. 4.3 and Fig. 4.4). A similar observation was made for the hydrogels without any gold on their surface (Fig. 4.3, C-E). The hydrogels with

densely packed patches of CALNN-capped gold nanoparticles did not show any cytosolic localization.

If the cytosolic localization of cationic core shell-polymers or hydrogels was not an artefact then how can this observation be explained? The overall positive surface charge of those hydrogels is likely to play a key role, since we observed no cytosolic localization of hydrogels with densely packed patches of CALNN-capped gold nanoparticles on their surface. It can be hypothesized that hydrogels with a sparse loading of 50% CALNN 50% (both mole/mole) PEG-capped gold nanoparticles on their surface still have enough positive moieties to pass the membrane barrier and enter into the cytosol. We should note, however, that even in those conditions (hydrogels with small number of nanoparticles or no particles), a significant proportion do enter by phagocytosis (Fig. 4.4, C-F).

In the experimental conditions for the results described above, both the surface chemistry (PEGylation or not) and the number of particles per hydrogel were varied simultaneously. To distinguish between those parameters, hydrogels functionalized with CALNN-capped nanoparticles using the same concentration ratio for both reagents as used for preparing hydrogels functionalized with 50% CALNN 50% (both mole/mole) PEG-capped gold nanoparticles have been studied for their interaction with the cell membrane and their cellular localization. As these hydrogels with few CALNN-capped gold nanoparticles on the surface were prepared from the second batch of hydrogels, this added one more variable to the experiment, as both the size and the shape appeared to be significantly different from the first batch (size 160 nm instead of 225nm; EM contrast suggests more porosity) (Fig. 4.1, C & D). The second hydrogel batch was also found to be more toxic to the cells and was, therefore, used at a reduced concentration (table 4.1, 3). The second batch of hydrogels with CALNN-capped gold nanoparticles on their surface, hardly showed any cytosolic localization (two EM images after scanning 7 cells, data not shown). Even the hydrogels without any CALNN-particles on the surface did not show any cytosolic localization. Efforts were made to determine the surface properties of the hydrogel with and without gold nanoparticles on their surface using zeta potential measurements, but due to the limited amount of sample and high concentration/volume required for these measurements, no conclusion could be reached. One additional issue was some apparent reactions of the gold decorated hydrogels with the electrode, which led to large fluctuations in the readings.

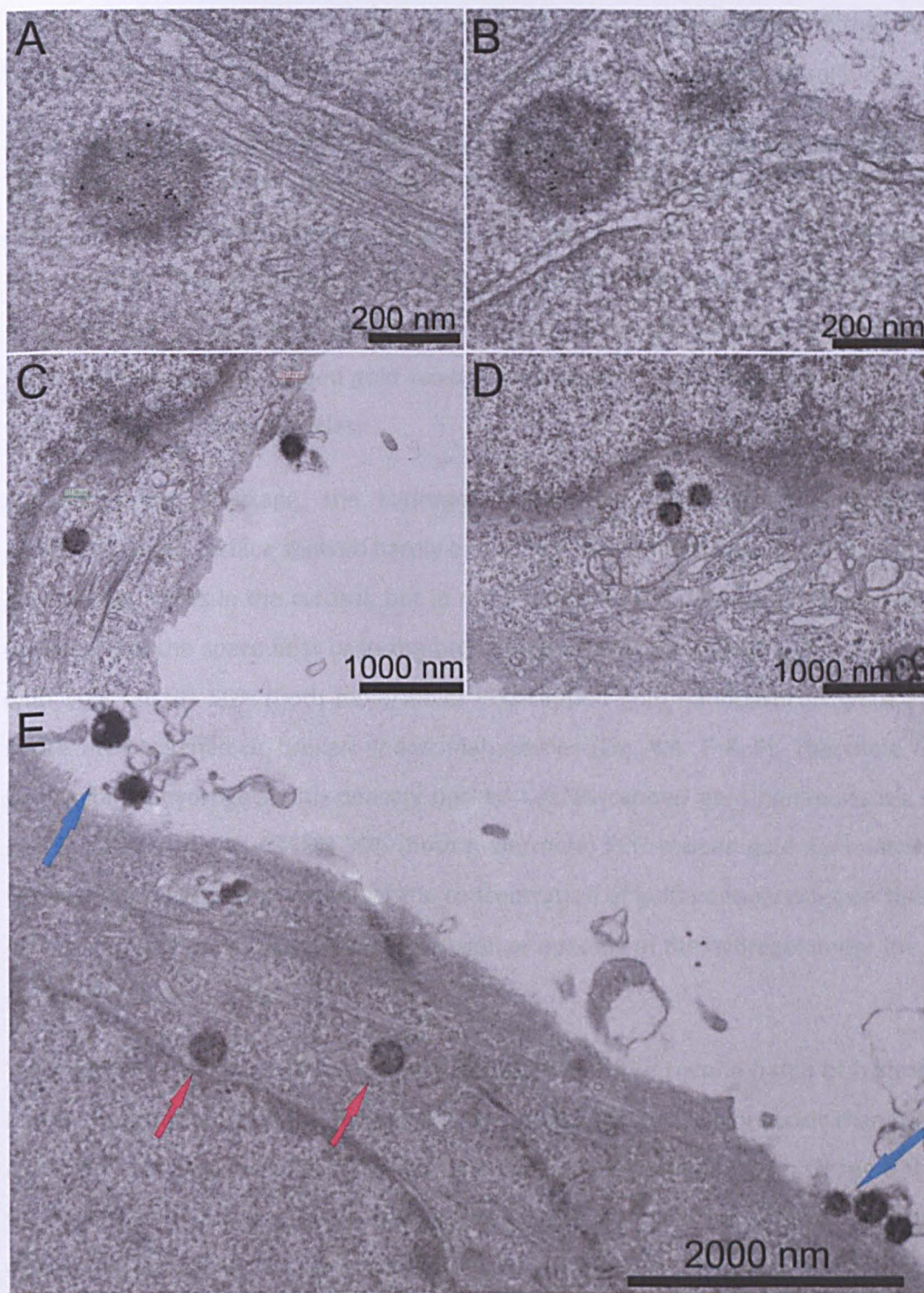


Fig. 4.3 Direct translocation into the cells

A, B) HeLa cells (5×10^5 /dish) were cultured Overnight and then incubated with hydrogels ($5 \mu\text{g/mL}$) functionalized with 9 nm 50% CALNN 50% (both mole/mole) PEG-capped gold nanoparticles (0.5 nM) for 6 (4+2) h, C-E) hydrogels only ($5 \mu\text{g/mL}$). Red arrows indicate hydrogels inside the cells and blue arrows indicate hydrogels outside the cells.

In the next section, we will discuss our observations in the context of the “endosomal breakage” model, which underpins the original design of these hydrogel colloids.

4.3.4 Did endosomal breakage help cytosolic delivery of gold nanoparticles?

The main purpose of using hydrogels for this study was to assess their ability to break the endosomes at low pH, thus delivering the gold nanoparticles, present on their surface, to the cytosol. The hydrogels with densely packed patches of CALNN-capped gold nanoparticles, or a low loading of CALNN-capped gold nanoparticles or of 50% CALNN 50% (both mole/mole) PEG-capped gold nanoparticles, were studied for estimating their ability to break the endosomal vesicles.

For endosomal breakage, the hydrogels having densely packed CALNN-capped gold nanoparticles on surface showed hardly one or two destabilized vesicle showing few CALNN-gold nanoparticles in the cytosol, but in most instances the gold nanoparticles were found stuck around the space near or in the broken endosomal vesicles (Fig. 4.4, A, B). Hydrogels with 50% CALNN 50% (both mole/mole) PEG-capped gold nanoparticles were also found inside the stretched or broken endosomal vesicles (Fig. 4.4, E & F). The same expansion behaviour of hydrogels with densely packed CALNN-capped gold nanoparticles or with a sparse loading of 50% CALNN 50% (both mole/mole) PEG-capped gold nanoparticles inside the vesicles suggested that at least the concentration of gold nanoparticles on the hydrogel surface can not hinder the volume expansion or opening of the hydrogel under the influence of low pH (Fig. 4.4, A, B & E, F).

The experiments described above were repeated with the second batch of hydrogels using half of the concentration for hydrogel, as the second batch was more toxic than the first one (table 4.1, 3). The time of incubation in medium was extended to 14 h to see if this affects the cytosolic delivery of gold nanoparticles after endosomal breakage. However, no endosomal breakage was observed for hydrogels functionalized with CALNN-capped gold nanoparticles (Fig. 4.4, C, D). The second batch of hydrogel was not functional either in terms for endosomal breakage or for gold nanoparticles loading compare to the first batch. The hydrogels incubated with 50% CALNN 50% (both mole/mole) PEG-capped gold nanoparticles didn't show any particles on their surface. The hydrogels (from second batch)

without any gold functionality were also located inside intact endosomes and no cytosolic localization was observed, in contrast to what was observed with the first batch of hydrogels.

The cellular localization of hydrogels functionalized with CALNN-capped gold nanoparticles using the same batch of hydrogels (second batch) at the same concentrations of hydrogels and gold nanoparticles was compared at different times of incubation. The TEM images and photothermal images show that the time of incubation (6 h or 14 h) had no effect on vesicular intracellular localization of gold nanoparticles (compare Fig. 4.5, B, D and Fig. 4.6, D-F).

Summarising the results presented so far, and ignoring the data from the “unfunctional” second batch of hydrogels, the results suggest that hydrogels were able to enter the cells by direct translocation along with parallel phagocytic entry (Fig. 4.3). The hydrogels covered with large numbers of gold nanoparticles did not show any direct translocation deep inside the cells. Inside the vesicles, the hydrogels were able to open, regardless of type or concentration of gold nanoparticles on their surface and few events of endosomal breakage were observed (Fig. 4.4). The hydrogels present in the cytosol due to what appears to be direct translocation showed gold nanoparticles still attached to their surface (Fig. 4.3, A, B).

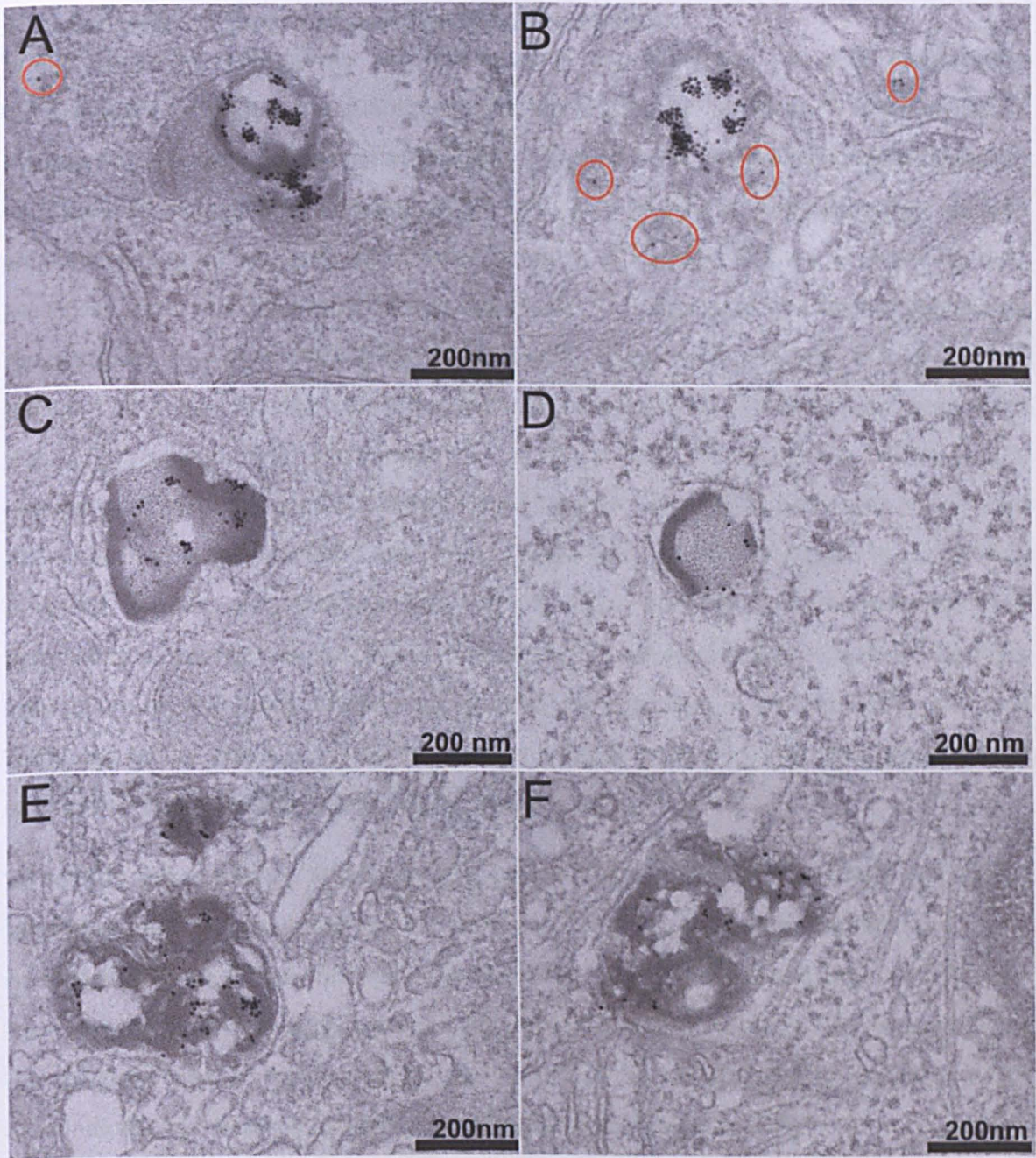


Fig. 4.4 possible low pH induced endosomal breakage by hydrogels

HeLa cells incubated with (A,B) hydrogels (1 $\mu\text{g}/\text{mL}$) functionalized with CALNN-capped gold nanoparticles (1.5 nM) for 10 h, (C, D) hydrogels (2.5 $\mu\text{g}/\text{mL}$) functionalized with CALNN-capped gold nanoparticles (0.25 nM) for (4+10) 14 h (E, F) hydrogels (4.5 $\mu\text{g}/\text{mL}$) functionalized with 50% CALNN and 50% (both mole/mole) PEG-capped gold nanoparticles (0.5 nM). All concentrations given here are final concentrations of reagents at the time of incubation with HeLa cells. The same batch of hydrogel was used in A, B and E, F images.

In the next section, a comparison between the cellular uptake of gold nanoparticles with and without hydrogels is presented.

4.3.5 Increased cellular uptake of gold nanoparticles

While doing the TEM study for investigating the behaviour of gold nanoparticle functionalized hydrogels, the quantitative uptake of gold nanoparticles in the absence of hydrogels was found to be almost negligible compared to the nanoparticle uptake observed with the gold nanoparticles-containing hydrogels. This result was found consistent with all experimental conditions, even with the second batch of hydrogel (Fig. 4.5, C, D and Fig. 4.6). Moreover, both the hydrogels functionalized with densely packed CALNN-capped gold nanoparticles or with a few CALNN-capped gold nanoparticles showed a high level of nanoparticle uptake into the cells compared to the uptake of free CALNN-gold nanoparticles (Fig. 4.5). Indeed, only one image out of 40 showed evidence for CALNN-capped nanoparticles in the cell at 0.25 nM (Fig. 4.5, C) Thus for 50% CALNN, 50% (both mole/mole) PEG-capped gold nanoparticles alone, not a single event of gold nanoparticle uptake was observed, whereas considerable cellular uptake occurred when these nanoparticles were loaded into a hydrogel (Fig. 4.4, E & F). This could be explained on the basis of the reduced interaction of PEGylated CALNN-capped gold nanoparticles with the cell membrane compared to the interaction showed by large cationic surface of the hydrogel decorated with a few PEGylated CALNN-capped gold nanoparticles.

To confirm this conclusion and to get a better overview of uptake at the whole cell level, a photothermal study was planned for hydrogels functionalized with CALNN-capped gold nanoparticles. The images of cells incubated with free CALNN-capped gold nanoparticles have showed almost no signal from the gold nanoparticles. In contrast CALNN-capped gold nanoparticles loaded on Hydrogels showed an intense punctate photothermal signal, which is an indication of endosomal localization of gold nanoparticles (Fig. 4.6).

The photothermal results confirms the TEM data and showed that hydrogels have considerably increased the cellular uptake of gold nanoparticles present in such low concentrations (250-500 pM), which could be hardly detectable even by electron microscopy (Fig. 4.5). Furthermore, the increased cellular uptake of gold nanoparticles (Fig. 4.5, 4.6) present on hydrogels is an observation, which was not affected by different variables, *e.g.*, incubation time, gold nanoparticle concentration, surface chemistry of gold nanoparticles and different batches of hydrogels.

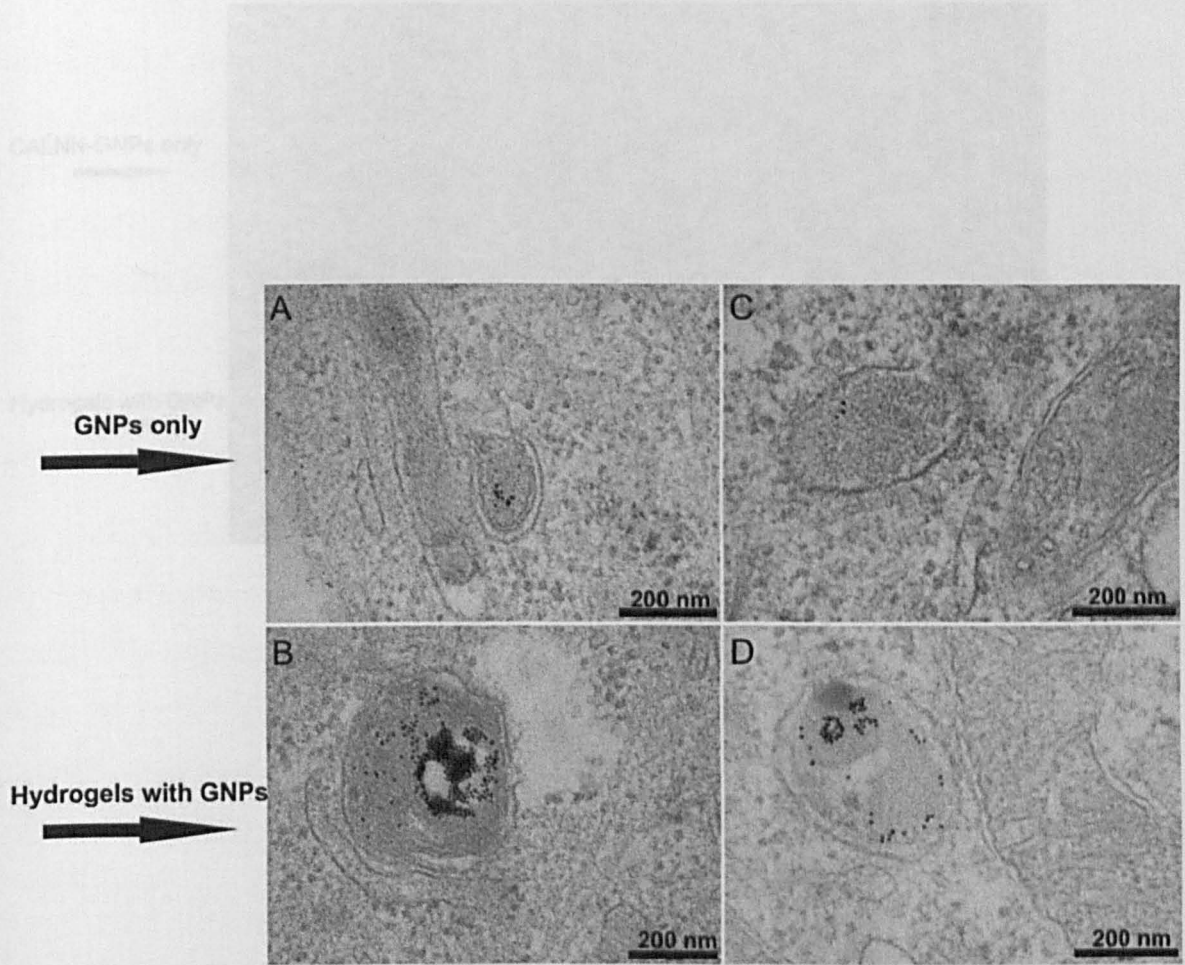


Fig. 4.5 Increased cellular uptake of gold nanoparticles in the presence of hydrogel (Electron microscopy)

HeLa cells were incubated with A) CALNN-capped gold nanoparticles (1.5 nM), B) hydrogels (1 $\mu\text{g}/\text{mL}$) functionalized with CALNN-capped gold nanoparticles (1.5 nM), C) CALNN-capped gold nanoparticles (0.25 nM), D) hydrogel (2.5 $\mu\text{g}/\text{mL}$) functionalized with CALNN-capped gold nanoparticles (0.25 nM). The image shown in C was the only one from a data set of 40 images, taken after searching 5 cells, which has showed some uptake of gold nanoparticles at 0.25 nM concentration.

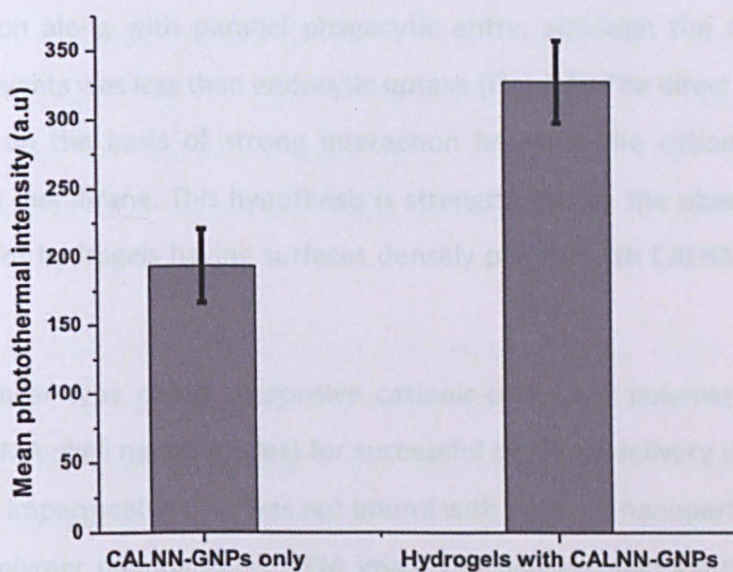
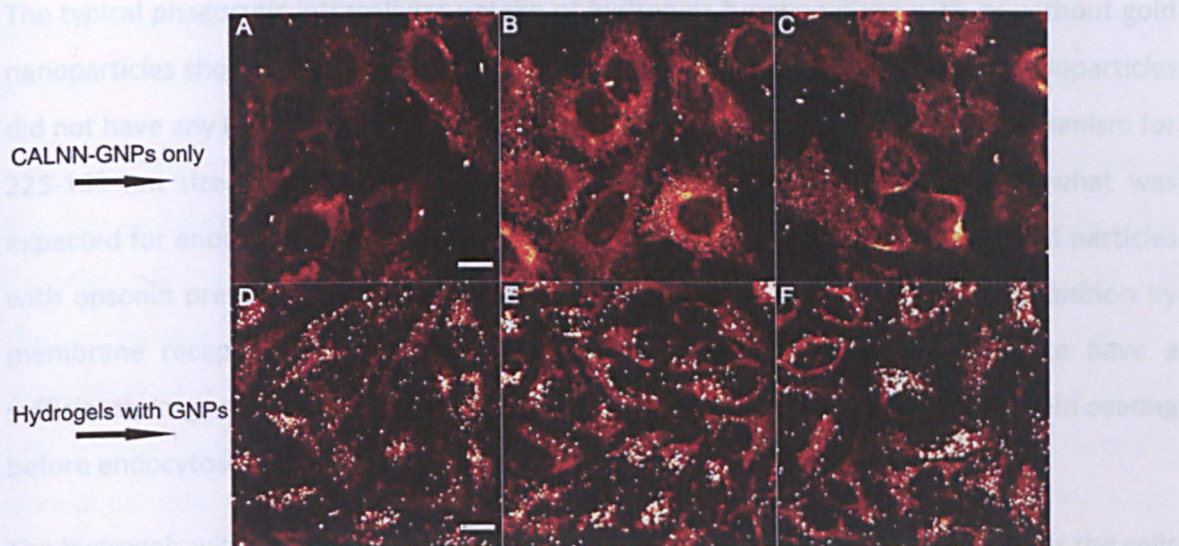


Fig.

Fig. 4.6 Increased cellular uptake of CALNN-capped gold nanoparticles (GNPs) in the presence of hydrogels

HeLa cells were incubated with A, B, C) CALNN-capped gold nanoparticles only (0.25 nM), D, F, G) hydrogels (2.5 $\mu\text{g}/\text{mL}$) functionalized with CALNN-capped gold nanoparticles (0.25 nM) for 4 h, then the cells were washed with warm medium and incubated for another 2 h in fresh medium and fixed for photothermal imaging. All concentrations given here are final concentrations of reagents at the time of incubation with HeLa cells. Scale bar represents 20 μm . Bar graph shows quantification based on whole field method (material and methods, section 2.18.1). Results are the mean \pm SE of the photothermal intensity of at least five different fields chosen at random.

4.4 Discussion

The typical phagocytic intracellular uptake of hydrogels functionalized with or without gold nanoparticles showed that concentration or the surface chemistry of the gold nanoparticles did not have any influence at least on the choice of endocytic cellular uptake mechanism for 225-160 nm size hydrogels (Fig. 4.2). This observation is in accordance with what was expected for endocytic uptake of such a big nanoparticle. Opsonization (coating of particles with opsonin present in serum) of particles is a necessary prerequisite for recognition by membrane receptors for phagocytic uptake, and particles above 200 nm size have a sufficiently large surface area to present for opsonin and complement serum protein coating before endocytosis by phagocytosis.¹

The hydrogels with less or no gold nanoparticles on their surface were able to enter the cells by direct translocation along with parallel phagocytic entry, although the abundance of direct translocation events was less than endocytic uptake (Fig. 4.3). The direct translocation might be explained on the basis of strong interaction between the cationic surface of hydrogel and the cell membrane. This hypothesis is strengthened by the observation of no direct translocation for hydrogels having surfaces densely packed with CALNN-capped gold nanoparticles.

Hu *et al.* used a similar type of pH responsive cationic-core shell polymer nanoparticle (PDEAEMA-core/PAEMA-shell nanoparticles) for successful cytosolic delivery of calcein. The calcein, a membrane impermeable dye, was not bound with polymer nanoparticles, but was co-incubated with polymer nanoparticles. TEM images of polymer nanoparticles revealed that they were present in cytosol, as well as in endosomes after 1 h incubation with dendritic cells. There were more polymer nanoparticles in cytosol (37 out of total 55 polymer particles) than found in endosomes (10 out of 55). The presence of polymer nanoparticles in cytosol was supported by the hypothesis that polymer nanoparticles were able to escape the endosomes after destabilizing them.¹⁰ This explanation for cytosolic presence can be justified, if one assumes the polymer nanoparticles were very efficient at breaking the endosomes within an hour after incubation. In our case, the hydrogels present in the endosomes did not show an intact round appearance, as was shown by the hydrogel present in cytosol after 6 h of incubation with cells. If we adapt Hu.'s hypothesis for explaining our results, then it can be thought that hydrogels escaped the endosomes after

an hour and then most were re-trapped inside vesicles, but a few still free and the polymer particles, which were re-trapped by vesicles were not able to remain intact anymore. This is a highly unlikely explanation.

Hu *et al.* have presented fluorescence images to demonstrate the non co-localization of polymer particles and Lyso Tracker Red DND-99 (an endosomal marker) to support the hypothesis of endosomal escape of polymer particles after 1 h of incubation with cells.¹⁰ If the fluorescence data presented by Hu *et al.* was a time course study to show the initial co-localization of polymer particles and Lyso Tracker Red DND-99 and then the separation of both signals happened, it could be strong evidence of polymer nanoparticles movement from endosomes into the cytosol. Balyes *et al.* have done a time course study, and showed the co-localization of Qdot functionalized hydrogel and DiO (endosomal marker), after 1 h of incubation. The signals for Qdots and DiO were then shown separated in the next 4 h and Qdots were found dispersed in the cytosol.¹² If the images after 1 h incubation are seen critically (in spite of really low resolution), some separate signals for Qdots functionalized hydrogels can be seen along with co-localized signals for Qdots functionalized hydrogels and DiO.

If we now accept the hypothesis that hydrogels have entered by direct translocation through cell membrane along with predominant endocytic uptake, then what factors have allowed this direct translocation and what is the mechanism responsible for the direct translocation of a hydrogel of 200 nm diameter are the questions that need to be answered? As stated in section 4.3.3, while explaining direct translocation, the overall positive surface charge of hydrogels is likely to play a key role, but does not explain the parallel predominant phagocytic uptake of hydrogels; it also does not provide a molecular level mechanism of passage of this object through the membrane. Certainly, more experiments are required, first for reproduction of data and secondly, to understand the direct translocation phenomenon further if there is some direct translocation.

Regardless of the entry mechanism adopted by the hydrogels, we were not able to show the cytosolic dispersion of gold nanoparticles, as was shown for Qdots and for calcein by Balyes *et al.* and by Hu *et al.* respectively.^{10,12}

The hydrogels trapped inside the vesicles were not able to deliver the cargo to cytosol in spite of the fact they were able to stretch regardless of type or concentration of gold nanoparticles on their surface. However, this stretching or expansion was not enough to destabilize a majority of the vesicles (Fig. 4.4). In our observations, the volume expansion of hydrogel was by a factor two and not a factor 50, as had been suggested by Bayles *et al.*¹² The shape of hydrogels was dramatically altered, while expanding under the influence of low pH inside the vesicles (Fig. 4.4). Surprisingly, the intact hydrogels present in cytosol showed the 50% CALNN 50% (both mole/mole) PEG-capped gold nanoparticles attached to their surface even after 6 h (Fig. 4.3, A). It can be hypothesized that CALNN peptide (even in the presence of 50% PEG in monolayer) on gold nanoparticles surface is making them irreversibly attached to the hydrogel surface even after 6 h long incubation time. If it is CALNN peptide responsible for the irreversible adsorption of gold nanoparticles with hydrogel surface, then this could be resolved by replacing CALNN peptide with any other suitable negatively charged peptide or simply using Streptavidin for coating gold nanoparticles as used by Bayles *et al.* for coating Qdots.

“The increased cellular uptake of gold nanoparticles present on hydrogel surface compare to much less cellular uptake of gold nanoparticles alone” is a result, which is in agreement what Bayles *et al.* and Kim *et al.* and Hu *et al.* have found.^{8,10-12}

Similarly, Kim *et al.* have showed significant increase in endocytic cellular uptake of both free and protein-conjugated Qdots encapsulated within poly (D,L-lactide-co-glycolide) (PLGA) nanosphere named as Qdots nanocomposite (QDNCs) compared to free Qdots alone.

The question arises as to why free gold nanoparticles were not able to show same level of cellular uptake as gold nanoparticles loaded in a hydrogel? To explain this difference Kim *et al.* have suggested that the tendency of free Qdots to form aggregates prevented their efficient internalization by SNB 19 cells.⁸ This cannot be taken as an explanation for peptide capped gold nanoparticles as CALNN-capped gold nanoparticles can readily be internalized so the possible answer to this question can be probed with more questions.

Is phagocytosis a more efficient endocytic uptake mechanism compares to other types of endocytic mechanisms, which can normally internalize objects as small as 9 or 8 nm gold nanoparticles?

The preference and efficiency of cellular uptake mechanism for different types of nanomaterials is a complicated phenomenon and will vary with the cell type, incubation conditions and the properties of the cargo to be internalized. It is probably not the matter of efficiency, but of preference. Large hydrogels present a large surface area for opsonin protein coating, which is essential for eliciting phagocytosis. Furthermore, if one takes the rate of endocytosis as equal for both the hydrogel and for an individual gold nanoparticle, the internalization of one hydrogel with many gold nanoparticles loaded on its surface will show more uptake of gold nanoparticles. The surface chemistry of gold nanoparticles is also responsible, as PEGylated CALNN-capped gold nanoparticles did not show cellular uptake, but the same PEGylated CALNN-capped gold nanoparticles loaded evenly and sparsely on hydrogel surface were taken up by the cells (Fig. 4.3, A, B).

Is it simply the larger contact area with cell membrane, which leads to an efficient endocytic uptake of the hydrogel as compared with peptide-capped gold nanoparticles?

This is probably the hypothesis, which can be put forward to explain the increased uptake of gold nanoparticles present on hydrogel compare to free gold nanoparticles alone. No doubt the CALNN-capped gold nanoparticles also show considerable interaction with the cell membrane due to their charged surfaces, but the charged surface presented by a 200 nm hydrogel is much more than that of 9 nm gold nanoparticles.

The observations and results discussed above provide some new insight. However, no definitive conclusions can be drawn from this chapter relating to uptake of gold nanoparticles into the cells, because of the difficulty of controlling all experimental parameters. These parameters include the batches of colloids used to prepare the hydrogels. It seemed that the cationic cores of hydrogels from the second batch were not fully coated, which could explain the induced cytotoxicity at 5 $\mu\text{g}/\text{mL}$, a concentration that was not toxic for the first batch of hydrogels. Furthermore the hydrogel from the second batch did not show any interaction with 50% CALNN 50% (both mole/mole) PEG-capped gold nanoparticles. Apart from size, the difference in shape and appearance of hydrogels of the two batches was also evident from the TEM images (Fig. 4.1, Fig. 4.4) again indicating difference in properties.

4.5 Conclusion and future perspective

The results presented in this chapter can be taken as preliminary, but nevertheless useful for planning further experiments. An integrated detailed study with robust experimental design is required to fully develop ideas about the cytosolic delivery potential of the hydrogels. The main problem raised during the study was the cytotoxicity and surface texture/properties, which were variable between the batches of hydrogels prepared/received at different times. The study needs to repeat with a less toxic batch of hydrogels similar to the first lot. The next step would be to see the working potential of the system for gold nanoparticles, as it appears to have worked for cytosolic distribution of streptavidin-coated Qdots. A detailed time course study will be helpful to understand the fate of polymer nanoparticles themselves either localized in cytosol or/and in endosomes. The direct entry mechanism of hydrogels could then be probed by blocking phagocytosis.

4.6 Bibliography

1. Hillaireau, H. & Couvreur, P. Nanocarriers' entry into the cell: relevance to drug delivery. *Cellular and Molecular Life Sciences* **66**, 2873-2896 (2009).
2. Duncan, R. The dawning era of polymer therapeutics. *Nat Rev Drug Discov* **2**, 347-360 (2003).
3. Ganta, S., Devalapally, H., Shahiwala, A. & Amiji, M. A review of stimuli-responsive nanocarriers for drug and gene delivery. *Journal of Controlled Release* **126**, 187-204 (2008).
4. Torchilin, V.P. Recent advances with liposomes as pharmaceutical carriers. *Nat Rev Drug Discov* **4**, 145-160 (2005).
5. Park, T.G., Jeong, J.H. & Kim, S.W. Current status of polymeric gene delivery systems. *Advanced Drug Delivery Reviews* **58**, 467-486 (2006).
6. Iversen, T.-G., Skotland, T. & Sandvig, K. Endocytosis and intracellular transport of nanoparticles: Present knowledge and need for future studies. *Nano Today* **6**, 176-185 (2011).
7. Kievit, F.M. et al. PEI-PEG-Chitosan-Copolymer-Coated Iron Oxide Nanoparticles for Safe Gene Delivery: Synthesis, Complexation, and Transfection. *Advanced Functional Materials* **19**, 2244-2251 (2009).
8. Kim, B.Y.S. et al. Biodegradable Quantum Dot Nanocomposites Enable Live Cell Labeling and Imaging of Cytoplasmic Targets. *Nano Letters* **8**, 3887-3892 (2008).
9. Duan, H. & Nie, S. Cell-penetrating quantum dots based on multivalent and endosome-disrupting surface coatings. *Journal of the American Chemical Society* **129**, 3333-3338 (2007).
10. Hu, Y. et al. Cytosolic delivery of membrane-impermeable molecules in dendritic cells using pH-Responsive core-shell nanoparticles. *Nano Letters* **7**, 3056-3064 (2007).
11. Hu, Y. et al. Cytosolic Delivery Mediated via Electrostatic Surface Binding of Protein, Virus, or siRNA Cargos to pH-Responsive Core-Shell Gel Particles. *Biomacromolecules* **10**, 756-765 (2009).
12. Bayles, A.R. et al. Rapid Cytosolic Delivery of Luminescent Nanocrystals in Live Cells with Endosome-Disrupting Polymer Colloids. *Nano Letters* **10**, 4086-4092 (2010).

Conclusion

Intracellular delivery and fate of probes and molecular cargos is an active research area due to its acute multidisciplinary significance not only in medical fields, but also for the understanding of molecular mechanisms at micro or nano levels. Different molecular probing techniques have been employed either to visualize the molecular mechanisms or for recording direct intracellular delivery events. These include organic dyes, genetically encoded fluorescent proteins, fluorescent nanocrystals and many other types of nanomaterials. Use of gold nanoparticles for probing the cellular machinery *in vivo* and *in vitro* is highly suitable, since their limited cytotoxicity and unique optical properties make them compatible with various imaging techniques. Furthermore, virtually any biomolecule can be easily attached to gold nanoparticles using thiol chemistry.

We have used peptide or/and PEG-capped gold nanoparticles for probing the efficacy of different cytosolic delivery strategies. Cytosolic delivery of biomolecular cargos (e.g. antisense oligos) is mandatory to utilise their full potential, as most of their targets are localized either in cytosol or in nucleus. The core problem all delivery system/vehicles are experiencing to date is endosomal entrapment, which greatly hampers the delivery systems. The fate of different biomolecular cargos *in vivo/in vitro* and the strategies to overcome the problem of endosomal entrapment have been reviewed in detail in chapter 1 and it was concluded that to date none of the delivery strategies, essentially based on non viral or non-invasive techniques, has showed robust cytosolic delivery. There is, therefore, plenty of room either to explore the real potential of different existing delivery systems or to design new delivery systems. Gold nanoparticles, with their ease of functionalisation and interesting optical properties, are an interesting model system for both imaging and delivery; yet there is currently no clear demonstration in the literature of efficient cytosolic delivery.

The potential of HA2 and TAT peptide-capped gold nanoparticles, as cytosolic delivery agents have been explored in detail in chapter 2. Gold nanoparticles having HA2 peptide in self assembled monolayer ligand shell have shown an increased cellular uptake, depending upon percentage of HA2 peptide in the SAM. For cellular localization, the analogues of HA2 peptide or the orientation of HA2 peptide did not result in any significant difference in terms of interaction with endosomal membranes. Though HA2 peptides were found

interacting with endosomal membrane, no robust cytosolic localization was shown by either of these peptides. HA2 fused TAT also showed increased cellular uptake of fluorescent-TAT with predominant vesicular localization of FITC-TAT.

The cellular localization of 5% CALNN-TAT 95% (mole/mole) PEG-capped gold nanoparticles was found vesicular, with few particles coming out of overfilled macropinosomes. These particles were shown to enter cells mainly through macropinocytosis, suggesting that the presence of a small proportion of particles in the cytosol is not due to direct translocation through the cell membrane, but some other mechanism, probably the bursting of macropinosomes due to the proton sponge effect, which is dependent upon the density of TAT peptide in the SAM of gold nanoparticles. This hypothesis needs to be checked with by titrating the TAT % (mole/mole) in the SAM of gold nanoparticles and monitoring overall cellular uptake and localization.

Then, the potential of a bacterial pore forming toxin Streptolysin O for cytosolic delivery of CALNN or/and CCALNN-PEG-capped gold nanoparticles has been explored in chapter 3. As a positive control, fluorescently labelled membrane impermeable dextran polymer molecules of varying sizes have been successfully delivered inside the cells in SLO treated cells and have displayed uniformly diffused cytosolic localization of polymers. Gold nanoparticles with varying amount of CCALNN-PEG have been functionalized, in order to see the maximum effect of SLO in the presence or absence of non-specific interaction of gold nanoparticles with the cellular membrane. No peptide or mix monolayer of peptide and PEG-capped gold nanoparticles have been found to have a cytosolic localization, but an increase of cellular uptake was observed for the gold nanoparticles having CCALNN-PEG in SAM, especially for 10% (mole/mole) CCALNN-PEG in the SAM. The observed increased endocytic uptake could be explained on the basis of the cell repair mechanism which comes to action to reseal the pores on the plasma membrane. However, the higher effect for 10% (mole/mole) PEGylated gold nanoparticles remains to be explained. Furthermore, successful cytosolic delivery of dextran under the same experimental conditions also suggested a key difference in interaction mechanisms of gold nanoparticles and dextran polymer with the pores. However, this possible difference of interaction between polymer and nanoparticle needs further exploration. One potential hypothesis to explain this difference may be the possible soft dimensions of polymer particle compare to a hard and solid gold nanoparticle, are responsible for entry through pore.

Lastly, the polymeric nanoparticle “hydrogels” were used for intracellular delivery of the gold nanoparticles. These hydrogels have a pH sensitive cationic core, which can swell at low pH inside the endosome, eventually bursting the vesicle. The surface coverage of hydrogel with the gold nanoparticles has been controlled by using the low concentration of gold nanoparticles and by introducing PEG in SAM of gold nanoparticles. Photothermal microscopy revealed a much higher uptake of gold particles bound to the hydrogel, as compared to free peptide-capped gold nanoparticles at the same concentration. This result was supported by the TEM investigation and the results of those two techniques were found consistent for all different experimental conditions. Together they suggested the potential of hydrogels as efficient carriers for cellular delivery of gold nanoparticles, even at pM concentration of the latter.

The cellular localization of hydrogels functionalized with evenly distributed CALNN and PEG capped gold nanoparticles on their surface showed direct translocation deep inside the cells, along with parallel endocytic uptake. In contrast, hydrogels densely packed with CALNN-capped gold nanoparticles showed no direct translocation. Inside the endosomes, in spite of considerable increase in volume due to expansion, probably under the influence of low pH, the hydrogels did not show the endosomal bursting events frequently and gold nanoparticles were found predominantly inside vesicles.

On the other hand, that hydrogel present in the cytosol had the gold nanoparticles attached to it even after 5-6 h incubation with cells. This suggested a strong interaction of gold nanoparticles with hydrogels mediated by CALNN peptide. The presence of hydrogels both in cytosol and in endosomes raises the question about which mechanism was responsible for the gradual increase in cytosolic signal for streptavidin-capped Qdots in the original study. The difference in surface properties and consequently the related cytotoxicity issues with the second batch of hydrogel hampered the further exploration and reproduction of data. However, the future perspective is really exciting for probing the mechanism of cytosolic delivery used by these hydrogels and their potential for the delivery of a variety of functional nanoparticles.

Materials and methods

1 Materials

Tissue culture medium was from Gibco Life Technologies (Invitrogen); fetal calf serum (FCS) from Harlan Sera lab (UK); The Peptides dCCALNN-HA2 (CCALNNGdimGewGneifGaiaGfIG-amide), HA2-NNALCC (GLFEAIEGFIENGWEGMIDGWYGGGGNNLACC), CCALNN-HA2 (CCALNNGGGGLFEAIEGFIENGWEGMIDGWYG), CALNN-Tat (CALNNAGRKKRRRQRRR), and CCALNN-PEG (CCALNN-(EG)₆-ol) were purchased from Peptides Proteins Research Ltd (Fareham, UK). The peptides CALNN and CCALNN-PEG (CCALNN-(EG)₆-ol) were either purchased from Anaspec (San Jose, CA) or from Peptides Proteins Research Ltd (Fareham, UK). The 11-Mercaptoundecyl-tetra ethylene glycol (SH-C₁₁-(EG)₄-ol) also called PEG; mol wt = 350 was from Prochimia (Poland).

Gold nanoparticles of 10 nm size were either from BBI international (Cardif, UK) or synthesized in laboratory (methods section, 2.2). Gold nanoparticles of 5 and 15 nm size were synthesized (methods section 2.2). Gold nanoparticles of 8 and 9 nm were either from BBI international (Cardif, UK) or synthesised as mentioned in methods section 2.2.

Glass cover slip dishes (35 mm) were from Iwaki (Japan) or MatTek (USA). Plastic cover slip dishes (35-mm), multiple well plates of 96-well and 384-well were from Corning (USA). Thiazolyl blue tetrazolium blue (MTT) powder, isopropanol and HCl were from Sigma Aldrich (UK). Streptolysin O (SLO), propidium iodide (PI) and fluorescein diacetate (FDA) were from Sigma Aldrich (UK). FITC-dextran was purchased from Sigma Aldrich (UK). The 16% (w/v) paraformaldehyde solution was from Agar Scientific (UK) and the 25% (w/v) glutaraldehyde solution from TAAB (UK). Centrifugation filters for nanoparticles purification and sterilisation were bought from VWR (PALL).

The polymeric hydrogel nanoparticles suspension was a gift from Brett A. Helms (Lawrence Berkeley National Laboratory, California). These are cationic core-shell polymer colloids of 160-225 nm size, made up of a pH-buffering proton sponge (2(diethylamino)ethylmethacrylate) (PDEAEMA) core cross-linked With poly(2-aminoethyl methacrylate) (PAEMA) shell via poly(ethylene glycol) dimethacrylate (PEGDMA).¹

2 Methods

2.1 Peptide stock solutions

Stock solutions (2 mM) of CALNN, dCCALNN-HA2, CCALNN-HA2, HA2-NNLACC and CCALNN-PEG (CCALNN-SH-C₁₁-(EG)₆-ol) were prepared by dissolving the peptides in concentrated phosphate buffered saline 10 x PBS pH 7.5 (recipe), aliquot and stored at -20°C. Stock solutions of CALNN-TAT (0.7 M) and FITC-TAT (1mg/mL) were prepared by dissolving the peptide in DMSO/ MQ water. 11-mercaptoundecyl-tetra (ethylene glycol) or PEG was dissolved in methanol at stock concentration of 100 mM. The resulting solution was aliquoted and stored at -20°C. The final concentration of PEG, for capping gold nanoparticles, was 2 mM by further diluting it in ethanol and water (ratio). The TAT-HA2 and FITC-TAT peptides were dissolved in Milli-Q water at stock concentrations of 1 mg/mL. The resulting solutions were aliquoted and stored at -80°C. The stock solution of hydrogel (1 mg/mL) was provided as suspension in 1 x PBS at pH 7.5 and stored at 4°C.

2.2 Gold nanoparticle synthesis

For 8-10 nm gold nanoparticles, the method is adapted and modified from Slot *et al.*^{2, 3} All glassware was meticulously cleaned with detergent, ethanol, and then washed thoroughly with Milli-Q water. To 79.75 mL of Milli-Q water 0.25 mL of 4% (w/v) HAuCl₄ (w/v) was added and stirred using magnetic stirrer. Whilst this mixture was kept on heating to 60°C, a 20 mL solution mixture containing; 4 ml of 1 % (w/v) trisodium citrate, 200 µL of 1% (w/v) tannic acid and 15.8 mL MQ water was prepared and added to the already hot and rapidly stirring gold solution. The solution turned from a light yellow to a deep red colour within 20-30 minutes. This solution was heated to 100°C for another 20 minutes to complete the reaction. The particles were cooled, filtered and stored at 4°C. Since the tannic acid was not sufficient to affect the overall pH, no K₂CO₃ solution was added.

For 15 nm citrate stabilized gold nanoparticles, the method was adapted and modified from Turkevich and Frens, G.^{4, 5} Briefly, a 50 mL of 0.01% (w/v) HAuCl₄ solution was heated to 60-100°C and then 1.75 mL-2 mL of 1% (w/v) tri-sodium citrate solution was added to it quickly and boiling was continued until a deep red wine colour appeared. The solution was cooled to room temperature, filtered and stored at 4°C.

For 5 nm gold nanoparticles, The method was adapted and modified from Slot *et al.*² Briefly, 395 mL of deionised water and 5mL of 1% (w/v) HAuCl₄ was heated to 60°C. 5 mL of 0.2 M

K_2CO_3 was added to gold solution when its temperature reached to 60°C and immediately after adding K_2CO_3 , reducing mixture solution (95 mL) containing, 20 mL 1% (w/v) trisodium citrate, 5 mL 1% (w/v) tannic acid and 70 mL of Milli-Q water is added and left to stir and reflux at 60°C until the reaction is completed. It usually takes 30-40 minutes. The cherry red solution of gold nanoparticles was cooled, filtered and stored at 4°C. Gold nanoparticles of size 8 nm from BBI were also being used. The size of gold nanoparticles was determined using TEM imaging and image analysis using Image J software.

2.3 Formation of peptide self-assembled monolayers for gold nanoparticles (general procedure)

The peptide solution was mixed in a 1:1 volume ratio with 10x PBS. A suspension solution of gold nanoparticles was added in a 9:1 volume ratio (gold:peptide) giving a 100 μ M final concentration of peptides. The solution was briefly agitated before the addition of Tween-20 to a final concentration of 0.05% (v/v). The solutions were left overnight at room temperature. For mix monolayers of CALNN and PEG or CCALNN-PEG, the diluted 2 mM PEG/ CCALNN-PEG solution was mixed with CALNN peptide solution at the required overall percentage concentration before adding 10 x PBS and gold nanoparticles at 1:1 and 1:9 ratios respectively.

2.4 Formation of peptide self-assembled monolayers containing 5% CALNN-TAT 95% PEG-ligands

2.4.1 First method

This method was adapted from Krpetic *et al.*⁶ The ligands mixture was prepared by adding the required volumes of 0.7 mM CALNN-TAT and 100 mM PEG (in order of first peptide and then PEG), to give 5% CALNN-TAT and 95% PEG (both mole/mole) in the self-assembled monolayer around gold nanoparticles. The addition and mixing of PEG was made as quickly as possible to avoid precipitation of the peptide in methanol followed immediately by addition of the citrate-stabilized gold nanoparticles. The suspension was vigorously shaken and left under agitation overnight at room temperature. The colour of the solution, an optical parameter for colloidal stability, was also observed carefully as it should remain red after addition of peptide and PEG. The total number of ligands per gold nanoparticles used for this ligand exchange reaction was 20500, out of which, 1025 were CALNN-TAT (5%) and 19475 of PEG (95%). For PEG-coated gold nanoparticles, only PEG was added to colloidal gold and kept overnight under agitation at room temperature.

2.4.2 Second method

Both stock solutions of CALNN-TAT (0.7mM) and PEG (0.1M) were diluted by factor of 6, before mixing them together, in order to increase the solubility of the mixture and to reduce the risk of peptide aggregation in the presence of methanol. The final total number of ligands per gold nanoparticles was kept the same, i.e., 20500 ligands / gold nanoparticle out of which, 1025 were CALNN-TAT molecules.

A stock solution of CALNN-TAT (0.7mM) in DMSO was diluted in ethanol to 0.116 mM while 100 mM stock solution of PEG was first diluted in methanol to 28.6 mM and then in ethanol to 16.6 mM. The peptide and PEG solutions were mixed together quickly and poured into the colloidal gold nanoparticles which were already put on vigorous vortex on magnetic stirring plate. Tween-20 0.05% (v/v) was added afterward and the resulting solution stirred overnight at room temperature. The 100% PEG-capped gold nanoparticles were made the same way, except there was no CALNN-TAT peptide added.

2.5 Nanoparticles purification procedure

The 10 nm nanoparticle solutions were centrifuged (13000 rpm, 60 minutes), and the pellet was resuspended in 1mL of 1 x PBS with 0.05% (v/v) Tween-20 before a second centrifugation step (13000 rpm, 60 minutes). This washing step was repeated three times with 1 x PBS only. The gold nanoparticles were then filtered by centrifugation using sterile ultrafree-MC GV 0.22 μm filters. Successful formation of the monolayer is immediately visible because of the increased colloidal stability and of a small red shift of the plasmon band. The repeated centrifugation procedure ensures that the concentration of excess of free peptide is in the pico molar range. For 14-15 nm gold nanoparticles, the purification procedure is exactly the same as for the 10 nm gold nanoparticles except for the fact that the nanoparticles solutions were centrifuged at 13000 rpm for 20 minutes each time. For 5 nm gold nanoparticles, to remove the excess of peptide, the suspension solution containing peptide and nanoparticles was centrifuged at 21000 rpm for 2 h at 4^oC. The supernatant was then discarded, the nanoparticles pellet was resuspended in 1 x PBS and eluted through a Sephadex G-25 column. The particles were then filtered by centrifugation using sterile ultrafree-MC GV 0.22 μm filters. UV-vis characterization for measuring concentrations of gold nanoparticles was done by diluting particles in 1 x PBS.

2.6 Nanoparticles purification procedure for 5% CALNN-TAT 95% PEG-containing gold nanoparticles

This method was applied to nanoparticles produced according to section 2.4.1. The nanoparticle solutions were centrifuged at 13000 rpm for 20 minutes and the pellet was resuspended in 0.8–1 mL of milli Q water. The gold nanoparticle solution was ultrasonicated for a few minutes for homogenous resuspension before a second centrifugation at 13000 rpm for 20 minutes. The washing procedure was repeated three times with water only, before final resuspension of gold nanoparticles in 1 x PBS. Successful formation of the monolayer is immediately visible because of the increased colloidal stability and of a small red shift of the plasmon band. The particles were then filtered by centrifugation using sterile ultrafree-MC GV 0.22 μm filters. The second method of purification correspond to second method of preparation (section 2.4.2), which was not much different from first method except the nanoparticles were washed and resuspended in 1 x PBS instead of milli-Q water.

2.7 Streptolysin O (SLO) preparation

As Streptolysin O is a thiol-activated toxin, a mixture of 0.1% (w/v) bovine serum albumin and 5 mM Dithiothreitol (DTT, molecular formula is $\text{C}_4\text{H}_{10}\text{O}_2\text{S}_2$), a strong reducing agent, was mixed with dried SLO to make a stock solution containing 14000 U/mL of SLO (3.8 μM). The stock solution was aliquoted and stored at -80°C .

2.8 Optimization of the optimum Streptolysin O amount

Optimization of streptolysin O (SLO) amount is required on a regular basis because even at -80°C oxidation results in a loss of toxin activity. In addition, the amount of SLO required is dependent on experimental parameters (number of cells per dish, medium type, cell line, resealing time, dish area and so on).

2.8.1 Optimization of SLO for cell suspension

Cells were detached using trypsin and pelleted at a concentration of 4×10^5 cells/per eppendorf, by centrifugation at 3000 rpm for 3 minutes. The supernatant was discarded to remove trypsin and serum. Cells were then washed by suspending in 400 μL serum free medium (MEM) and centrifuged again at 3000 rpm for 3 minutes. The entire supernatant medium was carefully removed as even traces of trypsin or serum can decrease or altogether inhibit the SLO activity. This washing procedure was repeated at least three times.

Cells were suspended in 200 μ L serum free medium mixed with propidium iodide (1 μ g/mL). Propidium iodide stains the DNA and cannot pass through the intact membrane of the cells. Then different concentrations of SLO pre-diluted in 200 μ L of serum free MEM were added to the cells. It was made sure that cells are properly resuspended before addition of SLO by flicking the tube several times. The cells were incubated for 10 minutes at 37°C and 5% CO₂. During incubation, cells were flicked after 5 minutes. Afterward 1 mL serum-containing medium was added and cells were again incubated for 20-30 minutes at 37°C. This step ensures both the inhibition of toxin activity and the subsequent resealing of the cell membrane. The cells were centrifuged for 4 minutes at 3000 rpm and medium was replaced with 1 mL fresh medium. The fluorescein diacetate (FDA) a non- fluorescent compound, was added at a final concentration of 2ng/mL, to check re-sealing as FDA is membrane permeable and is only fluorescent in live cells (esterases present in live cells converts the FDA into a green fluorescent molecule called fluorescein). The cells were again incubated for 10 minutes at 37°C. The medium was replaced with fresh medium and cells were visualized under confocal fluorescence microscope (Zeiss LSM 510, 710 or multiphoton). The cells showing both red and green fluorescence are considered permeabilized and resealed. The cells showing only red fluorescence are considered as dead and the cells showing only green fluorescence cells are considered alive but not permeabilized (Fig. 3.1). The overall cell shape and physical appearance was also taken into account. The SLO amount was considered as optimal when at least 50% of the cells were permeabilised and alive.

2.8.2 Optimization of SLO amount for adherent cells

The cells were seeded in 12 mm iwaki dishes (2.7 x 10³ cells/dish) or 14mm Matek glass bottom dishes (3 x 10³ cells /dish). After incubating for 24 h, the cells were washed with PBS twice and with MEM thrice. Mixture of PI and SLO diluted in MEM was carefully pipetted in the middle of the dish (150-200 μ L total volume) and cells are incubated at 37°C for 10 minutes at 5% (v/v) CO₂. Then 1mL normal warm serum medium was added to dishes in order to deactivate SLO. The medium was immediately replaced with fresh serum-containing medium. After adding fresh medium, the cells were kept at 37°C and at 5% (v/v) CO₂ for resealing. Resealing time was 40-45 minutes for adherent cells. It was experimentally observed that a better FDA fluorescence signal was obtained for the cells given long time for resealing. Fluorescein diacetate was added at a final concentration of 2-7

ng/mL, to check re-sealing. The presence of permeabilized and resealed cells was determined by looking at the fluorescence images of the cells. Cells with green and red fluorescence signal considered live and permeabilized while only red cells considered dead and only green cells were live but not permeabilized (Fig. 3.1).

These optimization experiments (on suspended cells or on adherent cells) were performed every time before proceeding with the experiments with gold nanoparticles.

2.9 Formation of nanoparticles-decorated hydrogels

The hydrogels were diluted at the appropriate concentration in 1 x PBS at pH 7.5 and left to spin on carousel with peptide or peptide and PEG-functionalized gold nanoparticles over night at 4°C. Spinning avoid sedimentation of hydrogel particles. These gold nanoparticles functionalized hydrogels were incubated with cells after further dilution in medium.

2.10 Cell culture and nanoparticle incubation (general procedure)

HeLa cells were incubated in Dulbecco's modified Eagle medium (DMEM) supplemented with 10% (v/v) FCS and 1% (v/v) non-essential amino acids, at 37°C, 5% CO₂. The cells (between passages 8 to 20) were plated at 1×10^{10} cells / flask and split every 48 h. From these main cell stock flasks, cells were either plated in 35 mm glass bottom dishes or used directly for suspension cells protocol.

For all HA2 and TAT/ PEG experiments, cells were seeded at 4×10^5 cells/dish in 35 mm Corning dishes day before the experiment. The nanoparticles were incubated directly into the complete medium (containing 10% (v/v) FCS) for indicated times at the stated final concentration.

For all SLO related experiments, peptide capped gold nanoparticles were incubated with medium (with or without 10% FCS in the presence or absence of the SLO respectively), for indicated times at the stated final concentration. The detail procedure for plated and for suspended cells incubation with gold nanoparticles is given in section 2.11.

For all hydrogel experiments, the cells were plated either in 35 mm Corning dishes or in 35 mm glass cover slip dishes at concentration of 5×10^5 cells/dish. Gold nanoparticles or gold nanoparticles functionalized hydrogels were incubated directly into the complete medium (containing 10% FCS) for 6-14 h. The final concentrations vary between 250-500 pM for the

gold nanoparticles and between 1-5 $\mu\text{g}/\text{mL}$ for the hydrogel as specified in the relevant figures (chapter 4).

2.11 Cells treatment with gold nanoparticles (with/without SLO)

2.11.1 Suspended cells (treated with /without SLO) and gold nanoparticles

Cells (between passages 8 to 20) were detached from the cell culture dish using trypsin, centrifuged and pelleted for removing trypsin. Cells were counted and resuspended in medium at the concentration of 4×10^5 cells/eppendorfs. The cells were washed with serum-free medium three times by centrifugation at 3000 rpm for 3 minutes, removing carefully all the medium each time.

The cells were resuspended in 200 μL of serum-free MEM and mixed with gold nanoparticles, which were already suspended in 200 μL serum-free MEM. The optimized amount of SLO was added to this mixture. The cells were left to incubate at 37°C for 10 minutes. Then 1 mL of serum containing MEM (10% FCS) was added and the tubes were placed in the incubator for 20-30 minutes for resealing. Later the medium was replaced by fresh medium (centrifugation of the cells for 3 minutes at 3000 rpm) to remove the excess nanoparticles. The cells were then seeded on Iwaki dishes for photothermal imaging or in Corning dishes for TEM imaging, and left for 4 h to attach to the dish before fixation. The fixed cells were kept in 1x PBS at 4°C with 0.05% (w/v) sodium azide until imaging. Gold nanoparticles incubation with HeLa cells, in the absence of streptolysin O, was done exactly the same way.

2.11.2 Adherent cells treated with /without SLO and gold nanoparticles

The cells (2.67×10^3 /dish) were seeded in 12 mm iwaki dishes the day before the experiment. For 14 mm Matek glass bottom dishes, 3×10^5 cells /dish were seeded. Cells were washed with 1 x PBS twice and MEM washes 3 times. Mixture of gold nanoparticles and SLO diluted in MEM was carefully pipetted in the middle of the dish (150-200 μL total volume) and cells were incubated for 10 minutes at 37°C , at 5% CO_2 . Afterward 1 mL normal warm serum medium was added to dishes in order to deactivate SLO. The medium was immediately replaced with fresh medium. After adding fresh medium, the cells were kept at 37°C and at 5% CO_2 for 45 minutes. Then the medium was replaced with warm 1 x PBS. After at least two PBS washes the cells were fixed for imaging. Gold nanoparticles incubation with HeLa cells, in the absence of streptolysin O, was done exactly the same way.

2.12 Cells treated with fluorescent isothiocyanate-dextran (FITC-dextran)

FITC-dextran molecules of different molecular weight were used to check the pore size, formed by SLO. The protocol for SLO treatment was the same as described in section 2.8.1/2.8.2 except no FDA was used for permeabilization confirmation as FITC-dextran itself was fluorescent and PI was added after resealing. Cells, either plated or suspended, were treated with SLO for 10 minute in the presence of 4KDa, 70KDa or 150KDa FITC-dextran (0.4-0.8% (w/v) final concentration) in serum-free medium. PI was added to confirm the resealing in the presence of serum-containing medium. The cells were then washed with warm serum-containing medium and incubated on the microscope stage at 37°C, 5% CO₂, and imaged by confocal fluorescence microscope. Five to eight fields were chosen randomly for imaging. The cells with only green fluorescence were considered permeabilized and live while red or colourless cells were considered dead or not permeabilized respectively (chapter 3, Fig. 3.2).

2.13 Cell proliferation assay: Thiazolyl blue tetrazolium bromide (MTT assay)

A cell proliferation assay was carried out using a colorimetric MTT assay. Cells were cultured at different densities per 200 µL/well in a 96-well plate in MEM medium with 10% (v/v) FBS and 1% (v/v) nonessential amino acid solution (NEAA) at 37°C in a humidified atmosphere containing 95% air and 5% (v/v) CO₂. One day after plating, cells were treated with SLO according to the protocol described in 2.6.2. The cells were then left to grow in normal MEM medium with 10% (v/v) FBS and 1% (v/v) NEAA for 24 h at 37°C, 5% (v/v) CO₂. The medium was aspirated and replaced by 100 µL /well MTT solution (5 mg /mL) and cells incubated at 37°C, 5% (v/v) CO₂ for 1 hr. the MTT solution was replaced with 100 µL /well isopropanol-HCl 0.04 N solution. The plate was shaken couple of times until complete dissolution of blue precipitates. The optical densities were assessed with a plate reader at 570 nm.

2.14 Transmission electron microscopy

The cells were plated in 35 mm plastic coverslipdishes. One day after plating, cells were washed with 1 x PBS and fixed with 4% (w/v) paraformaldehyde and 2% (v/v) glutaraldehyde in 0.1 M phosphate buffer solution (0.32 g NaH₂PO₄·2H₂O, and 2.08 g Na₂HPO₄·7H₂O in 100 ml final volume of deionized water, pH 7.4) for 1 h. Post fixation was done with 1% (v/v) aqueous solution of OsO₄ for 1 h. The cells were thoroughly washed with 1 x PBS, Milli-Q water and 30% (v/v) ethanol. The cells were stained with 0.5% (w/v) uranyl-acetate for 1 h.

Dehydration of the samples was carried out using increasing concentrations of ethanol from 30%, 60%, 70%, 80% and 100% (all v/v). Finally, the cells were processed for epoxy resin embedding. The cells were first treated with a mixture of 1:1 epoxy resin and 100% ethanol for 30 minutes and then with 100% resin at 60°C. The cells were left at 60°C for 48 h until the resin was polymerized. Ultrathin sections (50-70 nm) were cut with a LKB ultramicrotome with the help of a diamond knife. The cell's sections were collected on formvar-coated copper grids and post-stained with 5% (w/v) aqueous uranyl- acetate solution in 50% (v/v) ethanol and 2% (v/v) aqueous lead citrate solution before viewing in a FEI Tecnai Spirit transmission electron microscope at 100-120 KV.

2.15 TEM image analysis for gold content

Image analysis done by two different ways depending upon the fact that how the images were acquired and the purpose of quantification. The samples for which, images were taken randomly for recording endosomally localized gold nanoparticles events in different cell sections, the analysis was done by calculating the mean number of gold nanoparticles per unit micrometer area of endosomes using image J software. At least 15-20 images were selected randomly and quantified for each sample (chapter 2, Fig. 2.3).

The samples for which images were taken systematically by viewing through the whole cell section, the numbers of gold nanoparticles were calculated per cell section and sub-cellular localization was also recorded manually. On average, 15-20 images were taken for each cell section and at least 4-7 cell sections were searched thoroughly per condition/sample. Mean number of gold nanoparticles per cell section was calculated and then mean number of gold nanoparticles per samples was calculated by dividing the sum of means of each section with total number of cell sections (chapter 2, Fig. 2.5).

2.16 Gold nanoparticles sizing by TEM

The size of the bare gold nanoparticles was determined by taking TEM images of gold nanoparticles at high resolution (87 K-150 K). The procedure is as follows.

The 5 μ L colloidal suspension of gold was placed on formva coated aluminium grid and left to dry in air for at least 30 minutes. The dried grid was viewed in a FEI Tecnai Spirit transmission electron microscope and images were analysed using analySIS software (Soft Imaging Systems). At least 100 particles were measured using this software while the ImageJ

software was also used for size measurement. Some gold nanoparticles syntheses were exclusively measured using Image J software.

2.17 Confocal microscopy

Cells were plated in 35 mm glass coverslip cell culture dishes (Iwaki). One day after plating, cells were washed twice with warm 1 x PBS and warm fresh medium was added. The cells containing dishes then incubated on the microscope stage at 37°C, 5% (v/v) CO₂, and observed by confocal microscopy using a Zeiss LSM510 or multiphoton confocal with a Planapochromat 40 X or 63 X /1.3 NA oil immersion objective. Excitation of fluorescein was performed using an argon ion laser at 488 nm. Emitted light was detected through a 505-550 nm bandpass filter from a 545 nm dichroic mirror. Data capture was carried out with LSM510 version 3 software (Zeiss, Germany). These experiments were performed at least 2 times, and each time, five to eight random fields were chosen.

2.18 Photothermal microscopy

Briefly, a red laser (probing laser) detects a signal produced due to the change in refractive index of the surrounding medium of a gold probe. This change happens as a result of the heat dissipation by the gold nanoparticle into the medium after the absorption of the light coming from a green laser (heating laser). The photothermal images can be analysed by two following methods. The preference of one method or the other depends upon imaging conditions and feasibility. The goal of photothermal image analysis was to find a measure of the cells gold nanoparticle content to assess the amount of nanoparticles internalised by cells, and especially to allow for a comparison between different conditions, such as different self-assembled monolayer coating subsequently assessing the influence of the surface chemistry on the nanoparticle uptake.

2.18.1 Image analysis: method with threshold or whole field method

In this method the photothermal intensity, in an image, is measured above a threshold. The image analysis was processed using the software AQM Advance 6.0.2.23 (Kinetic Imaging Ltd, UK). For a given image the process is described in the following paragraph.

A TIFF image file composed of two image planes (bright field, photothermal) was used for the analysis. A region of interest (ROI) was drawn using the ellipse tool or free hand polygon image tool where no cells were present, using the bright field plane. The mean of the photothermal intensity of these ROIs was chosen as a measurement of the photothermal

background of the image. The bright field plane was used to draw a single ROI around all the cells appearing as whole. A value of 1.5 times the mean background photothermal intensity of the field of view was then used as a measurement threshold. A measurement of the mean photothermal intensity of that cell containing ROI was obtained by taking the mean of all the pixels above the threshold value.

To obtain a measurement of the cell population the same method was repeated on all acquired images. The values obtained for each image were averaged yielding mean photothermal intensity (mean nanoparticle uptake quantity) and a standard error.

2.18.2 Image analysis: single cell method

The analysis was processed using the software AQM Advance 6.0.2.23 (Kinetic Imaging Ltd, UK). For a given image the process is described in the following paragraph.

A TIFF image file composed of two image planes (brightfield, photothermal) was used for the analysis. Regions of interest were drawn using the ellipse tool or polygon tool where no cells were present, using the bright field plane. The mean of the photothermal intensity of these ROIs was chosen as a measurement of the photothermal background of the image. The bright field plane was used to draw ROIs around each of the cells appearing as whole. For a given cell, a measurement of the mean photothermal intensity of the cell was obtained by taking the mean of all the pixels in the ROI, after subtraction of the photothermal background intensity. The same treatment was applied to each cell within the image.

To obtain a measurement of the cell population the same method was repeated on all acquired images. The values obtained for each cell in each image were averaged yielding mean photothermal intensity (mean nanoparticle uptake quantity per cell) and a standard error.

2.18.3 Bright field microscopy

The bright field illumination system used was home built. It comprises a X-Cite Series 120 illuminator (EXFO UK, UK), an EXFO microscope adaptor and a lens (Thorlabs, USA) for collimation, a water dipping long working distance (2.5mm) objective (Achromplan 40x / 0.8 NA, Zeiss, Germany), and an oil objective (Achromplan 50x / 0.9 NA, Zeiss, Germany) for light collection. The illumination goes from the top of the microscope, through the water

dipping objective, the sample and the collecting objective before going to the camera. The sample adheres on the top surface of a glass coverslip bottom dish located between the two objectives. Images acquisition was handled via the HClmage 1.1.1.0 image acquisition software (Hamamatsu, Japan) and the air-cooled image EM EMCCD camera (Hamamatsu, Japan). The bright field images had the following characteristics: 16-bit TIFF file format, 512 x 512 pixels maximum frame size, 122 ms time exposure, camera gain $G=1$ and digital sensitivity gain $G=1$.

2.18.4 Cell fixation for photothermal microscopy

4% (w/v) paraformaldehyde (PFA) in 0.1 M phosphate buffer (PB) was used for cells fixed for photothermal imaging. The cells were washed twice with warm 1 x PBS (37⁰C) and fixed with warm 4% PFA fixative for 20 minutes. The fixative was then removed and the cells were washed twice with 1 x PBS, each time for at least 5 minutes. The cells were then kept at 4⁰C in 1 x PBS with 0.05% (w/v) sodium azide until imaging.

2.19 Bibliography

1. Bayles, A.R. et al. Rapid cytosolic delivery of luminescent nanocrystals in live cells with endosome-disrupting polymer colloids. *Nano Letters* **10**, 4086-4092 (2010).
2. Slot, J.W. & Geuze, H.J. Sizing of protein a-colloidal gold probes for immunoelectron microscopy. *Journal of Cell Biology* **90**, 533-536 (1981).
3. Kimling, J. et al. Turkevich method for gold nanoparticle synthesis revisited. *The Journal of Physical Chemistry B* **110**, 15700-15707 (2006).
4. Frens, G. Controlled nucleation for regulation of particle-size in monodisperse gold suspensions. *Nature-Physical Science* **241**, 20-22 (1973).
5. Turkevich, J., Stevenson, P.C. & Hillier, J. A study of the nucleation and growth processes in the synthesis of colloidal gold. *Discussions of the Faraday Society*, 55-& (1951).
6. Krpetic, Z. et al. Negotiation of intracellular membrane barriers by TAT-modified gold nanoparticles. *Acs Nano* **5**, 5195-5201 (2011).

Appendix

Publications arising from this thesis to date

Paper

Cathepsin-L digestion of nanobioconjugates upon endocytosis (ACS nano, 2009) Page 2461-2468, issue 9, volume 3. ISSN 1936-0851. DOI 10.1021/nn9006994.

Sée, V., Free, P., Cesbron, Y., Nativo, P., Shaheen, U., Rigden, D.J., Spiller, D.G., Fernig, D.G., White, M.R.H., Prior, I.A., Brust, M., Lounis, B., and Lévy, R.

Review

Gold nanoparticles delivery in mammalian live cells: a critical review (Nano reviews, 2010), volume 1. DOI: 10.3402/nano.v1i0.4889.

Lévy, R., Shaheen, U., Cesbron, Y., and Sée, V.